Numerical performance evaluation of a delugeable flat bare tube air-cooled steam condenser bundle

by

Ester Angula

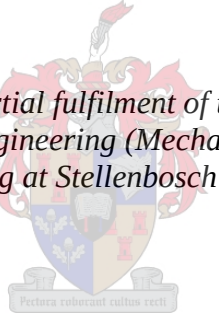

Project presented in partial fulfilment of the requirements for the degree of Master of Engineering (Mechanical) in the Faculty of Engineering at Stellenbosch University

Supervisor: Prof. H. C. R. Reuter

March 2015

Declaration

By submitting this project electronically, I declare that the entirety of the work contained therein is my own, original work, that I am the sole author thereof (save to the extent explicitly otherwise stated), that reproduction and publication thereof by Stellenbosch University will not infringe any third party rights and that I have not previously in its entirety or in part submitted it for obtaining any qualification.

Signature…….

Date: .....

Abstract

In this study, one and two-dimensional models are developed for the evaluation of the thermal performance of a delugeable flat tube bundle to be incorporated in the second stage of an induced draft hybrid (dry/wet) dephlegmator (HDWD) of a direct air-cooled steam condenser (ACSC). Both models are presented by a set of differential equations. The one-dimensional model is analysed analytically by using three methods of analysis which are: Poppe, Merkel, and heat and mass transfer analogy. The two-dimensional model is analysed numerically by means of heat and mass transfer analogy method of analysis whereby, the governing differential equations are discretised into algebraic equations using linear upwind differencing scheme. The two-dimensional model's accuracy is verified through a comparison of the two dimensional solutions to one dimensional solutions. Satisfactory correlation between the one and two-dimensional results is reached. However, there is a slight discrepancy in the solutions, which is mainly due to the assumptions made in one-dimensional model. The effect of tube height, tube pitch, tube width, deluge water mass flow rate, frontal air velocity, steam, and air operating conditions on the heat transfer rate and air-side pressure drop for both wet and dry operating modes are investigated. The long tube height, large tube width, small tube pitch, and high frontal air velocity are found to increase the tube bundle's performance. However, this performance is associated with a high air-side pressure drop. The performance of the deluged flat tube bundle is found to be less sensitive to the changes in the deluge water mass flow rate and air operating conditions. Furthermore, the best configuration of a delugeable flat tube bundle is identified through a comparison to round tube bundle presented by Anderson (2014). The performance of the round tube bundle is found to be around 2 times, and 1.5 times of that of flat tube bundle, when both bundles operate as an evaporative and dry air-cooled condenser respectively.

Opsoming

In hierdie studie is een en twee-dimensionele modelle ontwikkel vir die evaluering van die termiese prestasie van 'n benatbare plat buis bundel in die tweede stadium van 'n geïnduseerde ontwerp hibriede (droë / nat) deflegmator van 'n direkte lugverkoelde stoom kondensator. Beide modelle is aangebied deur 'n stel van differensiaalvergelykings. Die een-dimensionele model is analities ontleed deur die gebruik van drie metodes van analise wat: Poppe, Merkel, en die hitte en massa-oordrag analogie. Die twee-dimensionele model is numeries ontleed deur middel van hitte en massa-oordrag analogie metode van analise waardeur , die regerende differensiaalvergelykings gediskretiseer in algebraïese vergelykings met behulp van lineêre windop differensievorming skema. Die twee-dimensionele model se akkuraatheid is geverifieer deur 'n vergelyking van die twee dimensionele oplossings te een dimensionele oplossings. Bevredigende korrelasie tussen die een en twee-dimensionele resultate bereik word. Maar daar is 'n effense verskil in die oplossings, wat is hoofsaaklik te wyte aan die aannames wat gemaak in een-dimensional model. Die effek van buis hoogte, buis toonhoogte, buis breedte, vloed water massa-vloeitempo, frontale lug snelheid, stoom, en in die lug werktoestande op die hitte oordrag snelheid en lug - kant drukval vir beide nat en droë maatskappy modi word ondersoek. Die lang buis hoogte, groot buis breedte, klein buisie toonhoogte, en 'n hoë frontale lug snelheid gevind die buis bundel se prestasie te verhoog. Tog is hierdie prestasie wat verband hou met 'n hoë lug - kant drukval. Die prestasie van die oorstroom plat buis bundel gevind word minder sensitief vir die veranderinge in die vloed water massa-vloeitempo en lug werktoestande. Verder is die beste opset van 'n benatbare plat buis bundel geïdentifiseer deur 'n vergelyking met ronde buis bundel aangebied deur Anderson (2014). Die prestasie van die ronde buis bundel gevind word om 2 keer, en 1.5 keer van daardie plat buis bundel , wanneer beide bundels funksioneer as 'n damp en droë lugverkoelde kondensor onderskeidelik .

Dedication

This work is dedicated to the memory of my mother, who couldn't see the completion of this work.

Acknowledgements

I would like to acknowledge the following people for their valuable contributions:

- Prof. Reuter for his guidance and support throughout the project.
- University of Namibia, Faculty of Engineering and IT for funding my study.
- My family for their support.
- My God for his protection and guidance

Table of contents

Declaration i
Abstract ii
Opsoming iii
Dedication iv
Acknowledgements v
Table of contents vi
List of figures ix
List of tables xii
Nomenclature xiii
1. Introduction 1
1.1. Background 1
1.2. Deluge cooling systems 2
1.3. Adiabatic cooling systems 2
1.4. The role of the dephlegmator 3
1.5. The HDWD structure 4
1.6. Motivation 6
1.7. Project objectives 7
1.8. Project outline 7
2. Literature review 8
3. Analysis of thermal performance characteristics of a delugeable flat tube bundle 13
3.1. Numerical model 13
3.2. The governing equations of a one-dimensional model 15
3.2.1. Tube bundle operated as an evaporative condenser 15
3.2.2. Tube bundle operated as a dry air-cooled condenser 19
3.3. The governing equations of a two-dimensional model 19
3.3.1. Steam-side elementary control volume 20
3.3.2. Condensate-side elementary control volume 21
3.3.3. Tube wall-side elementary control volume 25
3.3.4. Deluge water elementary control volume 27
3.3.5. Air-side elementary control volume 31

3.3.6. The governing equations 33
3.4. Discretization of the governing equations 35
3.5. Solution methods 39
3.5.1. One-dimensional solution methods 39
3.5.2. Two-dimensional solution method 40
3.6. Validation of a two-dimensional numerical model 40
4. Parametric study 47
4.1. Effect of tube height and tube pitch on the heat transfer rate and air-side pressure drop 47
4.2. Effect of tube width on the heat transfer rate and air-side pressure drop 49
4.3. Effect of deluge water mass flow rate on the heat transfer rate and air-side pressure drop 51
4.4. Effect of frontal air velocity on the heat transfer rate and air-side pressure drop 53
4.5. Effect of steam operating conditions on the heat transfer rate and air-side pressure drop 55
4.6. Effect of air operating conditions on the heat transfer rate and air-side pressure drop 56
5. Tube bundle configurations 59
5.1. Introduction 59
5.2. Influence of tube pitch on the performance ratio of the bundles 60
5.3. Influence of tube height on the performance ratio of the bundles 61
5.4. Tube bundle selection 62
6. Conclusions and recommendations 65
6.1. Development of models 65
6.2. Effect of designing parameters on the bundle performance 65
6.3. Significant of the project 66
References 67
Appendix A.1
A. Properties of the fluids A.1
A.1. The thermo-physical properties of dry air from 220 K to 380 K at standard atmospheric pressure(1 atm.) A.1
A.2. The thermo-physical properties of saturated water vapour from 273.15 K to 380 K A.1

A.3. The thermo-physical properties of saturated water liquid from 273.15 K to 380 K.....A.2
A.4. Thermo-physical properties of mixtures of air and water vapour .A.2
B. Theories and empirical correlations.....B.1
B.1. Condensation heat transfer coefficient B.1
B.2. Deluge water heat transfer coefficients B.1
B.3. Air-side heat and mass transfer coefficients B.1
B.4. Air-side pressure drop.....B.2
C. Sample of calculation.....C.1

List of figures

Figure 1.1: Direct air-cooled steam condenser street 3

Figure 1.2: Diagram of steam flow in the ACC streets 4

Figure 1.3: Schematic diagram of the forced draft HDWD, Source: (Owen, 2013) 5

Figure 1.4: Schematic diagram of the induced draft HDWD 5

Figure 1.5: Diagram of steam flow in the ACC streets, incorporating the HDWD 6

Figure 3.1: Schematic diagram of two adjacent tubes in a delugeable flat plain tube bundle 13

Figure 3.2: The two-dimensional elementary control volume of the delugeable horizontal plain flat tube bundle 14

Figure 3.3: One-dimensional elementary control volume of the delugeable horizontal plain flat tube bundle 15

Figure 3.4: Steam-side elementary control volume and thermal resistance diagram 20

Figure 3.5: Condensate-side elementary control volume 21

Figure 3.6: Condensate-side thermal resistance diagram 22

Figure 3.7: Free body diagram for the control volume in the condensation film ..23

Figure 3.8: Tube wall-side elementary control volume and thermal resistance diagram 26

Figure 3.9: Deluge water-side elementary control volume.....27

Figure 3.10: Deluge water-side thermal resistance diagram.....28

Figure 3.11: Free body diagram for the control volume in deluge water film 29

Figure 3.12: Air-side elementary control volume.....31

Figure 3.13: Air-side thermal resistance diagram.....32

Figure 3.14: Grid points network.....35

Figure 3.15: General discretization using linear upwind differencing scheme. 36

Figure 3.16: Tube bundle section, illustrating the air-side flow between two adjacent tubes.....41

Figure 3.17: Graph illustrating the grid dependency of the numerical solutions ..42

Figure 3.18: The distribution of the temperature of air, deluge water, condensate and steam along the tube height.....43

Figure 3.19: Condensation heat transfer coefficient and film thickness along the tube height....43

Figure 3.20: Deluge water heat transfer coefficient and film thickness along the tube height....44

Figure 3.21: Air-side heat transfer coefficient and boundary layer thickness along the tube height....44

Figure 3.22: Friction coefficient, friction factor and boundary layer thickness along the tube height....44

Figure 4.1: Effect of tube height and pitch on the heat transfer rate - one dimensional model 48

Figure 4.2: Tube critical height as a percentage of tube height - one dimensional model 48

Figure 4.3: Effect of tube height and pitch on the air-side pressure drop - one dimensional model....49

Figure 4.4: Effect of tube width on the heat transfer rate - one dimensional model 50

Figure 4.5: Effect of tube width on the air-side pressure drop - one dimensional model 51

Figure 4.6: Effect of deluge water mass flow rate on the heat transfer rate - one dimensional model....52

Figure 4.7: Effect of deluge mass flow rate on the air-side pressure drop - one dimensional model....53

Figure 4.8: Effect of frontal air velocity on the heat transfer rate - one dimensional model 54

Figure 4.9: Effect of frontal air velocity on the air-side pressure drop - one dimensional model....55

Figure 4.10: Effect of steam temperature on the heat transfer rate - one dimensional model....56

Figure 4.11: Effect of steam temperature on the air-side pressure drop - one dimensional model....56

Figure 4.12: Effect of air operating conditions on the heat transfer rate - one dimensional model....57

Figure 4.13: Effect of air operating conditions on the air-side pressure drop - one dimensional model....58

Figure 5.1: Tube bundle presented by Anderson (2014) 59

Figure 5.2: Effect of the tube pitch on the heat transfer rate ratio of round and flat tube bundle....61

Figure 5.3: Effect of the tube pitch on the air-side pressure drop ratio of round and flat tube bundle 61

Figure 5.4: Effect of the tube height on the heat transfer rate ratio of round and flat tube bundle 62

Figure 5.5: Effect of the tube height on the air-side pressure drop ratio of round and flat tube bundle.....62

Figure 5.6: Tube bundle layout and dimensions.....64

List of tables

Table 3.1 Comparison of two-dimensional numerical solutions to one-dimensional results 45

Table 5.1: The performance data of a round tube bundle presented by Anderson (2014).....60

Table 5.2: Number of tubes per row for the flat tube bundle configurations 60

Table 5.3: Comparison of the performances of flat and round tube bundles for wet operating mode 63

Nomenclature

A	Area	m^2
c_p	Specific heat at constant pressure	$[J/kg\ K]$
C	Friction coefficient	
d	Diameter of duct	$[m]$
f	Friction factor	
G	Mass velocity	$[kg/m^2\ s]$
g	Gravitation acceleration	$[m/s^2]$
H	Height	$[m]$
h	Heat transfer coefficient	$[W/m\ K]$
h_d	Mass transfer coefficient	$[kg/m^2\ s]$
i	Enthalpy	$[J/kg]$
i_{fg}	Latent heat	$[J/kg]$
k	Thermal conductivity	$[W/mK]$
L	Length	$[m]$
m	Mass flow rate	$[kg/s]$
NTU	Number of transfer units	
n	Number	
P	Pitch	$[m]$
p	pressure	$[p_a]$
Q	Heat transfer rate	$[W]$
R	Gas constant or resistance	$[J/kgK]$
RH	Relative humidity	$[\%]$
t	Thickness	$[m]$
T	Temperature	$[℃]$
U	Overall heat transfer coefficient	$[W/m^2K]$
v	Velocity	$[m/s]$

W	Width	[m]
w	Humidity ratio	[kg (H_2O)/ kg dry air]
x	Co-ordinate or distance	[m]
y	Co-ordinate or distance	[m]
y_1, y_2, y_3, y_4, y_5	Distance	[m]
z	Co-ordinate or distance	[m]

Greeks symbols

Δ	Differential	
δ	Distance or thickness	[m]
μ	Dynamic viscosity	[kg/ms]
ρ	Density	[kg/m^3]
ϕ	Relative humidity	[%]
ν	Kinematic viscosity	[kg/ms]
τ	Tangential	

Dimensionless groups

Le_f	Lewis factor, $h_a/c_{pam}h_d$
NTU	Number of transfer units
Nu	Nusselt number, hL/k
Pr	Prandtl number, $\mu c_p/k$
Re	Reynolds number, $\rho vL/\mu$
Sc	Schmidt number, ν/D_{AB}
Sh	Sherwood number, $h_d L/D_{AB}$

Subscripts

a	Air
av	Air and water mixture
ac	Convection heat transfer

am	Mass transfer
b	Bundle
B	Buoyancy
cr	Critical
crw	Critical , wet
crd	Critical dry
c	Condensate
cm	Condensate mean
cs	Condensate surface
$c1$	Between condensate surface and mean
$c2$	Between condensate mean and tube wall
d	Dry
dw	deluge water
dwm	Deluge water mean
dws	Deluge water surface
$dw1$	Between tube wall and deluge water mean
$dw2$	Between deluge water mean and surface
f	Flat
fd	Fully developed
fr	Frontal
g	Gravity
i, j	Grind point index
m	mean
mdw	Deluge water mass flow rate
N, S, W, E	Grid cells
n, s, w, e	Interface grid points
o	outlet

r	Rows or intervals or round
ref	Reference
s	Surface or steam
sf	Steam flow
sw	Saturated water
t	Tube
tr	Tube row
y_1, y_2, y_3, y_4, y_5	Location or position
va	Air velocity
w	Wet
wb	Wet-bulb
x	Co-ordinate
y	Co-ordinate
z	Co-ordinate

1. Introduction

1.1. Background

Recent increase in water tariffs coupled with shortage of water in the arid regions, led to the widespread application of air-cooled steam condenser (ACSC) and dry cooling towers to reject heat into the environment in power plants incorporating steam turbines. However, these cooling systems experience performance penalties during the hot periods, which results in reduction of the output power of the steam turbine. Gadhamshetty et al. (2006) reported a 10 % reduction in power plant output at high ambient temperatures for plants with air-cooled condensers.

In an attempt to enhance the performance of dry air-cooled systems while utilising less amounts of water than for a fully wet cooling systems, combined cooling systems (dry/wet or wet/dry) can be considered. According to Maulbetsch (2002), the total water consumption of the combined cooling systems is in the range of 20 to 80 % of the total water consumption of fully wet cooling systems. The combined cooling systems consist of both wet and dry sections, which are arranged in different configurations that will influence their operating capabilities and capital costs. In comparison with fully dry air-cooled systems, the performance of the combined cooling systems is not affected by the high ambient operating conditions. However, their initial capital and maintenance costs are higher, because these systems consist of both dry and wet sections. Due to the fact that the wet section is operated only during the short period of high ambient operating conditions, the combined cooling system's economic viability is reduced.

This project aims to design and evaluate the thermal performance of a delugeable flat tube bundle to be incorporated in the second stage of a hybrid (dry/wet) dephlegmator (HDWD) of a direct air-cooled steam condenser. The HDWD is to replace a dry convectional dephlegmator in each street of an ACSC.

The HDWD concept was introduced by a group of researchers in the mechanical engineering department of Stellenbosch University. It was proposed as an enhancement technique in an attempt to improve the performance and availability of the ACSC during the high ambient temperature, as well as to level the power production rate by lowering fluctuations caused by the ambient condition's changes, and minimise the water usage. The HDWD has two stages: the first stage with finned tubes and second stage with a delugeable bundle of horizontal smooth galvanised steel tubes, which can operate in both dry and wet mode, depending on the ambient conditions.

Few studies have been conducted in an attempt to find a best configuration of the HDWD second stage's tube bundle that delivers a good performance. However, these studies have only considered round tube bundle. Heyns (2008) investigated a delugeable bundle performance of 38 mm diameter round tubes for the forced draft HDWD. Owen (2013) analysed 19 mm diameter round tube bundle for the

induced draft HDWD. In this study, a flat tube bundle for induced draft HDWD is considered.

In addition to combined cooling systems, other most commonly used techniques to maintain the performance of the dry air-cooled systems during hot periods are deluging the air-side heat transfer area of the heat exchangers with water, and pre-cooling of the inlet air (adiabatic cooling).

1.2. Deluge cooling systems

Dry air-cooled system's performance can be improved by spraying recirculating deluge water over the heat exchangers surface area. Some of the deluge water evaporates in the air stream. This enables both sensible and latent heat transfer from the heat exchanger's surface. In comparison with fully dry air-cooled systems operating under similar conditions, the deluge cooling systems increase heat transfer by a factor of up to five (Kröger, 2004). Although deluge cooling systems enhance the performance of dry air-cooled systems, there is a high risk of increase of pressure drop on the air-side, corrosion and fouling. Qureshi and Zubair (2005) asserted that fouling can decrease the effectiveness of both evaporative cooler and condenser up to 50%, and the outlet temperature of the process fluid can be increased by 5%. However, these risks are restricted for the plain tubes.

1.3. Adiabatic cooling systems

The fine water droplets are sprayed into the inlet ambient air before it enters the heat exchanger. The evaporation of water results in cooling of the inlet air closer to its wet-bulb temperature. For the adiabatic cooling systems, the return water loop is not required since all the water droplets are expected to evaporate. Wachtell (1974) and Duvenhage (1993) found that the complete evaporation of water droplets can be reached when the droplets' diameter is 20 and 50 micron, respectively. However, Branfield (2003) reported that it is impossible to achieve a complete evaporation of the water droplets, even when their sizes are significant small. Maulbetsch and DiFilippo (2003) analysed the reduction of the unevaporated water by introducing the drift eliminator. They conducted the nozzle tests, which demonstrated that only 60 to 70% of the water evaporates, and the drift eliminator cannot trap all the unevaporated water. Therefore, the tubes may be subjected to corrosion. Conradie and Kröger (1991) stated that for a particular power plant, the output power can be increased by 2.95% with the water consumption of 129.48 cubic meters per hour, if adiabatic pre-cooling is introduced to the air with a relative humidity of 70% at the dry temperature of 32°.

Due to the fact that in the deluge cooling systems evaporation takes place directly on the tubes surface rather than in the air, Charles and David (2002) asserted a high performance for the deluge cooling systems in comparison with the adiabatic cooling systems.

Apart from the above-mentioned enhancement methods, several approaches such as: increasing the maximum allowable exhaust pressure of the turbine or air flow, and over-sizing of the air-cooled condenser (ACC) can be employed to sustain the performance of the ACC during hot periods. Increasing the exhaust pressure of the turbine would lead to a corresponding increase in condenser temperature and the consequent reduction in power output. On the other hand, air flow increases the operating costs since it requires extra energy. Over-sizing of the ACC will increase the performance, however, the performance will be associated with high capital and operation costs. This is corroborated by Boulay et al. (2005) who argued that over-sizing is unreasonable.

1.4. The role of the dephlegmator

The ACSC of the power plant consists of numerous streets, which are made up of several primary condenser units, installed in A-frame arrangement. This arrangement enables the easier drainage of the condensate, minimises the length of the distribution duct of the steam, and reduces the occupied land surface area. The primary condenser units are connected in series to the secondary reflux condenser unit, which is known as dephlegmator as depicted in Figure 1.1.

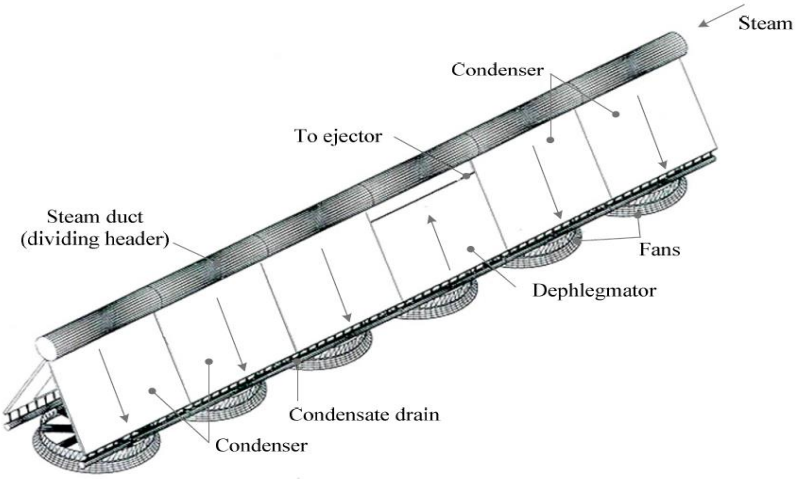

Figure 1.1: Direct air-cooled steam condenser street

The steam from the dividing header is partially condensed in the primary condenser units by the ambient air forced through the finned tube bundles by the axial fans. The extra steam from the primary condenser units is condensed in the dephlegmator. Figure 1.2 illustrates the flow of the steam in the streets of ACC. In the primary condenser units, the condensate and steam are flowing in the co-current direction.

The steam temperature in the primary condenser units of the multi-row tube bundle of the ACSC is accounted to be constant. The air temperature changes as it flows through the tube bundle's rows. As a result, the condensation rate of the steam in tubes of different rows is not the same. Subsequently, the variation in the steam-side pressure may occur. Since the tubes are connected parallel to the

dividing header, the vapour may enter into the tubes from both ends (vapour back flow) and form a stagnation region, which reduces the effective length of the tubes (Kröger, 2004).

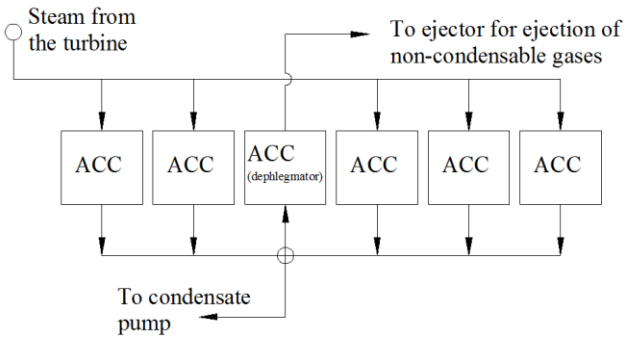

Figure 1.2: Diagram of steam flow in the ACC streets

The ACSC operates below atmospheric pressure; therefore the non-condensable gases may leak into the system. These gases accumulate at the stagnation point, and consequently a dead zone is formed inside the tubes. Furthermore, the presence of a dead zone in the tubes reduces the surface area of the heat transfer, worsens the performance of the ACSC during hot periods, and causes the corrosion and freezing of the tubes. To inhibit these problems as well as vapour back flow, the dephlegmator is required so that it expels the non-condensable gases, stabilises and accelerates the steam flow in the primary condenser units by drawing out and condensing the excess steam. Therefore, it is worthwhile to enhance the dephlegmator performance, since this will directly lead to the overall performance improvement of the ACSC.

1.5. The HDWD structure

The hybrid (dry/wet) dephlegmator can be forced or induced draft. The forced draft HDWD is shown in Figure 1.3. This HDWD has two stages connected in series and combined in one condenser unit. The first stage has inclined finned tubes and second stage with horizontal smooth galvanised steel tubes. In order to provide space for the second stage tube bundles, the first stage tubes are shorter compared to the convectional dephlegmator tubes. The second stage operates in the dry mode as an ACC during cold or off peak periods, and in the wet mode as evaporatively cooled condenser during hot and peak periods. Deluge water sprayed on the surface of the second stage tubes during the wet operating mode is collected in collecting troughs under the tube bundle, while the water droplets blown up by the air are trapped by the drift eliminator above the tube bundle. In order to mitigate the corrosion and fouling risk during the wet operating mode, the smooth plain tubes are used in the second stage.

Owen (2013) analysed the flooding occurrence in the forced draft HDWD when the second stage is operating as an evaporatively cooled condenser. The calculations performed shown that during the wet operating mode there can be a flooding in the primary condenser tubes. This is due to an increase in heat transfer

rate in the second stage tubes which results in an increase of steam flow inside the primary condenser tubes and subsequently, accumulation of condensate inside the tube.

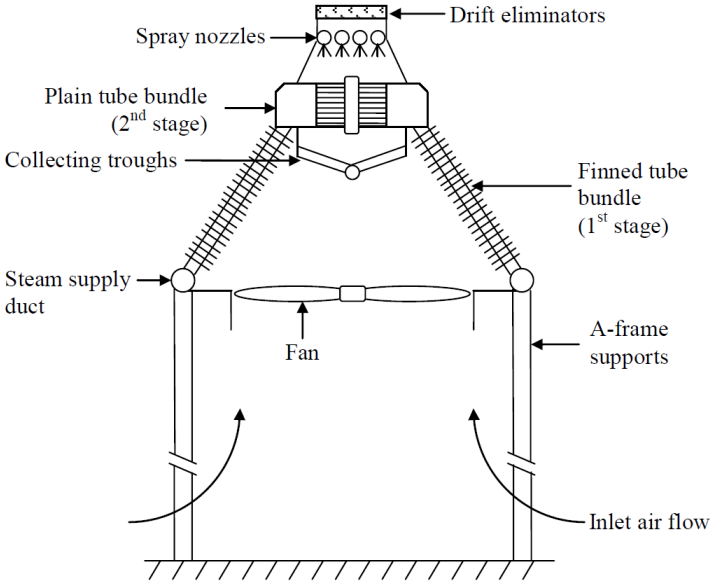

Figure 1.3: Schematic diagram of the forced draft HDWD, Source: (Owen, 2013)

As a result, the forced draft HDWD applications are limited to some operating conditions and tube geometries. However, these limitations can be addressed by changing the geometry of the tube in the primary condenser or alter the dephlegmator configuration to induced draft.

The structure and operating principles of the induced draft HDWD, presented in Figure 1.4 is similar to that of forced draft. In the induced draft HDWD the condensate and the vapour flow in the same direction, which is a reverse of the convectional dephlegmator. The co-current flow of condensate and vapour minimises the chances of flooding occurrence in primary condenser tubes.

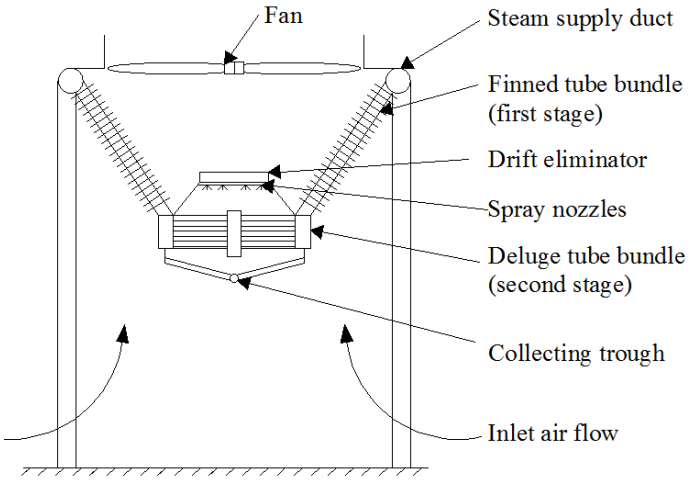

Figure 1.4: Schematic diagram of the induced draft HDWD

The flow chart of the steam flow in the ACSC street with five primary condenser units and incorporating the induced draft HDWD is shown in Figure 1.4.

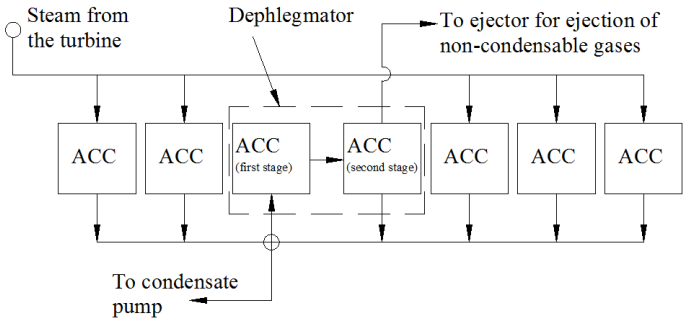

Figure 1.5: Diagram of steam flow in the ACC streets, incorporating the HDWD

The performance of the HDWD during the dry operating mode of the second stage's tube bundle is found to be lower than for the convectional dephlegmator. However, this disadvantage is outweighed by the substantial performance delivered during the wet operating mode. Owen (2013) compared the HDWD and convectional dephlegmator performance, on a component level (for the whole dephlegmator) and on a system level (for the whole ACC). On a component level , the HDWD performance is reported to be two to three times that of the convectional dephlegmator when operate in wet mode, while on a system level, the heat transfer rate of an ACC with five primary condensers and one HDWD is 15% -30% higher than for a similar ACC with convectional dephlegmator.

Heyns and Kröger (2012) in their study compared the output power of the steam turbine cooled by ACC incorporating the HDWD, ACC with pre-cooling of inlet air, and over-sized ACC by 33%. They found that during the hot period, the performance of all considered ACCs is the same. However, their study further found that the HDWD uses around 20% less water than for the pre-cooling technology, and the cost difference between the HDWD and the convectional dephlegmator is small. They concluded that, it is reasonable to employ the HDWD as an enhancement measurement of an ACC.

1.6. Motivation

As mentioned, during hot periods the ACSC experiences performance reduction. In order to meet the power demand during the high ambient temperature the power plant is operated more frequently than during cold period, which increases the fuel consumption. Consequently, the lifespan of the plant is reduced and more costs are spent on the fuels and labour which increases the operating cost of the plant. Moreover, intensive burning of fossil fuels is a significant source of air pollution and greenhouses gases emissions. Thus, there is need for research that will address the above cited shortfalls. The HDWD is found to be cost effective and use less water during the wet operating mode. However, the best configuration of the second stage tube bundle should be identified by evaluating its thermal performance.

In this work the delugeable flat tube air-cooled steam condenser bundle to be employed in the second stage of the induced draft HDWD is designed, and its thermal performance is analytically and numerically evaluated.

1.7. Project objectives

The specific objectives of this study are: to

1) Develop a method for establishing the validity of important thermal-hydraulic parameters that required in the design of a delugeable flat tube air-cooled steam condenser bundle to be incorporated in the HDWD's second stage.
2) Develop a one-dimensional model based on three methods of analysis: Poppe, Merkel and heat and mass transfer analogy.
3) Develop a two-dimensional numerical model based on heat and mass transfer analogy.
4) Carry out a parametric study and investigate the effects of the designing parameters on the heat transfer rate and air-side pressure drop.
5) Compare the performance of a delugeable flat tube bundle to the round tube bundle's performance.

1.8. Project outline

Chapter 1 provides the overview of HDWD as well as other enhancement technologies of an ACC, and highlights the main role of dephlegmator. The motivation, objectives and project outline are also presented in this chapter.

Chapter 2 summaries the literature reviews on the thermal performance analysis of the heat exchangers operating under wet conditions.

Chapter 3 presents the development of a one and two-dimensional numerical models, the solution methods employed in the analysis of the thermal performance of the tube bundle, and the validation of the numerical model.

Chapter 4 provides the parametric study of the impacts of the designing parameters on the thermal performance of the tube bundle.

Chapter 5 presents the comparison of performance of the deluged flat and round tube bundles

Chapter 6 discusses the conclusions and recommendations as well as the significance of the project.

2. Literature review

This chapter provides the summary of the literature reviews on the thermal performance analysis of the heat exchangers operating under wet conditions. During the wet operating mode, the HDWD operates as an evaporatively cooled condenser whereby the deluge water is sprayed over the tube bundle's surface, air is drawn through the bundle by axial fan and at the same time, steam is condensed inside the tubes. It is therefore worthwhile to know the studies carried out on the thermal performance evaluation of evaporatively cooled condensers/coolers as well as the methods of analysis employed.

Some of the previous studies were performed by Parker and Treybal (1961) who conducted the analytical analysis of the evaporative cooler. The heat and mass transfer coefficient was determined by assuming the Lewis factor equal to one, the evaporation of the deluge water was neglected and the enthalpy of the saturated air was considered being a linear function of the temperature. They found that the deluge water temperature varies along the height of the bundle. However, the variations are small and therefore the deluge water temperature can be considered constant. But, Finlay and Grant (1974) in their study of rating methods of the evaporative coolers indicated that the assumption of the constant deluge water temperature might leads to errors of more than 30%.

Mizushina et al. (1967) evaluated the evaporative cooler characteristics and implemented a similar approach to Parker and Treybal (1961). The two analysis techniques, numerical and analytical were employed, whereby for the former method the assumption of constant deluge water temperature throughout the evaporative cooler was not considered. Furthermore, the heat and mass transfer coefficient's correlations were derived.

Niitsu et al. (1969) performed an experimental study on the plain and finned round tube banks for the evaporative cooler. The results showed the lower heat and mass transfer coefficient for the finned tube bundle compared to plain. They concluded that the water hold between the fins might be a possible reason of the low fin efficiency.

Finlay and Grant (1972) employed the numerical technique in analysis of the evaporative cooler model, in which only the assumption of vapour pressure of the saturated air to be a linear function of the temperature was considered. For this reason, their model accounted to be more accurate.

Yang and Clark (1975) conducted an experimental analysis on the thermal performance characteristic of three compact plate finned heat exchangers (plain-finned, louvered, and perforated fin heat exchangers), deluged with water and ethylene glycol mixture. They found that the heat transfer depends on the wetted surface area, and therefore the geometry shape which provides a large surface area is more preferable. At the air speed of 1.26 to 2.52 ml/s, for the low Reynolds number of 500 and 1000, the air-side heat transfer coefficient increased from 40 to 45%, respectively. While for the high Reynolds number the results showed only

an increase of 6 and 12% for louvered and plain-finned heat exchangers respectively. There were no significant variations noted in the friction factors for all the heat exchangers. The significance of the evaporation on the heat transfer was neglected.

Leidenfrost and Korenic (1979) performed an analytical investigation on the performance of the counter flow evaporative condenser model. The model was evaluated by implementing the graphical procedure which derived by Bosnjakovic (1965). Moreover, the mass transfer coefficient was estimated from the dry heat transfer coefficient. Subsequently, the same model was employed in Leidenfrost and Korenic (1982) study, for investigating the performance of the finned counter flow evaporative condenser. They found that the air-side pressure drop across the wetted tubes increased up to 40%. Additionally, by increasing the air flow rate the condenser capacity increases until the air flow starts to break the water film on the tubes surface.

Perez-Blanco and Linkous (1983) studied the evaporative cooler's performance by deriving the overall heat transfer coefficient. They found that the heat transfer coefficient can be calculated accurately from the inlet and outlet measurements, only when the deluge water film enthalpy is neglected. Furthermore, due to the high resistance to the heat and mass transfer at the air-water interface, the authors concluded that enhancement of the heat and mass transfer at the interface is significant required.

Bykov at el. (1984) conducted a study on the heat and mass transfer as well as on the fluid flow characteristics in the evaporative condenser. They divided the evaporative condenser into three zones: the spray zone (above the tube bundle), the tube bundle zone, and the run-off zone (below the tube bundle). The water temperature and the air enthalpy in all zones, as well as the influence of the space above and below the tube bundle on the heat and mass transfer, were analysed. They found that the water temperature varies in all zones, and the run-off zone's size has a significant effect on the heat transfer rate than the spray zone's size.

Nakayama at el. (1988) investigated the heat transfer and pressure drop of the mist-cooled cross flow banks of circular smooth, micro finned and finned tubes. They introduced the concept of the effective wet area for the evaporation, which is a function of the water spray rate. The effective wet area increases with the increasing of the water spray rate up to a certain rate, whereby further spraying of water increases the thickness of the water film and build a resistance. Although high heat transfer coefficient was obtained for the finned tube bundle, it was found that the improvement in the performance of the finned tube bundle in the mist flow was lower than for the smooth tube bundle. Furthermore, they concluded that the water evaporation from the tubes surface plays a major role in the heat transfer enhancement. The changes in the pressure drop were found to be insignificant.

Erens and Dreyer (1989) presented procedures for analysing the horizontal and vertical evaporative coolers. The models based on the Poppe and Merkel's formulations for both evaporative coolers were presented, and the results obtained

were compared. They concluded that for the vertical evaporative cooler, the one-dimensional approach is adequate to provide the accurate results for forecasting the cooler's performance.

Hasan and Siren (2003) investigated and compared the performance of plain and plate-finned circular tube evaporative heat exchangers. The plain tube bundle showed higher mass transfer coefficient than finned. However, due to the large surface area of the finned tube bundle, the heat transfer rate for the finned tube bundle indicated an increase of 92-140%. Furthermore, in a continuation study Hasan and Siren (2004) conducted a comparative analysis between the plain circular and oval tube evaporative-cooled heat exchangers. Hasan and Siren (2004) reported that the oval tube bundle's performance is 79% of that of circular tube bundle, while the friction factor is 46% lower than for the circular tube bundle. Due to the larger surface area of the oval tube, its heat transfer coefficient between the tube wall and deluge water is 12% higher than for the circular. However, circular tube bundle showed high mass transfer coefficient than oval.

Qureshi and Zubair (2005) analysed the effect of the fouling on the thermal performance of the evaporative cooler and condenser. They developed the fouling model, which foreseen the changes in the heat transfer rate as the fouling increases. The obtained heat transfer rate was compared to Dreyer (1988) solutions, and showed an error of 2.2%. Their results indicated that the effectiveness of evaporative cooler and condenser decrease around 55% and 78%, respectively.

Jafari and Behfar (2010) developed a new rapid design algorithm (RDA), which was based on Mizushina et al. (1967) heat and mass transfer coefficients correlations for the plain tube evaporative coolers. The RDA depends on the relationship between the pressure drop, heat transfer area and heat and mass transfer coefficients. Unlike the traditional algorithm, RDA is straightforward, does not involve trial and error procedures and it has provision for the pressure drop limitations in the design. To validate the RDA, the results obtained by using RDA were compared to the traditional algorithm results as well as to the results obtained when the RDA run the sample specification presented in Kroger (2004). The RDA results showed an increase of 26.5%, 17.7% and 92.2% in the amount of mass transfer coefficient, deluge water film and tube side heat transfer coefficient, respectively

Heyns and Kröger (2010) performed a study of the thermal-flow performance characteristics of the round tube evaporative cooler. They investigated the effects of the deluge water and air mass flow rate as well as the deluge water temperature on the heat and mass transfer coefficients of the water film and air-water respectively. The correlations of the heat and mass transfer coefficient of the water film and air-water respectively, as well as of the air-side pressure drop were derived from the obtained experimental results. The optimum deluge water mass velocity needed for the evenly wetting of the tube's surface was reported to be 3.5 kg/m^2s. Their study found that the water film heat transfer coefficient depends on the air mass velocity, and deluge water temperature and mass velocity,

which did not agree with results obtained by neither with Mizushina et al. (1967) nor Parker and Treybal (1961). Mizushina et al. (1967) found that the water film heat transfer coefficient is a function of the deluge water mass velocity, while Parker and Treybal (1961) expressed it as a function of the deluge water mass velocity and temperature. Furthermore, they found that the air-water mass transfer coefficient depends on the air and deluge water mass velocity, which agrees with Mizushina et al. (1967) correlation, which derived as a function of Reynolds number of deluge water and air. The air-side pressure drop found to be a function of air and deluge water mass velocity, which agrees with Niitsu et al. (1969) correlation.

Jahangeer et al. (2011) performed a numerical investigation of the plain round tube evaporative-cooled condenser performance for air-conditioning applications. The dependence of the tube side, water and overall heat transfer coefficient on the deluge water film thickness as well as on the air velocity was analysed. They found that as the film thickness increases from 0.075 to 0.15 mm, the heat transfer coefficients decrease. While, as the air velocity increases from 1 to 4 m/s the tube side and the overall heat transfer coefficient increase from 29000 to $33000\ \mathrm{W/m^2K}$ and 330 to $800\ \mathrm{W/m^2K}$, respectively.

Zheng et al. (2012) investigated the thermal performance characteristic of the oval tube closed wet cooling tower. They determined the heat and mass transfer coefficient for the water film and air-water, respectively from the experimental results. The best deluging rate that ensures uniformly wetting of the tubes surface was found to be $1.2\ \mathrm{kg/m^2s}$. Furthermore, they found that the heat transfer coefficient for the water film is a function of temperature and mass flow rate of the deluge water as well as air mass velocity, which is in a good agreement with Heyns and Kroger (2010) results. While, the mass transfer coefficient for the air-water is a function of only air mass velocity, which agrees with Parker and Treybal (1961) and Niitsu et al. (1969)'s results.

Hwang et al. (2012) evaluated the performance of the compact round-tube louver-fin condenser, operating under wet and dry conditions. The heat exchanger capacity and air-side pressure drop at angle of $0°$ and $21°$ with the vertical were investigated. They found that at the air velocity of 1.4 m/s, the deluge water increased the heat exchanger capacity by 162% and 181%, and air-side pressure drop by 137% and 135% for the case of $0°$ and $21°$ angle with the vertical, respectively. Since the air-side pressure drop increases with air velocity, they concluded that increasing the air velocity beyond 1.4 m/s could not be the best way of enhancing the capacity of the heat exchanger condenser.

Zhang et al. (2014) conducted an experimental study on the evaporative mist pre-cooling; deluging cooling and the combination of the two cooling systems on the louver fin flat tube heat exchanger. The effects of the deluge water mass flow rate and air velocity on the heat exchanger capacity, the water drainage behaviour as well as on the air-side pressure drop were investigated. They found that at the higher deluge water flow rate, the rate of water drainage increases faster than the rate of evaporation of water. At $0.2\ \mathrm{g/m^2s}$ mass flow rate of water, 70 % of the

water evaporates and 30 % drains. While at 1 g/m^2s only about 30% of water evaporates and the rest drained. Furthermore, they found that the heat exchanger capacity and air-side pressure drop increase with water mass flow rate and air velocity, respectively.

Analysis of the thermal performance characteristics of the evaporatively cooled heat exchangers has been a subject of several works as indicated in the above-summarized studies. These studies have been conducted in an attempt to identify and address the heat and mass transfer resistance at the air-water interface, and enhancing the overall performance of the heat exchangers. In most of the studies, round finned and plain tube heat exchanger's performance was analysed, and few works investigated the oval and finned flattened tube heat exchanger's performance. Experimental and analytical methods have been employed in most of the works. However, numerical method has been also used in some studies such as in Mizushina et al. (1967), Finlay and Grant (1972) and Jahangeer et al. (2011).

The literatures lack information on specific performance investigation of the plain flattened tube bundle operating under deluging conditions as well as the comparison of its performance to other bundle of different tubes geometries operating under similar conditions. Therefore, this study evaluates the thermal performance of the plain flat tube air-cooled steam condenser bundle, operating under wet conditions. The bundle's performance is compared to the round tube bundle performance operating under similar conditions from the literature.

3. Analysis of thermal performance characteristics of a delugeable flat tube bundle

This chapter provides the development of a one and two-dimensional numerical models required for evaluating and forecasting the thermal performance of a delugeable flat tube bundle. Furthermore, the solution methods and validation of a two-dimensional numerical model are also discussed.

3.1. Numerical model

A schematic of two tubes in a delugeable flat tube bundle for the air-cooled condenser is shown in Figure 3.1.

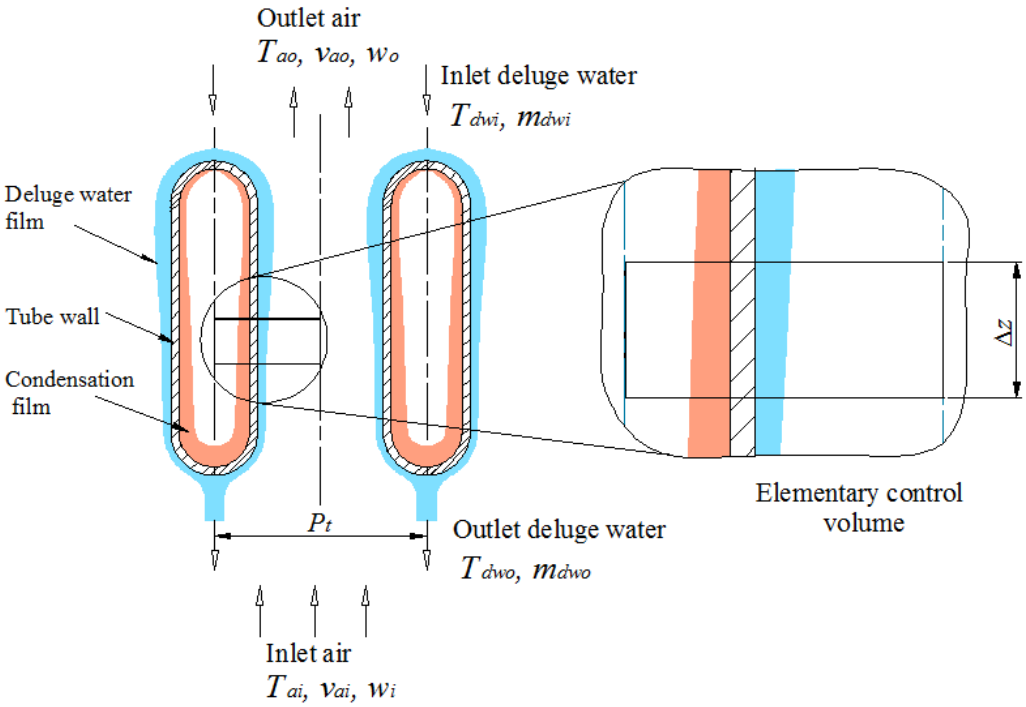

Figure 3.1: Schematic diagram of two adjacent tubes in a delugeable flat plain tube bundle

An elementary control volume with dimensions Δx, Δy and Δz and surface area (δA), is drawn from the centreline of the tube to the symmetry line between the two adjacent tubes as indicated in Figure 3.1. The parameters and the flow directions of all the media involving in the heat and mass transfer processes taking place in the control volume, and required for the derivations of the governing differential equations are illustrated in Figure 3.2.

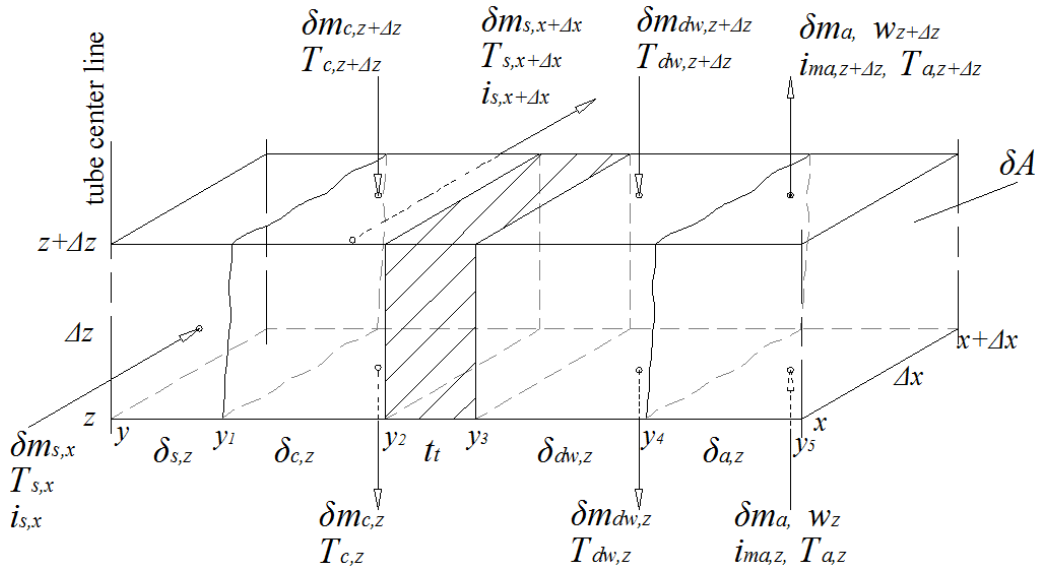

Figure 3.2: The two-dimensional elementary control volume of the delugeable horizontal plain flat tube bundle

The different y-values in Figure 3.2 can be written as:

$$y_1 = y + \delta_{s,z} \quad \textbf{(3. 1)}$$

$$y_2 = y_1 + \delta_{c,z} \quad \textbf{(3. 2)}$$

$$y_3 = y_2 + t_t \quad \textbf{(3. 3)}$$

$$y_4 = y_3 + \delta_{dw,z} \quad \textbf{(3. 4)}$$

$$y_5 = y_4 + \delta_{a,z} \quad \textbf{(3. 5)}$$

In this study, counter-current flow configuration of air and water over the surface of the tubes is considered. The steam flows inside the tubes in the *x*-direction, and the condensate drains in the negative *z*-direction. The steam is condensed by the deluge water and cooling air on the exterior of the tubes. A condensation film is formed inside the tubes, and runs down the tube wall along the height due to gravity. The recirculating deluge water is distributed over the tube surface in the negative *z*-direction, while the inlet air is drawn upward from the bottom of the tubes in the *z*-direction.

The heat is transferred from the condensed steam through the condensation film, tube wall, deluge water film, and finally crosses the air-water interface to the air stream. Due to the direct contact of air and water at the air-water interface, the deluge water evaporates into the air stream.

In the next two sections, the governing differential equations for the one and two-dimensional models are derived. These equations are to describe the heat transfer processes taking place in a delugeable flat tube bundle for non-saturated air.

3.2. The governing equations of a one-dimensional model

3.2.1. Tube bundle operated as an evaporative condenser

In order to obtain a one-dimensional model of a delugeable flat tube bundle, the following assumptions are considered:

1) The deluge water is distributed uniformly along the surface of the tubes.
2) The effect of steam velocity on the condensate film is not considered.

The governing equations are derived from the basic principle of conservation of mass and energy, and by using the approach presented in Dreyer (1988) and Kröger (2004). The one-dimensional elementary control volume of the delugeable tube bundle is shown in Figure 3.3.

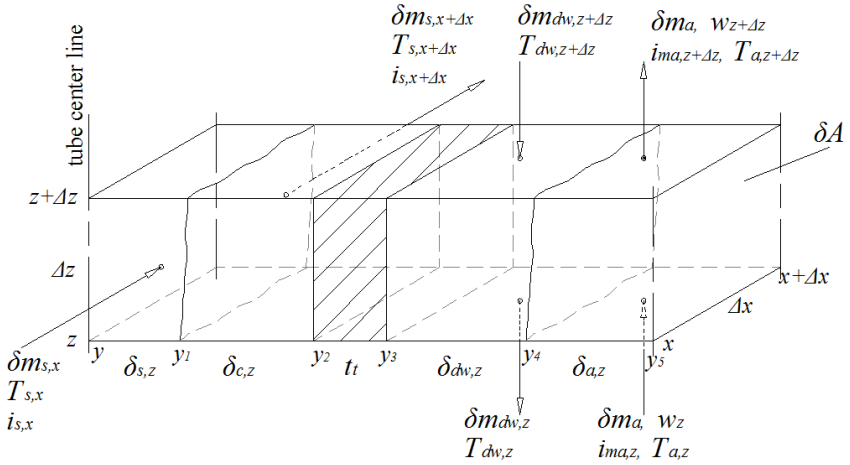

Figure 3.3: One-dimensional elementary control volume of the delugeable horizontal plain flat tube bundle

The mass balance for the control volume is

$$\delta m_s + \delta m_{dw,z+\Delta z} + \delta m_a(1 + w_z) = \delta m_s + \delta m_{dw,z} + \delta m_a(1 + w_{z+\Delta z}) \quad \textbf{(3. 6)}$$

That can be simplified as

$$\Delta\delta m_{dw} = \delta m_a \Delta w \quad \textbf{(3. 7)}$$

The overall energy balance for the control volume is

$$\delta m_s i_{s,x} + \delta m_{dw,z+\Delta z} c_{pdw} T_{dw,z+\Delta z} + \delta m_a i_{ma,z} = \delta m_s i_{s,x+\Delta x} + \delta m_{dw,z} c_{pdw} T_{dw,z} + \delta m_a i_{ma,z+\Delta z} \quad \textbf{(3. 8)}$$

Eq. (3.8) can be simplified to

$$\delta m_{dw,z} c_{pdw} \Delta T_{dw} + \Delta\delta m_{dw,z} c_{pdw} T_{dw,z} = \delta m_s \Delta i_s + \delta m_a \Delta i_{ma} \quad \textbf{(3. 9)}$$

Therefore,

$$\Delta T_{dw} = \frac{1}{\delta m_{dw,z} c_{pdw}} \left(\delta m_s \Delta i_s + \delta m_a \Delta i_{ma} - \Delta \delta m_{dw,z} c_{pdw} T_{dw,z} \right) \quad \textbf{(3. 10)}$$

The evaporation rate of the deluge water into the non-saturated air stream is given by Dalton's evaporation law as

$$\Delta \delta m_{dw} = h_d (w_{sw} - w) \delta A_a \quad \textbf{(3. 11)}$$

At the air-water interface, the heat transfer is due to the temperature and water vapour concentration difference between the saturated air at the interface and the air stream. Therefore, heat transfer across the air-water interface is expressed as

$$\delta Q_a = \delta Q_{ac} + \delta Q_{am} \quad \textbf{(3. 12)}$$

The enthalpy transfer can be defined as

$$\delta Q_{am} = \delta m_a \Delta w i_v = h_d i_v (w_{sw} - w) \delta A_a \quad \textbf{(3. 13)}$$

where, i_v is the water vapour enthalpy, which is determined at the deluge water film temperature (T_{dw}) as

$$i_v = i_{fgwo} + c_{pv} T_{dw} \quad \textbf{(3. 14)}$$

The sensible heat can be expressed as

$$\delta Q_{ac} = h_a (T_{dw} - T_a) \delta A_a \quad \textbf{(3. 15)}$$

Therefore, Eq. (3.12) can be re-written as

$$\delta Q_a = h_a (T_{dw} - T_a) \delta A_a + h_d i_v (w_{sw} - w) \delta A_a = \delta m_a \Delta i_{ma} \quad \textbf{(3. 16)}$$

To replace the temperature differential $(T_{dw} - T_a)$ in Eq. (3.16) by the enthalpy differential, first saturated air enthalpy at the air-water interface, which is evaluated at the local bulk deluge water temperature, is computed, and then the air-water interface vapour mixture enthalpy per unit of dry air is determined. The saturated air enthalpy is defined as

$$i_{masw} = c_{pa} T_{dw} + w_{sw} \left(i_{fgwo} + c_{pv} T_{dw} \right) = c_{pa} T_{dw} + w_{sw} i_v \quad \textbf{(3. 17)}$$

and can be re-written as

$$i_{masw} = c_{pa} T_{dw} + w i_v + (w_{sw} - w) i_v \quad \textbf{(3. 18)}$$

The air-water interface vapour mixture enthalpy is computed as

$$i_{ma} = c_{pa} T_a + w \left(i_{fgwo} + c_{pv} T_a \right) \quad \textbf{(3. 19)}$$

Subtract Eq. (3.19) from Eq. (3.18) and simplify the resultant equation by ignoring the small difference in the specific heats, which is determined at different temperatures to obtain

$$i_{masw} - i_{ma} = (c_{pa} + wc_{pv})(T_{dw} - T_a) + (w_{sw} - w)i_v \quad \textbf{(3. 20)}$$

Then Eq. (3.20) can be rearranged as

$$T_{dw} - T_a = [(i_{masw} - i_{ma}) - (w_{sw} - w)i_v]/c_{pma} \quad \textbf{(3. 21)}$$

where

$$c_{pma} = c_{pa} + wc_{pv} \quad \textbf{(3. 22)}$$

Substitute Eq. (3.21) into (3.16) to yield

$$\delta m_a \Delta i_{ma} = h_d \left[\frac{h_a}{c_{pma}h_d}(i_{masw} - i_{ma}) + \left(1 - \frac{h_a}{c_{pma}h_d}\right) i_v(w_{sw} - w)\right] \delta A_a \quad \textbf{(3. 23)}$$

Therefore,

$$\Delta i_{ma} = \frac{h_d \delta A_a}{\delta m_a}\left[\frac{h_a}{c_{pma}h_d}(i_{masw} - i_{ma}) + \left(1 - \frac{h_a}{c_{pma}h_d}\right) i_v(w_{sw} - w)\right] \quad \textbf{(3. 24)}$$

where $h_a/c_{pma}h_d$ is a Lewis factor, which determines the relation between the heat and mass transfer. In terms of the overall heat transfer coefficient, the heat transfer rate from the condensed steam to the deluge water film can be expressed as

$$\delta Q_c = \delta m_s \Delta i_s = U_a \delta A_a (T_s - T_{dws}) \quad \textbf{(3. 25)}$$

where U_a is the overall heat transfer coefficient, which accounts for the transfer of the heat between the steam and the deluge water, and it is determined as

$$U_a = \left[\frac{1}{h_c} + \frac{t_t}{k_t} + \frac{1}{h_{dw}}\right]^{-1} \quad \textbf{(3. 26)}$$

where h_c is the condensation film heat transfer coefficient, and h_{dw} is deluge water film heat transfer coefficient, which accounts for the transfer of the heat at the interface of tube wall and deluge water, as well at the air-water interface. From Eq. (3.26), the changes in the steam enthalpy can be expressed as

$$\Delta i_s = \frac{U_a \delta A_a}{\delta m_s}(T_s - T_{dws}) \quad \textbf{(3. 27)}$$

For Poppe's formulation, the heat transfer processes taking place within the one-dimensional control volume of a delugeable tube bundle are described by differential equations (3.7), (3.10), (3.11), (3.24) and (3.27). For Merkel's formulation, the deluge water evaporation is neglected and Lewis factor is equal to one. Therefore Eq. (3.10) and (3.24) become

$$\Delta T_{dw} = \frac{1}{\delta m_{dw,z} c_{pdw}}(\delta m_s \Delta i_s + \delta m_a \Delta i_{ma}) \quad \textbf{(3. 28)}$$

$$\Delta i_{ma} = \frac{h_d \delta A_a}{\delta m_a}(i_{masw} - i_{ma}) \quad \textbf{(3. 29)}$$

The condenser capacity can be determined as

$$\delta Q = \delta m_a \Delta i_{ma} = \delta m_s (x_i - x_o) i_{fg} \quad \textbf{(3. 30)}$$

where, x_i and x_o are inlet and outlet steam quality. When all the steam is condensed to saturated liquid, the condenser capacity is

$$\delta Q = \delta m_a \Delta i_{ma} = \delta m_s i_{fg} \quad \textbf{(3. 31)}$$

For Merkel's simplified model, the deluge water temperature is assumed to be constant. Therefore, the heat transfer from the condensed steam to the deluge water is equal to the heat transfer from the air-water interface to the air stream.

$$\delta m_a \Delta i_{ma} = U_a (T_s - T_{dws}) \delta A_a \quad \textbf{(3. 32)}$$

and also

$$\delta m_a \Delta i_{ma} = h_d \delta A_a (i_{masw} - i_{ma}) \quad \textbf{(3. 33)}$$

Integrate Eq. (3.32) and (3.33) between the inlet and outlet air enthalpy

$$\frac{i_{mao} - i_{mai}}{T_s - T_{dws}} = \frac{U_a}{m_a} A_a \quad \textbf{(3. 34)}$$

$$ln\left(\frac{i_{masw} - i_{mai}}{i_{masw} - i_{mao}}\right) = \frac{h_d}{m_a} A_a = NTU_a \quad \textbf{(3. 35)}$$

Substitute Eq. (3.34) into (3.35)

$$ln\left(\frac{i_{masw} - i_{mai}}{i_{masw} - i_{mao}}\right) = \frac{h_d}{U_a}\left(\frac{i_{mao} - i_{mai}}{T_s - T_{dws}}\right) \quad \textbf{(3. 36)}$$

Eq. (3.36) can be used for rating of the condenser. The outlet air enthalpy can be obtained from Eq. (3.34) and (3.35) as

$$i_{mao} = i_{mai} + \frac{U_a A_a}{m_a}(T_s - T_{dws}) \quad \textbf{(3. 37)}$$

$$i_{mao} = i_{masw} - (i_{masw} - i_{mai}) e^{-NTU_a} \quad \textbf{(3. 38)}$$

Combine Eq. (3.37) and (3.38)

$$i_{mai} + \frac{U_a A_a}{m_a}(T_s - T_{dws}) = i_{masw} - (i_{masw} - i_{mai}) e^{-NTU_a} \quad \textbf{(3. 39)}$$

The deluge water's surface temperature can be determined either using Eq. (3.32) or (3.39) as

$$T_{dws} = T_s - \frac{m_a (i_{mao} - i_{mai})}{U_a A_a} \quad \textbf{(3. 40)}$$

$$T_{dws} = T_s - \frac{m_a(i_{masw} - i_{mai})(1 - e^{-NTU_a})}{U_a A_a} \quad \textbf{(3. 41)}$$

When the deluge water film thickness is very thin, the air-water interface area (A_a) can be considered to be the same as tube outside surface area (A_o).

3.2.2. Tube bundle operated as a dry air-cooled condenser

The tube bundle is operated as a dry air-cooled condenser during the cold and off-peak periods. The governing equation for a dry air-cooled condenser can be derived from Figure 3.3 and through the same procedures as in section 3.2.1. However, deluge water is neglected, and therefore $m_{dw} = 0\ kg/s$. The governing equation for a dry air-cooled condenser can be written as

$$m_a c_{pa}(T_{ao} - T_{ai}) = UA_a(T_s - T_a) \quad \textbf{(3. 42)}$$

where U is overall heat transfer coefficient, which accounts for the heat transfer between condensed steam inside the tubes and air on the tubes' outside surface. The overall heat transfer coefficient is determined as

$$U = \left[\frac{1}{h_c} + \frac{t_t}{k_t} + \frac{1}{h_a}\right]^{-1} \quad \textbf{(3. 43)}$$

where h_a is air-side heat transfer coefficient, which accounts for the heat transfer between the tube wall and air.

3.3. The governing equations of a two-dimensional model

The two-dimensional approach provides more detailed information on the heat and mass transfer processes. However, it is more complicated, thus its applications have been limited to simple structures (Chan et al., 2003). The two-dimensional elementary control volume shown in Figure 3.2 is divided into five elementary control volumes which are: steam-side, condensate-side, tube wall-side, deluge water-side and air-side, which are shown in Figures 3.4(a), 3.5, 3.8(a), 3.9 and 3.12, respectively. The two-dimensional model is developed from the principle of conservation of mass, energy and momentum.

3.3.1. Steam-side elementary control volume

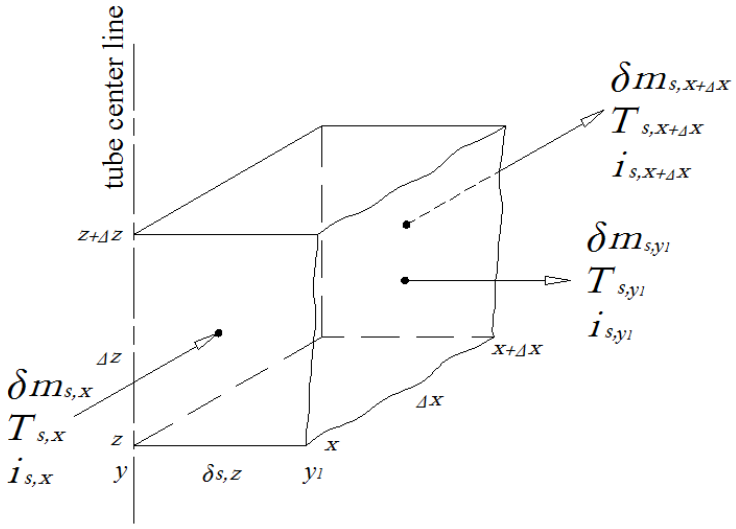

(a) Elementary control volume

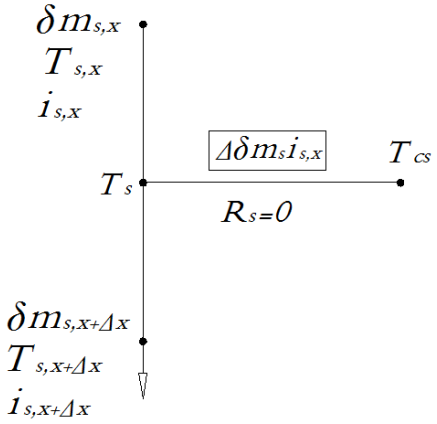

(b) Thermal resistance diagram

Figure 3.4: Steam-side elementary control volume and thermal resistance diagram

a) The mass balance for the elementary control volume

$$\delta m_{s,x} = \delta m_{s,x+\Delta x} + \delta m_{s,y_1} \quad \textbf{(3. 44)}$$

That can be simplified as

$$\delta m_{s,x} = \delta m_{s,x} - \Delta\delta m_{s,x} + \delta m_{s,y_1} \quad \textbf{(3. 45)}$$

$$\Delta\delta m_{s,x} = \delta m_{s,y_1} \quad \textbf{(3. 46)}$$

b) The energy balance for the elementary control volume

$$\delta m_{s,x} i_{s,x} = \delta m_{s,x+\Delta x} i_{s,x+\Delta x} + \delta m_{s,y_1} i_{s,y_1} \quad \textbf{(3. 47)}$$

Assume that $i_{s,x} = i_{s,x+\Delta x} = i_{s,y_1}$ then,

$$\delta m_{s,x} i_{s,x} = \delta m_{s,x+\Delta x} i_{s,x} + \delta m_{s,y_1} i_{s,y_1} \quad \textbf{(3. 48)}$$

Eq. (3.48) becomes

$$\delta m_{s,x} i_{s,x} = \left(\delta m_{s,x} - \Delta\delta m_{s,x}\right) i_{s,x} + \delta m_{s,y_1} i_{s,y_1} \quad \textbf{(3. 49)}$$

$$\Delta\delta m_{s,x} i_{s,x} = \delta m_{s,y_1} i_{s,y_1} \quad \textbf{(3. 50)}$$

3.3.2. Condensate-side elementary control volume

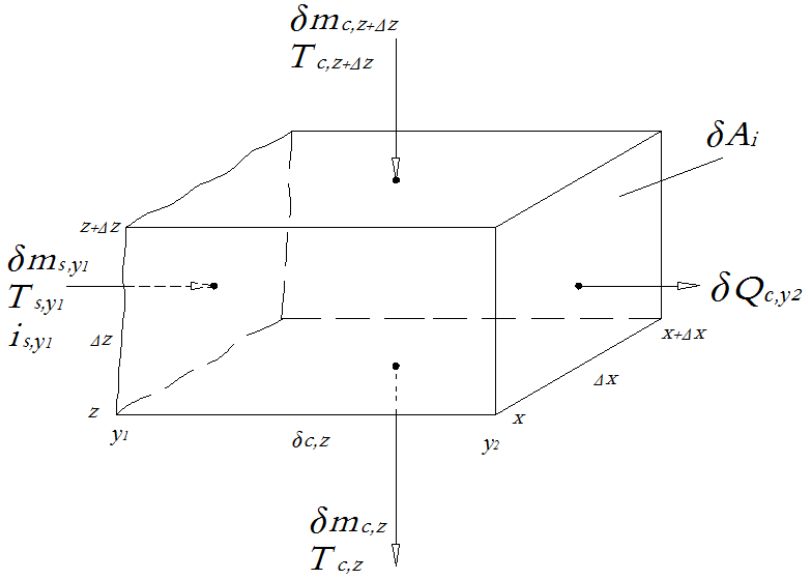

Figure 3.5: Condensate-side elementary control volume

a) The mass balance for the elementary control volume

$$\delta m_{s,y_1} + \delta m_{c,z+\Delta z} = \delta m_{c,z} \quad \textbf{(3. 51)}$$

That can be simplified as

$$\delta m_{s,y_1} + \delta m_{c,z} - \Delta\delta m_{c,z} = \delta m_{c,z} \quad \textbf{(3. 52)}$$

$$\delta m_{s,y_1} = \Delta\delta m_{c,z} \quad \textbf{(3. 53)}$$

Substitute Eq. (3.46) into (3.53)

$$\Delta\delta m_{s,x} = \Delta\delta m_{c,z} \quad \textbf{(3. 54)}$$

b) The energy balance for the elementary control volume

$$\delta m_{s,y_1} i_{s,y_1} + \delta m_{c,z+\Delta z} c_{pc} T_{c,z+\Delta z} = \delta m_{c,z} c_{pc} T_{c,z} + \delta Q_{c,y_2} \quad \textbf{(3. 55)}$$

That can be simplified as

$$\delta Q_{c,y_2} = \delta m_{s,y_1} i_{s,y_1} + \left(\delta m_{c,z} - \Delta\delta m_{c,z}\right) c_{pc} T_{c,z+\Delta z} - \delta m_{c,z} c_{pc} T_{c,z} = \delta m_{s,y_1} i_{s,y_1} + \delta m_{c,z} c_{pc} \Delta T_{c,z} - \Delta\delta m_{c,z} c_{pc} T_{c,z+\Delta z} \quad \textbf{(3. 56)}$$

Substitute Eq. (3.50) into (3.56)

$$\delta Q_{c,y_2} = \Delta\delta m_{c,z} i_{s,x} + \delta m_{c,z} c_{pc} \Delta T_{c,z} - \Delta\delta m_{c,z} c_{pc} T_{c,z+\Delta z} = \Delta\delta m_{c,z} (i_{s,x} - c_{pc} T_{c,z+\Delta z}) + \delta m_{c,z} c_{pc} \Delta T_{c,z} \quad \textbf{(3. 57)}$$

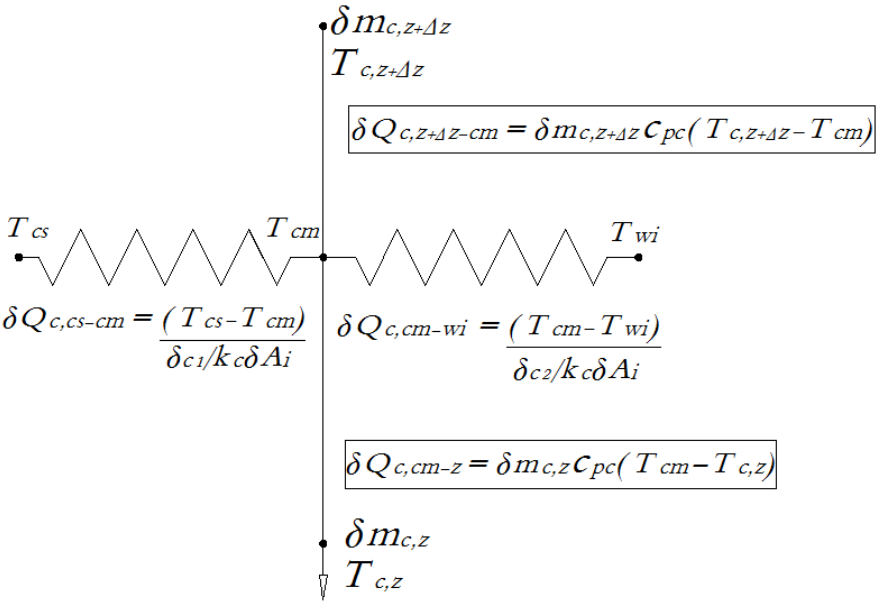

Figure 3.6: Condensate-side thermal resistance diagram

c) The heat transfer balance for the thermal resistance diagram

$$\delta Q_{c,cs-cm} + \delta Q_{c,z+\Delta z-cm} = \delta Q_{c,cm-wi} + \delta Q_{c,cm-z} \quad \textbf{(3. 58)}$$

where

$$\delta Q_{c,cs-cm} = \frac{k_c \delta A_i (T_{cs} - T_{cm})}{\delta_{c1}} \quad \textbf{(3. 59)}$$

$$\delta Q_{c,cm-wi} = \frac{k_c \delta A_i (T_{cm} - T_{wi})}{\delta_{c2}} = \frac{k_c \delta A_i (T_{cs} - T_{wi})}{\delta_c} \quad \textbf{(3. 60)}$$

$$\delta Q_{c,z+\Delta z-cm} = \delta m_{c,z+\Delta z} c_{pc} \left(T_{c,z+\Delta z} - T_{cm}\right) \quad \textbf{(3. 61)}$$

$$\delta Q_{c,cm-z} = \delta m_{c,z} c_{pc} (T_{cm} - T_{c,z}) \quad \textbf{(3. 62)}$$

$$\delta_c = \delta_{c1} + \delta_{c2} \quad \textbf{(3. 63)}$$

d) Coupling of the elementary control volume to thermal resistance diagram

$$\delta Q_{c,cs-cm} = \delta m_{s,y_1} i_{s,y_1} = \Delta\delta m_s i_{s,x} = \Delta\delta m_{c,z} i_{s,x} \quad \textbf{(3. 64)}$$

$$\delta Q_{c,cm-wi} = \delta Q_{c,y_2} \quad \textbf{(3. 65)}$$

e) The momentum balance of the elementary control volume

Consider the control volume $((y - y_1)\Delta x\Delta z)$ shown in Figure 3.7. The forces acting in the control volume are due to buoyancy (F_B), gravity (F_g) and friction which is due to viscosity (F_τ).

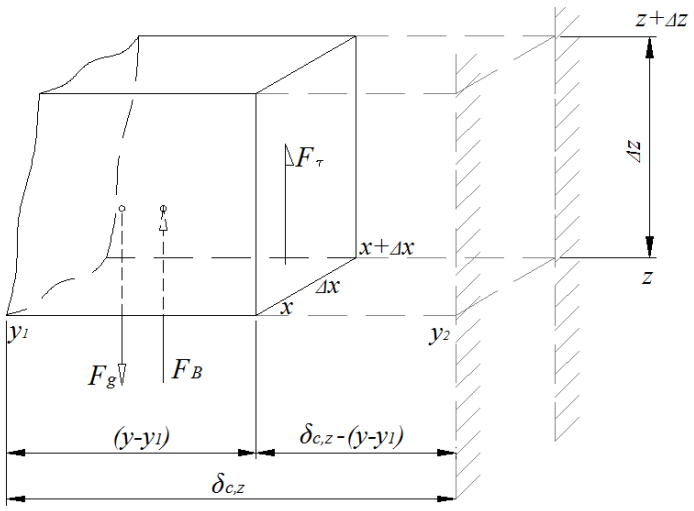

Figure 3.7: Free body diagram for the control volume in the condensation film

The Newton's second law of motion for the free body diagram shown in Figure 3.7 can be written as

$$\sum F_z = ma_z = F_\tau + F_B - F_g = 0 \quad \textbf{(3. 66)}$$

Eq. (3.66) can be re-written as

$$F_g = F_\tau + F_B \quad \textbf{(3. 67)}$$

And then

$$\rho_c g(y - y_1)(\Delta x\Delta z) = \mu_c \frac{dw_c}{d(y-y_1)}(\Delta x\Delta z) + \rho_s g(y - y_1)(\Delta x\Delta z) \quad \textbf{(3. 68)}$$

Divide Eq. (3.68) by $(\Delta x\Delta z)$ to obtain $\frac{dw_c}{d(y-y_1)}$

$$\frac{dw_c}{d(y-y_1)} = \frac{g(\rho_c-\rho_s)}{\mu_c}(y - y_1) \quad \textbf{(3. 69)}$$

In order to obtain the velocity profile of the condensate inside the condensation film, integrate Eq. (3.69), so that

$\frac{dw_c}{d(y-y_1)} = 0$ at y_1 where $(y - y_1) = 0$, and $w_c = 0$ at y_2 where $(y - y_1) = \delta_{c,z}$.

$$\int_0^{w_c} dw_c = \frac{g(\rho_c - \rho_s)}{\mu_c} \int_0^{(y-y_1)} (y - y_1)\, d(y - y_1) \qquad \textbf{(3. 70)}$$

The velocity profile of the condensate

$$w_c(y - y_1) = \frac{g(\rho_c - \rho_s)}{2\mu_c} (y - y_1)^2 \qquad \textbf{(3. 71)}$$

The condensate mass flow rate at the location *z*, where the film thickness is $\delta_{c,z}$, is determined as

$$\begin{aligned} \delta m_{c,z} &= \int_0^{\delta_{c,z}} \rho_c w_c (y - y_1) \Delta x d(y - y_1) \\ &= \frac{\rho_c g \Delta x (\rho_c - \rho_s)}{2\mu_c} \int_0^{\delta_{c,z}} (y - y_1)^2 d(y - y_1) \\ &= \frac{\rho_c g \Delta x (\rho_c - \rho_s)}{6\mu_c} \delta_{c,z}{}^3 \end{aligned} \qquad \textbf{(3. 72)}$$

The changes in the condensation rate of the steam in the *z*-direction is defined as

$$\Delta \delta m_{c,z} = \frac{\rho_c g \Delta x (\rho_c - \rho_v)\, \delta_{c,z}{}^2}{2\mu_c} \Delta \delta_{c,z} \qquad \textbf{(3. 73)}$$

In order to describe the heat transfer in the internal flow, the mean temperature of the fluid is required. This is due to the absence of the fixed free stream temperature as in the external flow (Incropera & De Witt, 1990). At a known cross section, the mean temperature is determined in terms of the enthalpy transferred by the fluid as it flows through that cross section. The enthalpy of the condensate, which flows through the cross section $(\Delta x \delta_c)$, can be written as

$$\delta m_c c_{pc} T_{cm} = c_{pc} \int_0^{\delta_c} \rho_c w_c (y - y_1) T_c (y - y_1) \Delta x d(y - y_1) \qquad \textbf{(3. 74)}$$

The temperature distribution in the condensation film in the *y*-direction is assumed to be linear, and can be written as

$$T_c(y - y_1) = T_{cs} - \frac{(T_{cs} - T_{wi})}{\delta_c} (y - y_1) \qquad \textbf{(3. 75)}$$

so that $T_c(y - y_1) = T_{cs}$ at y_1, where $(y - y_1) = 0$ and $T_c(y - y_1) = T_{wi}$ at y_2, where $(y - y_1) = \delta_c$.

Therefore Eq. (3.74) can be re-written as

$$\delta m_c c_{pc} T_{cm} = c_{pc} \int_0^{\delta_c} \frac{\rho_c g (\rho_c - \rho_s)}{2\mu_c} (y - y_1)^2 \left[T_{cs} - \frac{(T_{cs} - T_{wi})}{\delta_c} (y - y_1) \right] \Delta x d(y - y_1) \qquad \textbf{(3. 76)}$$

Divide Eq. (3.76) by c_{pc}

$$\begin{aligned}\delta m_c T_{cm} &= \frac{\rho_c g \Delta x(\rho_c-\rho_s)}{2\mu_c}\left[\begin{matrix} T_{cs}\int_0^{\delta_c}(y-y_1)^2 d(y-y_1) - \\ \frac{(T_{cs}-T_{wi})}{\delta_c}\int_0^{\delta_c}(y-y_1)^3 d(y-y_1)\end{matrix}\right] \\ &= \frac{\rho_c g \Delta x(\rho_c-\rho_s)}{2\mu_c}\left[\frac{T_{cs}}{3}(\delta_c)^3 - \frac{(T_{cs}-T_{wi})}{4\delta_c}(\delta_c)^4\right] \\ &= \frac{\rho_c g \Delta x(\rho_c-\rho_s)\delta_c{}^3}{2\mu_c}\left[\frac{T_{cs}}{3} - \frac{(T_{cs}-T_{wi})}{4}\right]\end{aligned} \quad \textbf{(3. 77)}$$

For the cross section $(\Delta x \delta_c)$, Eq. (3.72) is re-written as

$$\delta m_c = \frac{\rho_c g \Delta x(\rho_c-\rho_s)\delta_c{}^3}{6\mu_c} \quad \textbf{(3. 78)}$$

Substitute Eq. (3.78) into (3.77)

$$\frac{\rho_c g \Delta x(\rho_c-\rho_s)\delta_c{}^3}{6\mu_c} T_{cm} = \frac{\rho_c g \Delta x(\rho_c-\rho_s)\delta_c{}^3}{2\mu_c}\left[\frac{T_{cs}}{3} - \frac{(T_{cs}-T_{wi})}{4}\right] \quad \textbf{(3. 79)}$$

which can be simplified as

$$\frac{T_{cm}}{6} = \frac{1}{2}\left[\frac{T_{cs}}{3} - \frac{(T_{cs}-T_{wi})}{4}\right] \quad \textbf{(3. 80)}$$

Therefore, the weighted mean temperature of the condensate in the condensation film is

$$T_{cm} = T_{cs} - \frac{3(T_{cs}-T_{wi})}{4} \quad \textbf{(3. 81)}$$

3.3.3. Tube wall-side elementary control volume

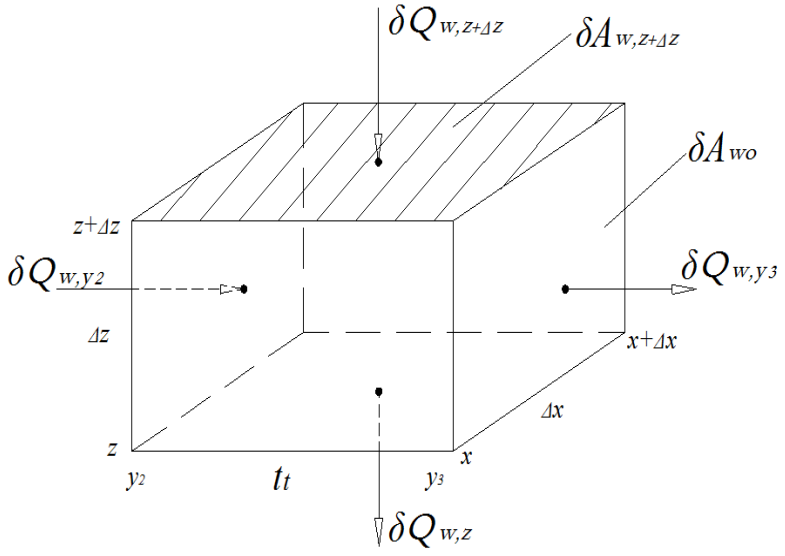

(a) Control volume

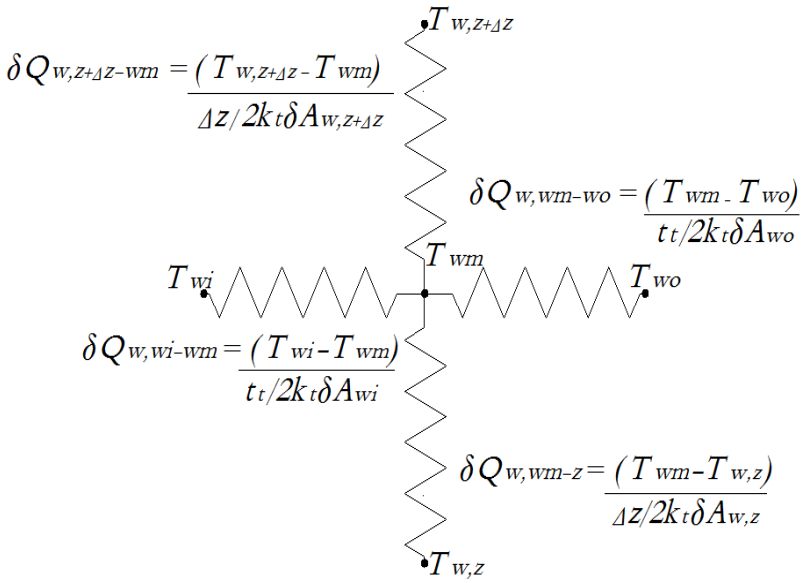

(b) Thermal resistance diagram

Figure 3.8: Tube wall-side elementary control volume and thermal resistance diagram

a) The heat transfer balance for the thermal resistance diagram

$$\delta Q_{w,wi-wm} + \delta Q_{w,z+\Delta z-wm} = \delta Q_{w,wm-wo} + \delta Q_{w,wm-z} \quad \textbf{(3. 82)}$$

where

$$\delta Q_{w,wi-wm} = \frac{2k_t\delta A_{wi}(T_{wi}-T_{wm})}{t_t} \quad \textbf{(3. 83)}$$

$$\delta Q_{w,z+\Delta z-wm} = \frac{2k_t\delta A_{w,z+\Delta z}(T_{w,z+\Delta z}-T_{wm})}{\Delta z} \quad \textbf{(3. 84)}$$

$$\delta Q_{w,wm-wo} = \frac{2k_t\delta A_{wo}(T_{wm}-T_{wo})}{t_t} \quad \textbf{(3. 85)}$$

$$\delta Q_{w,wm-z} = \frac{2k_t\delta A_{w,z}(T_{wm}-T_{w,z})}{\Delta z} \quad \textbf{(3. 86)}$$

and

$$\delta A_{wi} = \delta A_{wo} \quad \textbf{(3. 87)}$$

$$\delta A_{w,z} = \delta A_{w,z+\Delta z} \quad \textbf{(3. 88)}$$

b) Coupling of the elementary control volume to thermal resistance diagram

$$\delta Q_{w,wi-wm} = \delta Q_{w,y_2} = \delta Q_{c,y_2} \quad \textbf{(3. 89)}$$

$$\delta Q_{w,z+\Delta z-wm} = \delta Q_{w,z+\Delta z} \quad \textbf{(3. 90)}$$

$$\delta Q_{w,wm-wo} = \delta Q_{w,y_3} \quad \textbf{(3. 91)}$$

$$\delta Q_{w,wm-z} = \delta Q_{w,z} \quad \textbf{(3. 92)}$$

3.3.4. Deluge water elementary control volume

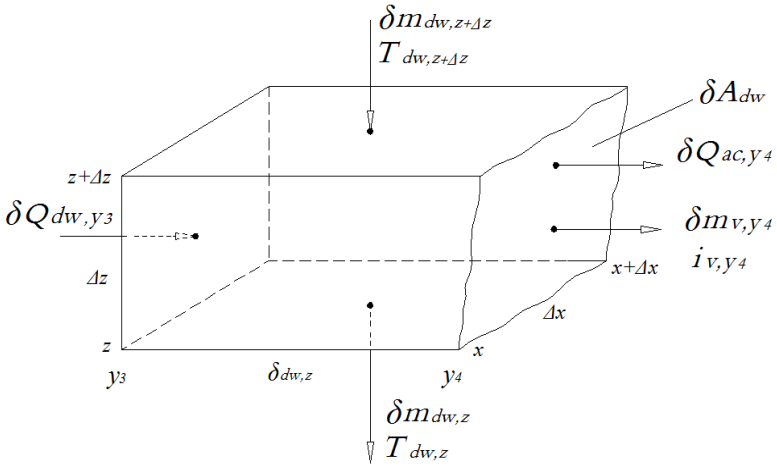

Figure 3.9: Deluge water-side elementary control volume

a) The water mass balance for the elementary control volume

$$\delta m_{dw,z+\Delta z} = \delta m_{dw,z} + \delta m_{v,y_4} \quad \textbf{(3. 93)}$$

That can be simplified as

$$\delta m_{dw,z} + \Delta\delta m_{dw,z} = \delta m_{dw,z} + \delta m_{v,y_4} \quad \textbf{(3. 94)}$$

$$\Delta\delta m_{dw,z} = \delta m_{v,y_4} \quad \textbf{(3. 95)}$$

b) The energy balance for the elementary control volume

$$\delta Q_{dw,y_3} + \delta m_{dw,z+\Delta z} c_{pdw} T_{dw,z+\Delta z} = \delta m_{dw,z} c_{pdw} T_{dw,z} + \delta Q_{ac,y_4} + \delta m_{v,y_4} i_{v,y_4} \quad \textbf{(3. 96)}$$

The heat transfer ($\delta Q_{dw,y_4}$), leaving the control volume is the sum of sensible and latent heat crossing the air-water interface therefore,

$$\delta Q_{dw,y_4} = \delta Q_{ac,y_4} + \delta m_{v,y_4} i_{v,y_4} \quad \textbf{(3. 97)}$$

Then eq. (3.96) is re-written as

$$\delta Q_{dw,y_3} + \delta m_{dw,z+\Delta z} c_{pdw} T_{dw,z+\Delta z} = \delta m_{dw,z} c_{pdw} T_{dw,z} + \delta Q_{dw,y_4} \quad \textbf{(3. 98)}$$

Re-arrange the terms to obtain $\delta Q_{dw,y_4}$

$$\delta Q_{dw,y_4} = \delta Q_{dw,y_3} + \delta m_{dw,z+\Delta z} c_{pdw} T_{dw,z+\Delta z} - \delta m_{dw,z} c_{pdw} T_{dw,z} \quad \textbf{(3. 99)}$$

$$= \delta Q_{dw,y_3} + \left(\delta m_{dw,z} + \Delta\delta m_{dw,z}\right) c_{pdw} T_{dw,z+\Delta z} - \delta m_{dw,z} c_{pdw}$$

$$= \delta Q_{dw,y_3} + \delta m_{dw,z} c_{pdw} \Delta T_{dw,z} + \Delta\delta m_{dw,z} c_{pdw} T_{dw,z+\Delta z}$$

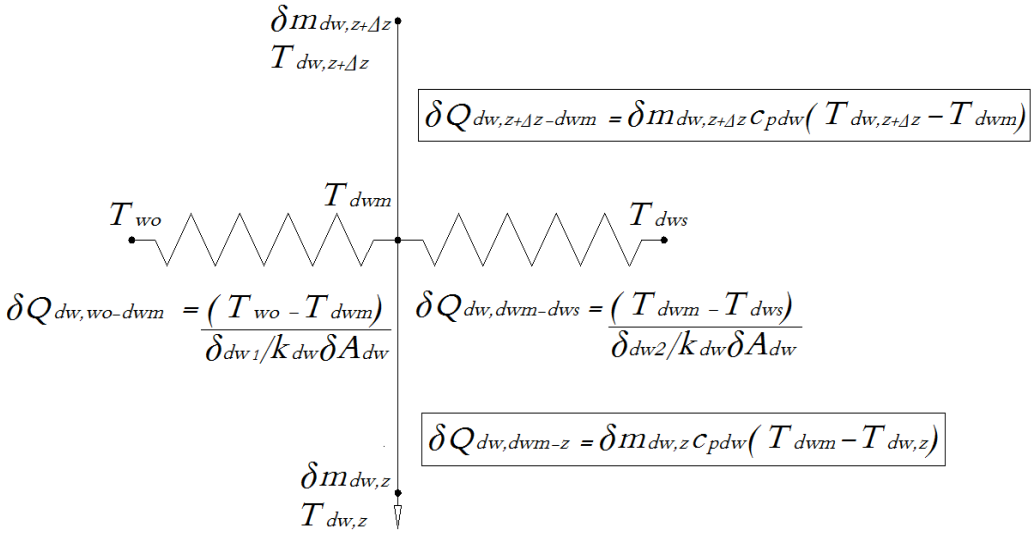

Figure 3.10: Deluge water-side thermal resistance diagram

c) The heat transfer balance for the thermal resistance diagram

$$\delta Q_{dw,wo-dwm} + \delta Q_{dw,z+\Delta z-dwm} = \delta Q_{dw,dwm-dws} + \delta Q_{dw,dwm-z} \quad \textbf{(3. 100)}$$

where

$$\delta Q_{dw,wo-dwm} = \frac{k_{dw}\delta A_{dw}(T_{wo}-T_{dwm})}{\delta_{dw1}} \quad \textbf{(3. 101)}$$

$$\delta Q_{dw,dwm-dws} = \frac{k_{dw}\delta A_{dw}(T_{dwm}-T_{dws})}{\delta_{dw2}} = \frac{k_{dw}\delta A_{dw}(T_{wo}-T_{dws})}{\delta_{dw}} \quad \textbf{(3. 102)}$$

$$\delta Q_{dw,z+\Delta z-dwm} = \delta m_{dw,z+\Delta z} c_{pdw}(T_{dw,z+\Delta z} - T_{dwm}) \quad \textbf{(3. 103)}$$

$$\delta Q_{dw,z} = \delta m_{dw,z} c_{pdw}(T_{dwm} - T_{dw,z}) \quad \textbf{(3. 104)}$$

$$\delta_{dw} = \delta_{dw1} + \delta_{dw2} \quad \textbf{(3. 105)}$$

d) Coupling of the elementary control volume to thermal resistance diagram

$$\delta Q_{dw,wo-dwm} = \delta Q_{dw,y_3} = \delta Q_{w,y_3} \quad \textbf{(3. 106)}$$

$$\delta Q_{dw,dwm-dws} = \delta Q_{dw,y_4} \quad \textbf{(3. 107)}$$

e) The momentum balance of the elementary control volume

Consider the control volume $\left[\left[\delta_{dw,z}-(y-y_3)\right]\Delta x\Delta z\right]$ shown in Figure 3.11. The forces acting in the control volume are due to buoyancy (F_B), gravity (F_g) and friction which is due to viscosity (F_τ).

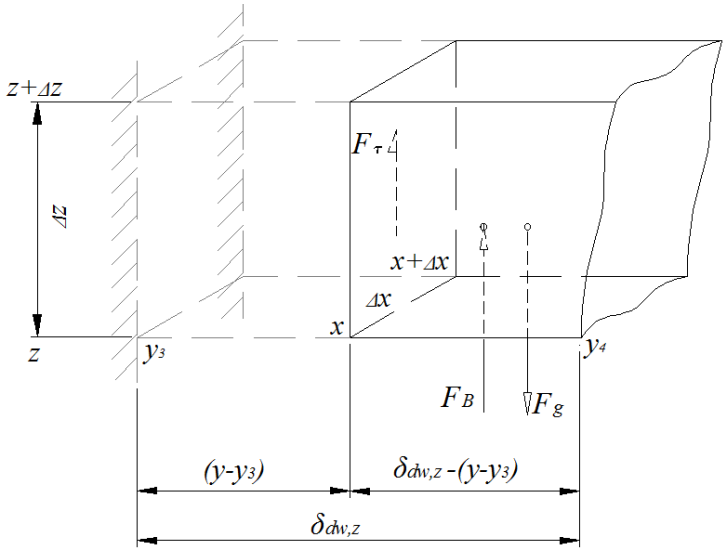

Figure 3.11: Free body diagram for the control volume in deluge water film

The Newton's second law of motion for the free body diagram shown in Figure 3.11 can be written as

$$\sum F_z = ma_z = F_\tau + F_B - F_g = 0 \qquad \textbf{(3. 108)}$$

which can be re-written as

$$F_g = F_\tau + F_B \qquad \textbf{(3. 109)}$$

Then,

$$\rho_{dw}g\left[\delta_{dw,z}-(y-y_3)\right](\Delta x\Delta z) = \mu_{dw}\frac{dw_{dw}}{d(y-y_3)}(\Delta x\Delta z) + \rho_a g\left[\delta_{dw,z}-(y-y_3)\right](\Delta x\Delta z) \qquad \textbf{(3. 110)}$$

Divide Eq. (3.110) by $(\Delta x\Delta z)$ to obtain $\frac{dw_{dw}}{d(y-y_3)}$

$$\frac{dw_{dw}}{d(y-y_3)} = \frac{g(\rho_{dw}-\rho_a)\left[\delta_{dw,z}-(y-y_3)\right]}{\mu_{dw}} \qquad \textbf{(3. 111)}$$

Integrate Eq. (3.11) so that, $w_{dw}=0$ at y_3, where $(y-y_3)=0$ and $\frac{dw_{dw}}{d(y-y_3)}=0$ at y_4, where $(y-y_3)=\delta_{dw}$.

$$\int_0^{w_{dw}} dw_{dw} = \frac{g(\rho_{dw}-\rho_a)}{\mu_{dw}} \int_0^{(y-y_3)}\left[\delta_{dw,z}-(y-y_3)\right]d(y-y_3) \qquad \textbf{(3. 112)}$$

Then the velocity profile of the deluge water inside the film

$$w_{dw}(y-y_3)=\frac{g(\rho_{dw}-\rho_a)}{\mu_{dw}}\left[(y-y_3)\delta_{dw,z}-\frac{(y-y_3)^2}{2}\right] \quad \textbf{(3. 113)}$$

The deluge water mass flow rate is determined as

$$\begin{aligned}&\delta m_{dw,z}=\int_0^{\delta_{dw,z}}\rho_{dw}w_{dw}(y-y_3)\Delta x d(y-y_3)=\\&\int_0^{\delta_{dw,z}}\rho_{dw}\frac{g(\rho_{dw}-\rho_a)\Delta x}{\mu_{dw}}\left[(y-y_3)\delta_{dw,z}-\frac{(y-y_3)^2}{2}\right]d(y-y_3)=\\&\frac{\rho_{dw}g\Delta x(\rho_{dw}-\rho_a)}{3\mu_{dw}}\delta_{dw,z}{}^3\end{aligned} \quad \textbf{(3. 114)}$$

The deluge water film thickness is defined as

$$\delta_{dw,z}=\left(\frac{3\mu_{dw}\delta m_{dw,z}}{\rho_{dw}g\Delta x(\rho_{dw}-\rho_a)}\right)^{\frac{1}{3}} \quad \textbf{(3. 115)}$$

The mean temperature of the deluge water is determined in term of the enthalpy of the deluge water, flows through the cross section $(\Delta x\delta_{dw})$, which is written as

$$\begin{aligned}&\delta m_{dw}c_{pdw}T_{dwm}\\&=c_{pdw}\int_0^{\delta_{dw}}\rho_{dw}w_{dw}(y-y_3)T_{dw}(y-y_3)\Delta x d(y-y_3)\end{aligned} \quad \textbf{(3. 116)}$$

The temperature distribution in the deluge water film in the *y*-direction is assumed to be linear and can be written as

$$T_{dw}(y-y_3)=T_{wo}-\frac{(T_{wo}-T_{dws})}{\delta_{dw}}(y-y_3 \quad \textbf{(3. 117)}$$

so that $T_{dw}(y-y_3)=T_{wo}$ at y_3, where $(y-y_3)=0$ and $T_{dw}(y-y_3)=T_{dws}$ at y_4, where $(y-y_3)=\delta_{dw,z}$.

Substitute Eq. (3.113) and (3.117) into (3.116)

$$\begin{aligned}&\delta m_{dw}c_{pdw}T_{dwm}=c_{pdw}\int_0^{\delta_{dw}}\frac{\rho_{dw}g(\rho_{dw}-\rho_a)}{\mu_{dw}}\left[(y-y_3)\delta_{dw,z}-\right.\\&\left.\frac{(y-y_3)^2}{2}\right]\left[T_{wo}-\frac{(T_{wo}-T_{dws})}{\delta_{dw}}(y-y_3)\right]\Delta x d(y-y_3)\end{aligned} \quad \textbf{(3. 118)}$$

Divide Eq. (3.118) by c_{pdw} and re-arrange the terms

$$\begin{aligned}&\delta m_{dw}T_{dwm}=\frac{\rho_{dw}g\Delta x(\rho_{dw}-\rho_a)}{\mu_{dw}}\left[\int_0^{\delta_{dw}}\left((y-y_3)\delta_{dw}T_{wo}\right)d(y-y_3)-\right.\\&\int_0^{\delta_{dw}}(y-y_3)^2(T_{wo}-T_{dws})d(y-y_3)-\int_0^{\delta_{dw}}\left(\frac{(y-y_3)^2}{2}T_{wo}\right)d(y-\\&y_3)+\left.\int_0^{\delta_{dw}}\left(\frac{(y-y_3)^3}{2}\frac{(T_{wo}-T_{dws})}{\delta_{dw}}\right)d(y-y_3)\right]\\&=\frac{\rho_{dw}g\Delta x(\rho_{dw}-\rho_a)}{\mu_{dw}}\left[\frac{(\delta_{dw})^3}{2}T_{wo}-\frac{(\delta_{dw})^3}{3}(T_{wo}-\right.\\&\left.T_{dws})-\frac{(\delta_{dw})^3}{6}T_{wo}+\frac{(\delta_{dw})^3}{8}(T_{wo}-T_{dws})\right]\end{aligned} \quad \textbf{(3. 119)}$$

$$= \frac{\rho_{dw} g \Delta x (\rho_{dw} - \rho_a) \delta_{dw}^{\ 3}}{\mu_{dw}} \left[\frac{T_{wo}}{3} - \frac{5(T_{wo} - T_{dws})}{24} \right]$$

The mass flow rate of the deluge water, which flows through the cross section $(\Delta x \delta_{dw})$ is defined as

$$\delta m_{dw} = \frac{\rho_{dw} g \Delta x (\rho_{dw} - \rho_a)}{3\mu_{dw}} \delta_{dw}^{\ 3} \quad \textbf{(3. 120)}$$

Substitute Eq. (3.120) into (3.119)

$$\frac{\rho_{dw} g \Delta x (\rho_{dw} - \rho_a) \delta_{dw}^{\ 3}}{3\mu_{dw}} T_{dwm} = \frac{\rho_{dw} g \Delta x (\rho_{dw} - \rho_a) \delta_{dw}^{\ 3}}{\mu_{dw}} \left[\frac{T_{wo}}{3} - \frac{5(T_{wo} - T_{dws})}{24} \right] \quad \textbf{(3. 121)}$$

That can be simplified as

$$\frac{T_{dwm}}{3} = \left[\frac{T_{wo}}{3} - \frac{5(T_{wo} - T_{dws})}{24} \right] \quad \textbf{(3. 122)}$$

Therefore, the deluge water weighted mean temperature is

$$T_{dwm} = T_{wo} - \frac{5(T_{wo} - T_{dws})}{8} \quad \textbf{(3. 123)}$$

3.3.5. Air-side elementary control volume

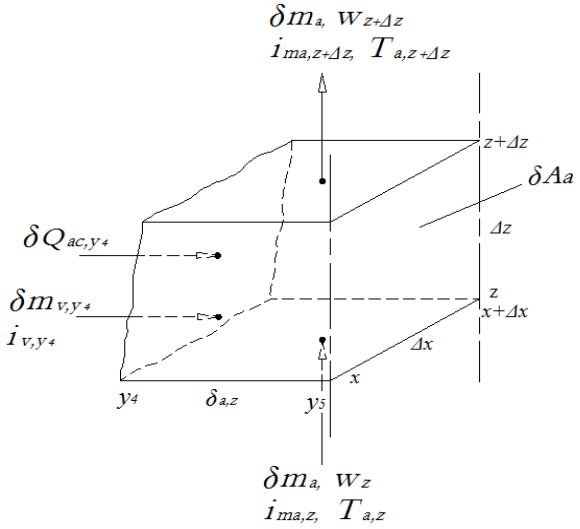

Figure 3.12: Air-side elementary control volume

a) The water mass balance for the elementary control volume

$$\delta m_{v,y_4} + \delta m_a (1 + w_z) = \delta m_a (1 + w_{z+\Delta z}) \quad \textbf{(3. 124)}$$

That can be simplified as

$$\delta m_{v,y_4} + \delta m_a(1 + w_z) = \delta m_a(1 + w_z + \Delta w) \quad \textbf{(3. 125)}$$

$$\delta m_{v,y_4} = \delta m_a \Delta w \quad \textbf{(3. 126)}$$

Substitute Eq. (3.95) into (3.126)

$$\Delta\delta m_{dw,z} = \delta m_a \Delta w \quad \textbf{(3. 127)}$$

b) The energy balance for the elementary control volume

$$\delta Q_{ac,y_4} + \delta m_{v,y_4} i_{v,y_4} + \delta m_a i_{ma,z} = \delta m_a i_{ma,z+\Delta z} \quad \textbf{(3. 128)}$$

That can be simplified as

$$\delta Q_{ac,y_4} + \delta m_{v,y_4} i_{v,y_4} + \delta m_a i_{ma,z} = \delta m_a \left(i_{ma,z} + \Delta i_{ma,z}\right) \quad \textbf{(3. 129)}$$

$$\delta Q_{ac,y_4} + \delta m_{v,y_4} i_{v,y_4} = \delta m_a \Delta i_{ma,z} = \delta Q_{a,y_4} \quad \textbf{(3. 130)}$$

Substitute Eq. (3.126) into (3.130)

$$\delta Q_{ac,y_4} + \delta m_a \Delta w i_{v,y_4} = \delta m_a \Delta i_{ma,z} \quad \textbf{(3. 131)}$$

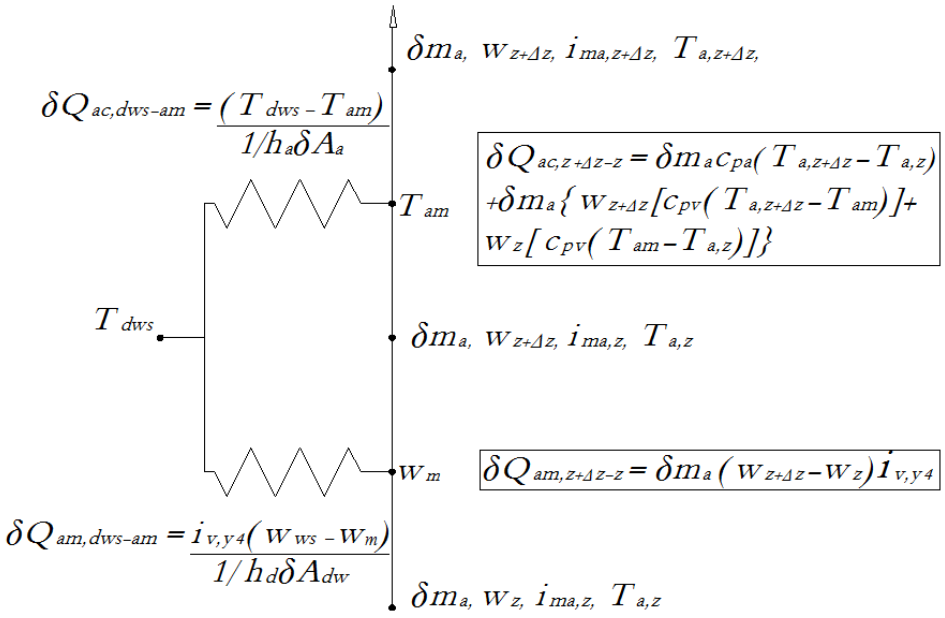

Figure 3.13: Air-side thermal resistance diagram

c) The heat transfer balance for the thermal resistance diagram

$$\delta Q_{ac,dws-am} = h_a \delta A_a (T_{dws} - T_{am}) = \delta m_a c_{pa}\left(T_{a,z+\Delta z} - T_{a,z}\right) + \delta m_a w_{z+\Delta z} c_{pv}\left(T_{a,z+\Delta z} - T_{am}\right) + \delta m_a w_z c_{pv}\left(T_{am} - T_{a,z}\right) \quad \textbf{(3. 132)}$$

$$\delta Q_{am,dws-am} = h_d \delta A_{dw} i_{v,y_4}(w_{sw} - w_m) = \delta m_a i_{v,y_4}(w_{z+\Delta z} - w_z) \quad \textbf{(3. 133)}$$

d) Coupling of the elementary control volume to thermal resistance diagram

$$\delta Q_{am,dws-am} = \delta Q_{am,z+\Delta z-z} = \delta m_{v,y_4} i_{v,y_4} \quad \textbf{(3. 134)}$$

$$\delta Q_{ac,dws-am} = \delta Q_{ac,z+\Delta z-z} = \delta Q_{ac,y_4} \quad \textbf{(3. 135)}$$

3.3.6. The governing equations

In order to obtain the governing equations, describing the processes taking place in each elementary control volume as well as in the entire two-dimensional elementary control volume, the differential equations derived in sections 3.3.1, 3.3.2, 3.3.3, 3.3.4, and 3.3.5 are coupled and simplified.

a) Condensate-side

From Eq. (3.60)

$$\frac{k_c \delta A_i (T_{cm} - T_{wi})}{\delta_{c2}} = \frac{k_c \delta A_i (T_{cs} - T_{wi})}{\delta_c} \quad \textbf{(3. 136)}$$

Divide Eq. (3.136) by $k_c \delta A_i$ to obtain δ_{c2}

$$\delta_{c2} = \frac{(T_{cm} - T_{wi})\delta_c}{(T_{cs} - T_{wi})} \quad \textbf{(3. 137)}$$

Substitute Eq. (3.137) into (3.63)

$$\delta_c = \delta_{c1} + \frac{(T_{cm} - T_{wi})\delta_c}{(T_{cs} - T_{wi})} \quad \textbf{(3. 138)}$$

Then solve for δ_{c1}

$$\delta_{c1} = \frac{(T_{cs} - T_{cm})\delta_c}{(T_{cs} - T_{wi})} \quad \textbf{(3. 139)}$$

Substitute Eq. (3.59) into (3.64)

$$\frac{k_c \delta A_i (T_{cs} - T_{cm})}{\delta_{c1}} = \Delta \delta m_{c,z} i_{s,x} \quad \textbf{(3. 140)}$$

Then solve for $\Delta \delta m_{c,z}$

$$\Delta \delta m_{c,z} = \frac{k_c \delta A_i (T_{cs} - T_{cm})}{\delta_{c1} i_{s,x}} \quad \textbf{(3. 141)}$$

Substitute Eq. (3.139) into (3.141) and simplify

$$\Delta\delta m_{c,z} = \frac{k_c \delta A_i (T_{cs} - T_{cm})}{i_{s,x}} \frac{1}{\frac{(T_{cs} - T_{cm})\delta_c}{(T_{cs} - T_{wi})}} = \frac{k_c \delta A_i (T_{cs} - T_{wi})}{i_{s,x} \delta_c} \quad \textbf{(3. 142)}$$

Substitute Eq. (3.73) into (3.142)

$$\frac{\rho_c g \Delta x (\rho_c - \rho_v) {\delta_c}^2}{2\mu_c} \Delta\delta_{c,z} = \frac{k_c \delta A_i (T_{cs} - T_{wi})}{i_{s,x} \delta_c} \quad \textbf{(3. 143)}$$

Replace δA_i in Eq. (3.143) by $\Delta x \Delta z$ and re-arrange the terms

$${\delta_c}^3 \Delta\delta_{c,z} = \frac{2 k_c \mu_c \Delta z \ (T_{cs} - T_{wi})}{\rho_c g (\rho_c - \rho_v) i_{s,x}} \quad \textbf{(3. 144)}$$

Integrate Eq. (3.144) from $z = 0$, where $\delta_c = 0$ to z, where $\delta_c = \delta_c$ to obtain the condensation film thickness.

$$\delta_c = \left[\frac{8 k_c \mu_c \ (T_{cs} - T_{wi}) z}{\rho_c g (\rho_c - \rho_v) i_{s,x}}\right]^{1/4} \quad \textbf{(3. 145)}$$

where $i_{s,x}$ is the steam enthalpy and is determined as

$$i_{s,x} = i_{fg,x} + c_{pv} T_v \quad \textbf{(3. 146)}$$

The differential equations (3.53), (3.64), (3.65), (3.81), (3.137), (3.139), (3.141) and (3.145) describe the heat transfer processes taking place in the condensate-side elementary control volume.

b) Tube wall-side

The heat conducted through the tube wall is defined by Eq. (3.82).

c) Deluge water-side

Combine Eq. (3.101) and (3.106)

$$\frac{k_{dw} \delta A_{dw} (T_{wo} - T_{dwm})}{\delta_{dw1}} = \delta Q_{dw,y_3} \quad \textbf{(3. 147)}$$

Re-arrange the terms to obtain δ_{dw1}

$$\delta_{dw1} = \frac{k_{dw} \delta A_{dw} (T_{wo} - T_{dwm})}{\delta Q_{dw,y_3}} \quad \textbf{(3. 148)}$$

From Eq. (3.102)

$$\frac{k_{dw} \delta A_{dw} (T_{dwm} - T_{dws})}{\delta_{dw2}} = \frac{k_{dw} \delta A_{dw} (T_{wo} - T_{dws})}{\delta_{dw}} \quad \textbf{(3. 149)}$$

Divide Eq. (3.149) by $k_{dw} \delta A_{dw}$ to obtain δ_{dw2}

$$\delta_{dw2} = \frac{(T_{dwm} - T_{dws}) \delta_{dw}}{(T_{wo} - T_{dws})} \quad \textbf{(3. 150)}$$

Substitute Eq. (3.150) into (3.105), and solve for δ_{dw1}

$$\delta_{dw1} = \frac{(T_{wo} - T_{dwm})\delta_{dw}}{(T_{wo} - T_{dws})} \quad \textbf{(3. 151)}$$

Therefore, Eq. (3.148) is equal to Eq. (3.151). The differential equations (3.95), (3.106), (3.107), (3.115), (3.123), (3.150) and (3.151) describe the heat transfer processes taking place in the deluge water-side elementary control volume.

d) Air-side

The heat transfer processes taking place in the air-side elementary control volume are described by differential equations (3.127), (3.131), (3.132) and (3.133).

3.4. Discretization of the governing equations

In order to derive the governing equations for the computational model, the governing differential equations are discretised into simple and solvable algebraic equations. The tube is divided into several control volumes in the *z*-direction as depicted in Figure 3.14. The discretised equations are obtained by integrating the governing differential equations over the corresponding individual control volumes, and maintaining the conservation laws (Verseteeg & Malalasekera, 2007). The balance of the heat transfer over the control volume face is expressed through the temperature at the main grid point.

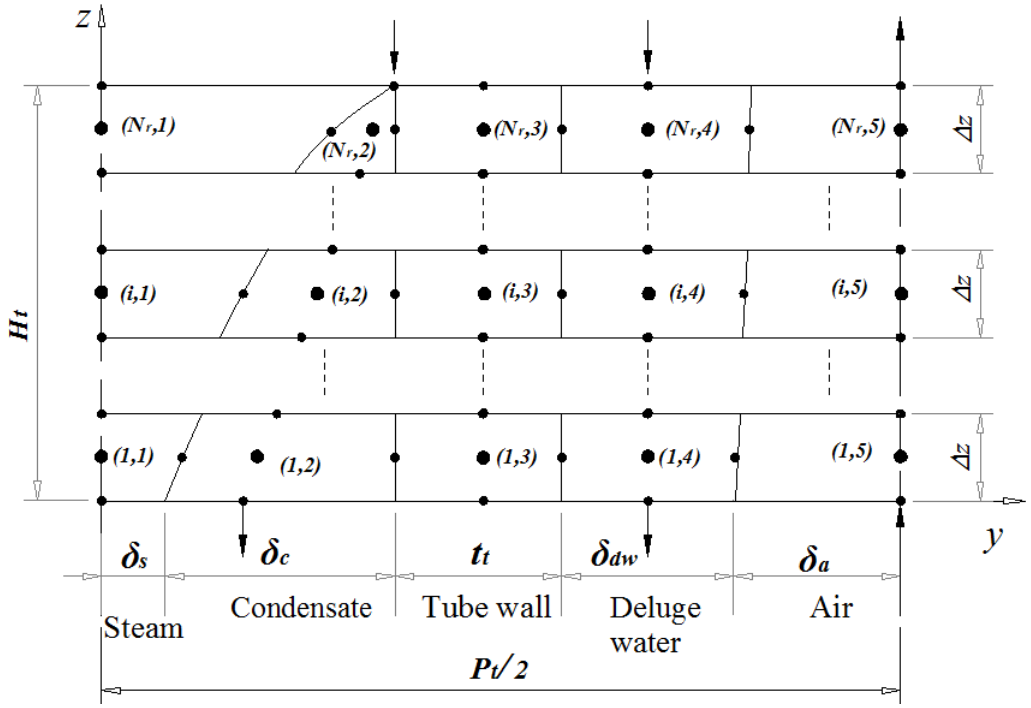

Figure 3.14: Grid points network

The discretised governing equations are achieved by employing the linear upwind differencing scheme. The linear upwind differencing scheme is mainly used in the convection dominated flows, because it provides the numerical stable solutions and takes into account the flow direction (Suhas, 1980).

To show the generally application of the linear upwind differencing scheme, the nodal grid point *P* at the centre of the cell (*i*, *j*) is considered. The neighbouring cells of point *P* are denoted as *N*, *S*, *W* and *E*, and the interface grid points between them and point *P* are designated as *n*, *s*, *w* and *e*, as illustrated in Figure 3.15.

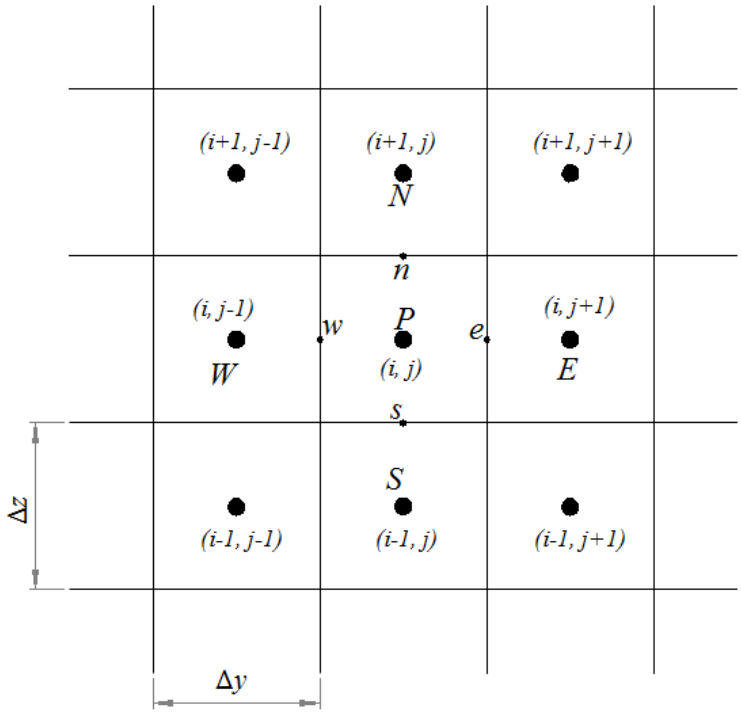

Figure 3.15: General discretization using linear upwind differencing scheme.

The derivatives of a considered property (ϕ) at nodal point *P* in the *z*-direction can be expressed as

$$\left.\frac{d\phi}{dz}\right|_{P(i,j)} = \frac{\phi_{n(i,j)} - \phi_{s(i,j)}}{\Delta z} \qquad \textbf{(3. 152)}$$

where $\phi_{n(i,j)}$ and $\phi_{s(i,j)}$ are values of property (ϕ) at the interface grid points *n* and *s*, respectively.

$$\phi_{n(i,j)} = \frac{\phi_{P(i,j)} + \phi_{N(i,j)}}{2} = \frac{\phi_{(i,j)} + \phi_{(i+1,j)}}{2} \qquad \textbf{(3. 153)}$$

$$\phi_{s(i,j)} = \phi_{P(i,j)} + \frac{\phi_{P(i,j)} - \phi_{N(i,j)}}{2} = \phi_{(i,j)} + \frac{\phi_{(i,j)} - \phi_{(i+1,j)}}{2} \qquad \textbf{(3. 154)}$$

The values of property (ϕ) at the interface grid points *w* and *e* in the *y*-direction are expressed as

$$\phi_{w(i,j)} = \frac{\phi_{P(i,j)}+\phi_{W(i,j)}}{2} = \frac{\phi_{(i,j)}+\phi_{(i,j-1)}}{2} \quad \textbf{(3. 155)}$$

$$\phi_{e(i,j)} = \phi_{P(i,j)} + \frac{\phi_{P(i,j)}-\phi_{W(i,j)}}{2} = \phi_{(i,j)} + \frac{\phi_{(i,j)}-\phi_{(i,j-1)}}{2} \quad \textbf{(3. 156)}$$

In order to demonstrate the discretization of the obtained governing differential equations in section 3.3.6, the i^{th}-interval in Figure 3.14 is considered. The first number or subscript i of the indices notation used in Figure 3.14 denotes the grid point index in the *z*-direction, and the second number or subscript j denotes the grid point index in the *y*-direction.

The height of each grid cell is determined as

$$\Delta z = H_t/N_r \quad \textbf{(3. 157)}$$

where, H_t is tube height and N_r is the number of intervals/rows in the *z*-direction.

a) Grid point (*i*, 2)

The governing equations (3.53), (3.64), (3.65), (3.81), (3.137), (3.139), (3.141) and (3.145) are discretised as follows

$$\begin{aligned}\Delta\delta m_{s(i,1)} = \Delta\delta m_{c(i,2)} &= \left(\delta m_{c,s} - \delta m_{c,n}\right)_{(i,2)} \\ &= \frac{\delta m_{c(i,2)}+\delta m_{c(i+1,2)}}{2} - \left(\delta m_{c(i,2)} + \frac{\delta m_{c(i,2)}-\delta m_{c(i+1,2)}}{2}\right)\end{aligned} \quad \textbf{(3. 158)}$$

$$\delta Q_{c,w(i,2)} = \Delta\delta m_{c(i,2)}\left(i_{fg} + c_{pc}T_v\right) = k_c\Delta x\Delta z\left[\frac{\left(T_{c,w}-T_c\right)}{\delta_{c1}}\right]_{(i,2)} \quad \textbf{(3. 159)}$$

$$\begin{aligned}\delta Q_{c,e(i,2)} &= \Delta\delta m_{c(i,2)}\left[i_{fg} + c_{pc}\left(T_v - T_{c,n(i,2)}\right)\right] \\ &\quad + \delta m_{c,s(i,2)}c_{pc}\Delta T_{c(i,2)} \\ &= k_c\Delta x\Delta z\left[\frac{\left(T_{c,w}-T_{c,e}\right)}{\delta_c}\right]_{(i,2)} = k_c\Delta x\Delta z\left[\frac{\left(T_c-T_{c,e}\right)}{\delta_{c2}}\right]_{(i,2)} \\ &= \left(\delta Q_{c,w} + \delta Q_{c,n} - \delta Q_{c,s}\right)_{(i,2)}\end{aligned} \quad \textbf{(3. 160)}$$

$$T_{c(i,2)} = \left[T_{c,w} - \frac{3\left(T_{c,w}-T_{c,e}\right)}{4}\right]_{(i,2)} \quad \textbf{(3. 161)}$$

$$\delta_{c2(i,2)} = \left[\frac{\left(T_c-T_{c,e}\right)\delta_c}{\left(T_{c,w}-T_{c,e}\right)}\right]_{(i,2)} \quad \textbf{(3. 162)}$$

$$\delta_{c1(i,2)} = \left[\frac{\left(T_{c,w}-T_c\right)\delta_c}{\left(T_{c,w}-T_{c,e}\right)}\right]_{(i,2)} \quad \textbf{(3. 163)}$$

$$\Delta\delta m_{c(i,2)} = \frac{k_c\Delta x\Delta z}{\left(i_{fg}+c_{pc}T_v\right)}\left[\frac{\left(T_{c,w}-T_c\right)}{\delta_{c1}}\right]_{(i,2)} \quad \textbf{(3. 164)}$$

$$\delta_{c(i,2)} = \left[\frac{8k_c\mu_c\left(T_{c,w}-T_{c,e}\right)_{(i,2)}z}{\rho_c g(\rho_c-\rho_v)\left(i_{fg}+c_{pc}T_v\right)}\right]^{1/4} \quad \textbf{(3. 165)}$$

b) Grid point (*i*, 3)

The governing equation (3.82) is discretised as

$$\delta Q_{w,e(i,3)} = \left(\delta Q_{w,w} + \delta Q_{w,n} - \delta Q_{w,s}\right)_{(i,3)} \quad \textbf{(3. 166)}$$

$$\delta Q_{w,w(i,3)} = \delta Q_{c,e(i,2)} \quad \textbf{(3. 167)}$$

$$\delta Q_{w,n(i,3)} = \frac{2k_t t_t \Delta x}{\Delta z}\left(T_{w,n} - T_w\right)_{(i,3)} \quad \textbf{(3. 168)}$$

$$\delta \mathrm{Q}_{\mathrm{w,s(i,3)}} = \frac{2\mathrm{k_t t_t}\Delta \mathrm{x}}{\Delta \mathrm{z}}\left(\mathrm{T_w} - \mathrm{T_{w,s}}\right)_{\mathrm{(i,3)}} \quad \textbf{(3. 169)}$$

c) Grid point (*i*, 4)

The governing equations (3.95), (3.106), (3.107), (3.115), (3.123), (3.150) and (3.151) are discretised as follows

$$\begin{aligned}\Delta\delta m_{dw(i,4)} &= \delta m_a \Delta w_{(i,5)} = \delta m_a [w_n - w_s]_{(i,5)} \\ &= \delta m_a \left[\frac{w_{(i,5)}+w_{(i+1,5)}}{2} - \left(w_{(i,5)} + \frac{w_{(i,5)}-w_{(i+1,5)}}{2}\right)\right]\end{aligned} \quad \textbf{(3. 170)}$$

$$\delta Q_{dw,w(i,4)} = \delta Q_{w,e(i,3)} \quad \textbf{(3. 171)}$$

$$\begin{aligned}\delta Q_{dw,e(i,4)} &= \delta Q_{dw,w(i,4)} + \delta m_{dw,s(i,4)} c_{pdw} \Delta T_{dw(i,4)} \\ &\quad + \Delta\delta m_{dw(i,4)} c_{pdw} T_{dw,n(i,4)} \\ &= k_{dw}\Delta z \Delta x \left[\frac{\left(T_{dw,w}-T_{dw,e}\right)}{\delta_{dw}}\right]_{(i,4)} \\ &= k_{dw}\Delta z \Delta x \left[\frac{\left(T_{dw}-T_{dw,e}\right)}{\delta_{dw2}}\right]_{(i,4)} \\ &= \left(\delta Q_{dw,w} + \delta Q_{dw,n} - \delta Q_{dw,s}\right)_{(i,4)}\end{aligned} \quad \textbf{(3. 172)}$$

$$\delta_{dw(i,4)} = \left[\frac{3\mu_{dw}\delta m_{dw(i,4)}}{\rho_{dw} g \Delta x(\rho_{dw}-\rho_a)}\right]^{\frac{1}{3}} \quad \textbf{(3. 173)}$$

$$T_{dw(i,4)} = \left[T_{wo} - \frac{5(T_{wo}-T_{dws})}{8}\right]_{(i,4)} \quad \textbf{(3. 174)}$$

$$\delta_{dw1(i,4)} = \left[\frac{\left(T_{dw,w}-T_{dw}\right)\delta_{dw}}{\left(T_{dw,w}-T_{dw,e}\right)}\right]_{(i,4)} \quad \textbf{(3. 175)}$$

$$\delta_{dw2(i,4)} = \left[\frac{\left(T_{dw}-T_{dw,e}\right)\delta_{dw}}{\left(T_{dw,w}-T_{dw,e}\right)}\right]_{(i,4)} \quad \textbf{(3. 176)}$$

d) Grid point (*i*,5)

The governing equation (3.127), (3.131), (3.132) and (3.133) are discretised as

$$\begin{aligned}\left(\delta Q_{ac,w} + \delta m_a \Delta w i_v\right)_{(i,5)} &= \delta m_a \Delta i_{ma(i,5)} \\ &= \delta m_a \left(i_{ma,n} - i_{ma,s}\right)_{(i,5)}\end{aligned} \quad \textbf{(3. 177)}$$

$$\begin{aligned}\delta Q_{ac,w(i,5)} &= h_a \Delta z \Delta x \left(T_{a,w} - T_a\right)_{(i,5)} \\ &= \delta m_a c_{pa}\left(T_{a,n} - T_{a,s}\right)_{(i,5)} + \delta m_a \left[w_{n(i,5)} c_{pv}\left(T_{a,n} - T_a\right)_{(i,5)} + w_{s(i,5)} c_{pv}\left(T_a - T_{a,s}\right)_{(i,5)}\right]\end{aligned} \quad \textbf{(3. 178)}$$

$$\delta Q_{am,w(i,5)} = \delta m_a (i_v \Delta w)_{(i,5)} = h_d \Delta z \Delta x i_{v(i,5)} (w_{sw} - w)_{(i,5)} \quad \textbf{(3. 179)}$$

3.5. Solution methods

In this study, both one and two-dimensional techniques are employed in the evaluation of thermal performance of a delugeable flat tube air-cooled steam condenser bundle. The one-dimensional methods are performed in order to validate the numerical two-dimensional solutions, and to find out whether the numerical method is adequate to provide the correct results, to predict the bundle's performance.

3.5.1. One-dimensional solution methods

For one-dimensional model, the bundle's performance is investigated based on three methods of analysis: Merkel, Poppe, and heat and mass transfer analogy. The major assumption made in all these methods is the constant temperature difference between the steam and deluge water or air.

For both Merkel and Poppe analysis, the mass transfer coefficient at the air-water interface is attained from the relationship between heat and mass transfer coefficient at the air-water interface through a Lewis factor, which can be determined as

$$Le_f = \frac{h_a}{c_{pma} h_d} \quad \textbf{(3. 180)}$$

Then, the mass transfer coefficient is defined as

$$h_d = \frac{h_a}{c_{pma} Le_f} \quad \textbf{(3. 181)}$$

For Merkel's analysis, Lewis factor assumed to be equal to one ($Le_f = 1$), and outlet air is assumed to be saturated with water vapour, while for Poppe approach, the Lewis factor is determined by employing Bosnjakovic (1965) equation as

$$Le_f = 0.866^{0.667} \left(\frac{w_{sw}+0.622}{w+0.622} - 1\right) / ln\left(\frac{w+0.622}{w+0.622}\right) \quad \textbf{(3. 182)}$$

For the heat and mass transfer analogy method, the mass transfer convection coefficient is determined from the analogy between heat and mass transfer at the air-water interface. Since the air flows from the bottom of the tube bundle, the boundary values of inlet air temperature, air mass flow rate and humidity ratio are known at the bottom of the tube bundle. Therefore, outlet air temperature and air humidity ratio, as well as deluge water inlet and outlet temperature can be obtained through an iteration process, whereby the initial values are guessed. The iteration process is completed when the inlet and outlet temperature values of deluge water are the same.

3.5.2. Two-dimensional solution method

For the comprehensive assessment of thermal performance of the tube bundle, a two-dimensional analysis is conducted based on heat and mass transfer analogy method of analysis. Unlike one-dimensional analysis, two-dimensional analysis takes into account the heat transfer in both z and y-directions. The discretised governing equations of a two-dimensional model are solved numerically. The numerical method is complex and consumes time. However, it is analogous to the laboratory experiment and provides a set of solutions that indicate the distribution of the variables within the domain (Suhas, 1980).

For each control volume the local temperature value at each grid point as well as the local heat transfer across the control volume is determined. The evaluation and calculations are performed interval by interval starting from the top of the tube.

Procedure of solving method:

1) The boundary initial values of condensate temperature and mass flow rate, tube wall temperature, deluge water inlet temperature, outlet air temperature and humidity ratio for the top grid cells are assumed. The steam condensation is assumed to take place at constant condensing temperature.
2) The calculations are performed for the whole top interval, until all the discretised governing equations are satisfied.
3) The input values of the top interval are then taken as the output values of the interval below.

This procedure is repeated for each interval until the given boundary conditions at the bottom of the tube bundle are satisfied. The sample of calculation of the two-dimensional numerical model is presented in appendix C.

3.6. Validation of a two-dimensional numerical model

The accuracy of the numerical solutions is sensitive to grid cell sizes. Therefore, in this section, a two-dimensional numerical model is validated by performing the grid dependency, and by comparing its solutions to the one-dimensional results. The manual grid refinement method is employed to investigate the impacts of the grid dependency on the numerical solutions. In order to attain the grid

independent numerical results, the tube is divided into several intervals/rows (N_r) in the z-direction. As the number of the intervals increases the size of the grid cells become smaller and the variations in the numerical solutions become lesser, and therefore solutions tend toward constant values.

The model's validation is performed based on the following typical designing conditions of the delugeable tube bundle: steam temperature - $T_s = 45$ ℃, atmospheric pressure - $p_a = 101325$ Pa; ambient inlet air temperature - $T_a = 15$ ℃; relative humidity - $\phi = 60$ %; air velocity - $v_a = 2\ m/s$; and deluge water mass flow rate - $m_{dw} = 10\ \Delta m_{dw}$. For this validation, the flow on the air-side is considered based on Figure 3.16. The critical tube height (H_{cr}) at which two air-side boundary layers reach the symmetric line between the tubes as shown in Figure 3.16 is computed. The flow within the critical height is considered to be a developing flow, and therefore the heat transfer rate and air-side pressure drop within this region are determined by employing the external flow theories. The flow in the rest of the air flow channel (δ_a) is considered to be a fully developed flow.

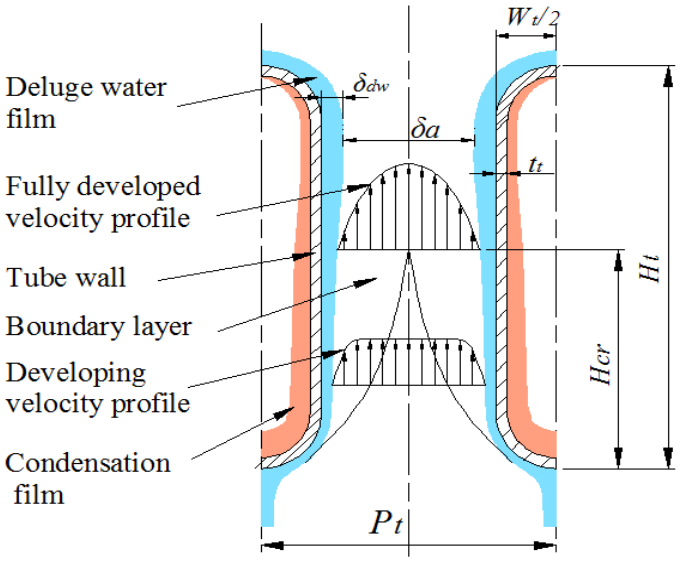

Figure 3.16: Tube bundle section, illustrating the air-side flow between two adjacent tubes

The effect of the physical grid cells' size on the numerical solutions is shown in Figure 3.17. The normalised values of calculated variables, as presented in the legends of the graph, are plotted against the number of intervals. From Figure 3.17, it is clear that up to interval number 15, ($N_r = 15$), the numerical results highly vary with grid cells' size; while beyond interval number 15, the variations in the numerical solutions are slight smaller and the solutions can be taken as constant. Therefore, the solutions are grid independent as from interval number 15, and that further grid refinement will provide grid independent solutions.

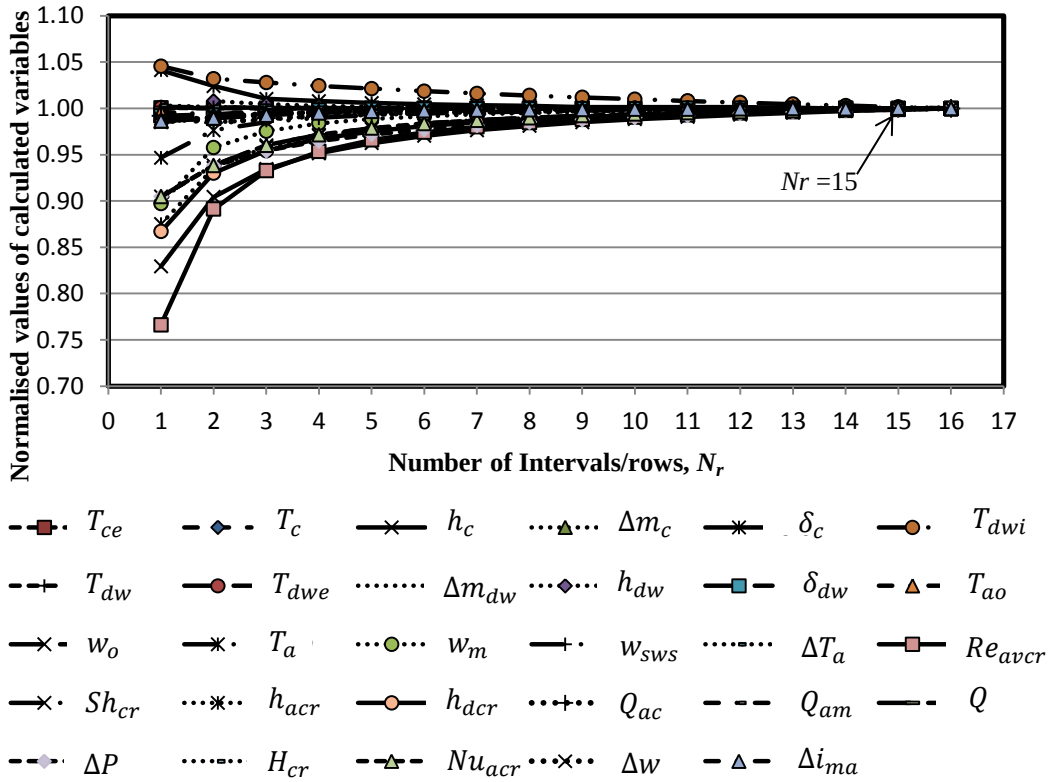

Figure 3.17: Graph illustrating the grid dependency of the numerical solutions

For the converged numerical solutions ($N_r = 15$), the temperature profiles of the condensate, deluge water and air along the tube height are depicted in Figure 3.18. From Figure 3.18, it can be seen that the deluge water temperature increases as water hits the tube's surface and decreases as water flows downward, while the air temperature increases as air flows upward. The temperature of deluge water deviated from the mean temperature value by less than 4.5 %.

The condensation and deluge water heat transfer coefficients are found to be more depending on the film thicknesses and variations of the properties. Figure 3.19 and 3.20 show the condensation and deluge water heat transfer coefficients, respectively as well as the films' thickness along the tube height. The maximum values of both heat transfer coefficients occur at the location where the film thickness is minimum. On the air-side, the boundary layer thickness increases in the flow direction until the flow becomes fully developed. Therefore, as expected in the critical region the heat transfer and friction coefficient decrease in the flow direction as illustrated in Figure 3.21 and 3.22, respectively. However, in the fully developed flow region the heat transfer coefficient and friction factor become constant. Since the mass transfer coefficient is determined from the analogy between heat and mass transfer at the air-water interface, its changes along the tube height is the same as that of air-side heat transfer coefficient.

The comparison of two-dimensional numerical solutions to one-dimensional results is presented in table 3.1. Solutions obtained from all methods are

comparable. Poppe method provides slightly high heat transfer rate followed by Merkel analysis, and heat and mass transfer analogy method delivers the lowest. The two-dimensional numerical solutions are closer to the solutions of heat and mass transfer analogy method with 1.98% difference in heat transfer rate. The difference in air-side pressure drop yielded from all methods is found to be insignificant. The discrepancies between one and two-dimensional solutions are mainly attributed to the assumptions made in one-dimensional model and variation of air and water properties in two-dimensional model.

Furthermore, one can conclude that there are no substantial differences between solutions obtained using one or two dimensional model. Thus, the two-dimensional model is demonstrated to be valid for the analysis of the thermal performance of a delugeable flat tube air-cooled steam condenser bundle.

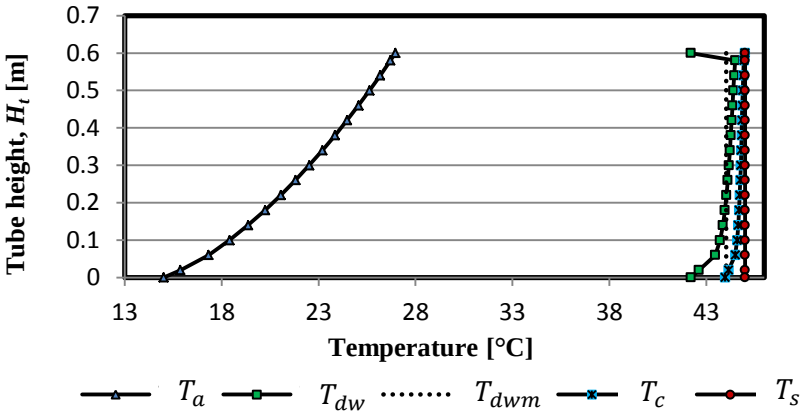

Figure 3.18: The distribution of the temperature of air, deluge water, condensate and steam along the tube height

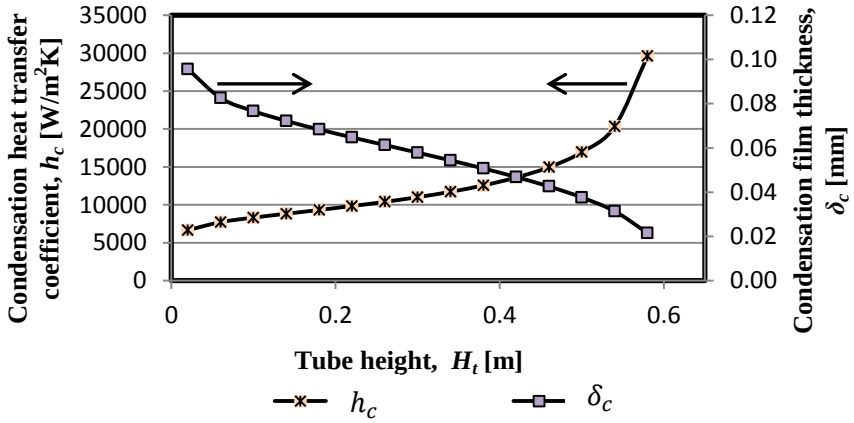

Figure 3.19: Condensation heat transfer coefficient and film thickness along the tube height

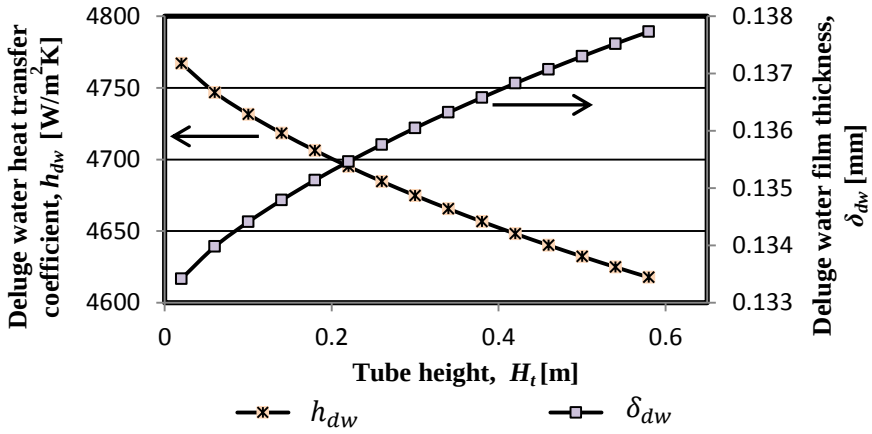

Figure 3.20: Deluge water heat transfer coefficient and film thickness along the tube height

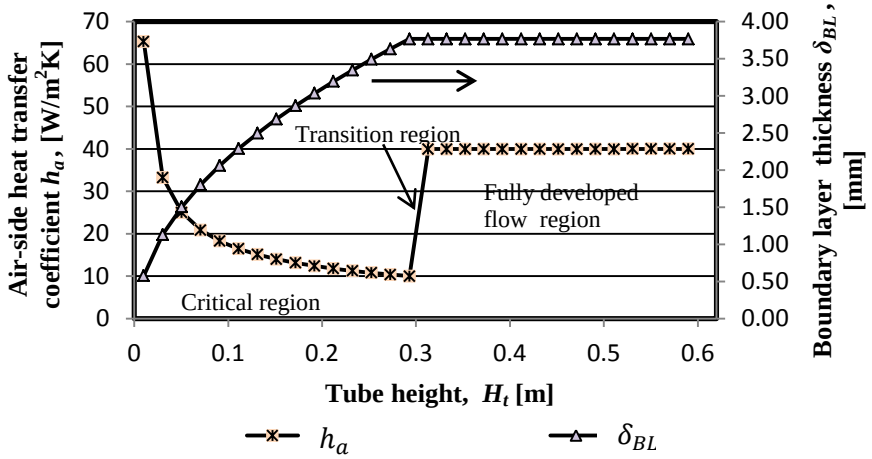

Figure 3.21: Air-side heat transfer coefficient and boundary layer thickness along the tube height

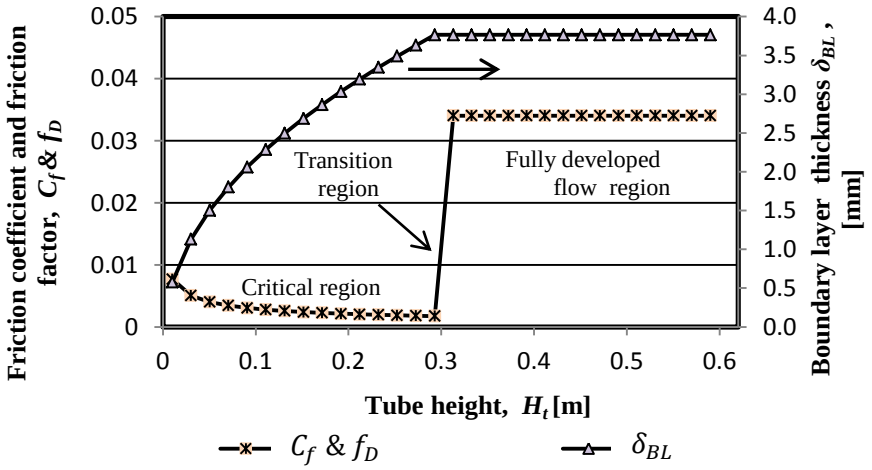

Figure 3.22: Friction coefficient, friction factor and boundary layer thickness along the tube height

Table 3.1 Comparison of two-dimensional numerical solutions to one-dimensional results

			One-dimensional model			Two-dimensional model
Description	**Symbol**	**Units**	**Poppe**	**Merkel**	**Heat and mass transfer analogy**	
Condensate mean temperature	T_{cm}	℃	44.738	44.748	44.769	44.727
Tube wall temperature	T_{wi}	℃	44.651	44.664	44.692	44.635
Condensation rate	m_c	kg/s	0.002047	0.001990	0.001863	0.001763
Condensation heat transfer coefficient	h_c	W/m² K	11720.21	11831.16	12093.52	12785.56
Deluge water inlet temperature,	T_{dwi}	℃	43.936	44.007	44.062	42.208
Deluge water mean temperature	T_{dwm}	℃	43.936	44.007	44.062	44.029
Deluge water surface temperature	T_{dws}	℃	43.589	43.692	43.757	43.736
Deluge water evaporation rate	Δm_{dw}	kg/s	0.001585	0.001420	0.001416	0.001389
Deluge water mass flow rate	m_{dw}	kg/s	0.015855	0.014203	0.014160	0.01389
Deluge water heat transfer coefficient	h_{dw}	W/m² K	4412.01	4579.32	4585.80	4680.70
Outlet air temperature,	T_{ao}	℃	27.261	29.846	27.224	26.88
Outlet air humidity ratio	w_o	kg/kg	0.02948	0.02707	0.02714	0.02661
Air mean temperature	T_{am}	℃	21.130	22.423	21.112	22.0598
Air mean humidity ratio	w_m	kg/kg	0.01792	0.01672	0.01675	0.01821
Air humidity ratio at the air-water interface	w_{sw}	℃	0.06151	0.06175	0.06088	0.06084
Air temperature difference	ΔT_a	℃	12.261	14.846	12.224	11.881
Air humidity ratio difference	Δw	kg/kg	0.02311	0.02071	0.02078	0.02025
Air-vapour mixture enthalpy difference	Δi_{ma}	J/kg	71492.64	68079.34	65483.56	63778.03
Reynolds number (critical region)	$Re_{av,cr}$		149103.09	148128.77	147236.36	145996.16
Nusselt number(critical region)	$Nu_{a,cr}$		228.84	228.05	227.41	224.95
Sherwood number(critical region)	Sh_{cr}		0.00	0.00	217.61	215.25
Air-side heat transfer coefficient (critical region)	$h_{a,cr}$	W/m² K	19.453	19.499	19.425	19.180

Table 3. 1: Comparison of two-dimensional numerical solutions to one-dimensional results, continued…

			One-dimensional model			Two-dimensional model
Description	**Symbol**	**Units**	**Poppe**	**Merkel**	**Heat and mass transfer analogy**	
Mass transfer coefficient (critical region)	$h_{d,cr}$	m/s	0.01991	0.01878	0.01781	0.01777
Air-side heat transfer coefficient (fully developed region)	$h_{a,fd}$	$W/m^2 K$	40.013	39.995	39.746	39.954
Mass transfer coefficient (fully developed region)	$h_{d,fd}$	m/s	0.04095	0.03852	0.03577	0.03582
Sensible heat	Q_{ac}	W	0	0	802.34	783.43
Latent heat	Q_{am}	W	0	0	3661.11	3591.05
Heat transfer rate	Q_a	W	4903.93	4767.16	4463.33	4374.76
Friction coefficient	C_f		0.00344	0.00346	0.00347	0.00299
Friction factor	f_D		0.03402	0.03406	0.03409	0.03405
Air-side pressure drop	ΔP	p_a	30.915	31.001	30.555	29.599
Fan power	P_F	W	1.779	1.792	1.747	1.709
Tube critical height	H_{cr}	m	0.30324	0.30266	0.30176	0.30317

4. Parametric study

In this chapter, a study of the effects of tube height, tube pitch, tube width, deluge water mass flow rate, frontal air velocity, steam, and air operating conditions on the heat transfer rate and air-side pressure drop of the deluged flat tube bundle is performed. The parametric study is conducted by employing the heat and mass analogy method of analysis. During the parametric study, the examined parameter is varied, while keeping the other parameters constant, and then the changes in heat transfer rate and air-side pressure drop are observed. The investigation of the impacts of tube height, tube pitch, tube width, deluge water mass flow rate, and frontal air velocity is executed at two different standard operating conditions: $T_s = 38$ ℃; $T_a = 32$ ℃; $RH = 38\%$ and $T_s = 45$ ℃; $T_a = 15$ ℃; $RH = 60$ %.

To ensure that the obtained results are independent from the tube geometry, the air velocity between the tubes is kept constant for all cases in which air velocity effects are not investigated. Meanwhile, the deluge water mass flow rate is considered to be ten times the evaporation rate, and tube width is taken to be 20 mm for all cases in which the deluge water mass flow rate and tube width effects are not examined. Throughout the study, the tube wall thickness is kept constant at 1.5 mm. The investigation is conducted for both wet and dry operating modes.

4.1. Effect of tube height and tube pitch on the heat transfer rate and air-side pressure drop

To study the influences of tube height and tube pitch on the heat transfer rate and air-side pressure drop, the tube height is varied from 0.2 to 1 m, whereas tube pitches of 25, 28 and 30 mm are considered. The obtained results of the heat transfer rate (Q_w and Q_d) and air-side pressure drop (ΔP_w and ΔP_d) for wet and dry operating mode are plotted in Figure 4.1 to 4.3.

From the yielded results, it is found that both tube height and pitch have measurable effects on the heat transfer rate and air-side pressure drop, regardless of the operating conditions and operating mode. The heat transfer rate and air-side pressure drop increase as the tube height varies from 0.2 to 1 m. This is due to the fact that the tube height increases the heat transfer surface area and the length of the air flow channel between the tubes, which in turn directly impact on the rate of heat transfer and air-side pressure drop. The increase of the tube pitch widens the air flow channel, thins the boundary layer thickness, and lengthens the tube critical height. Consequently, the air-side heat transfer and friction coefficients drop. As a result, the heat transfer rate and air-side pressure drop decrease.

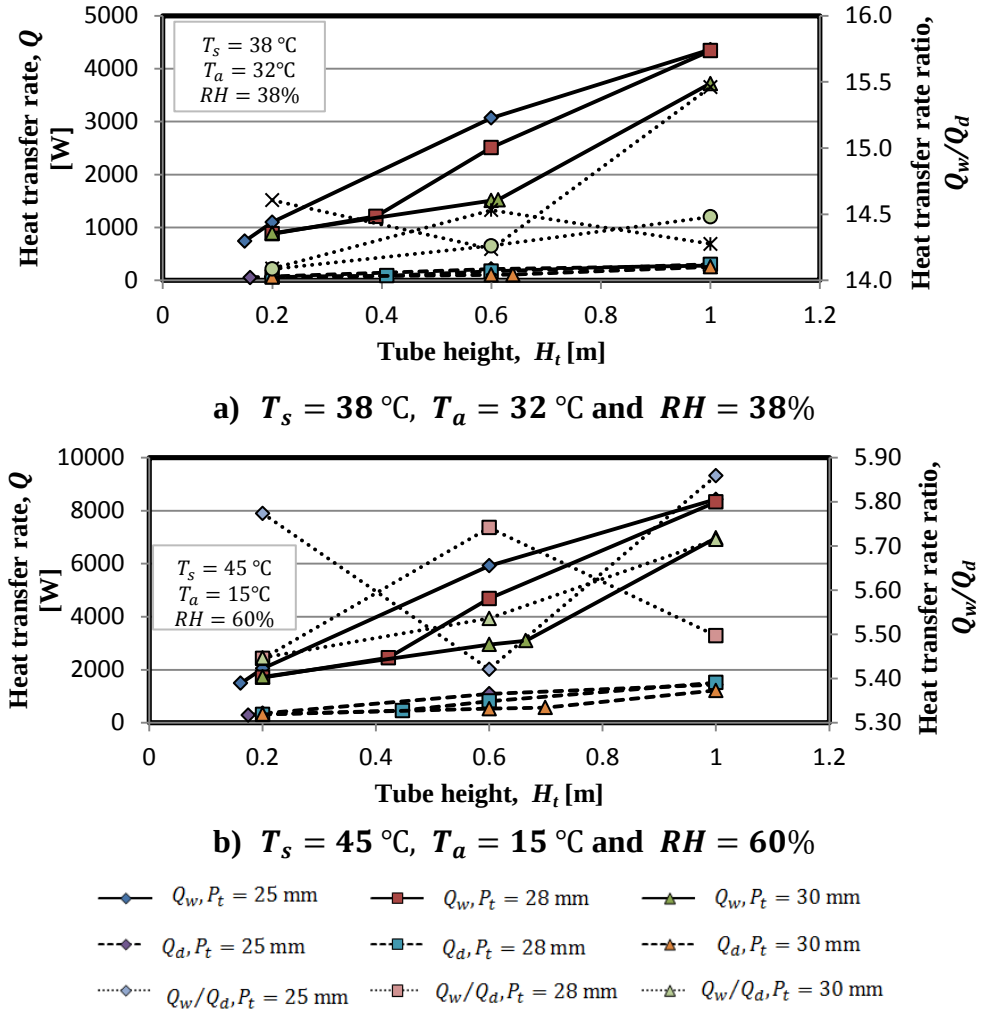

Figure 4.1: Effect of tube height and pitch on the heat transfer rate - one dimensional model

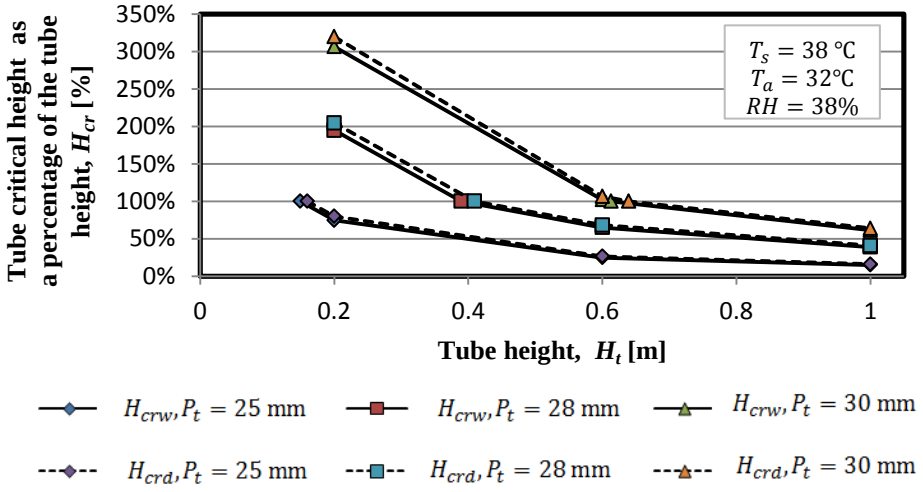

Figure 4.2: Tube critical height as a percentage of tube height - one dimensional model

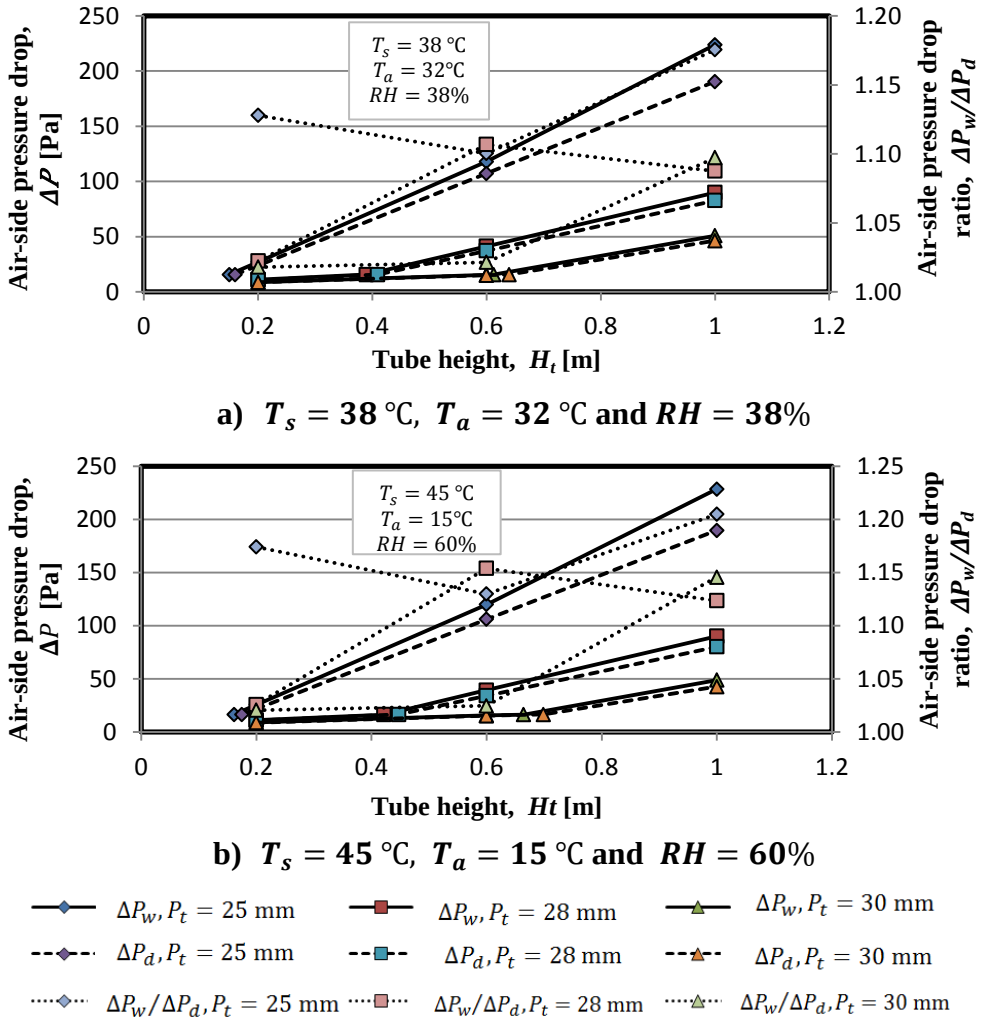

Figure 4.3: Effect of tube height and pitch on the air-side pressure drop - one dimensional model

4.2. Effect of tube width on the heat transfer rate and air-side pressure drop

To examine the impact of tube width on the heat transfer rate and air-side pressure drop, the tube width of 20 and 23 mm are considered. The investigation is conducted for a fixed tube pitch of 28 mm, since this tube pitch provides the best heat transfer rate at a reasonable air-side pressure drop. For the same reason, the 28 mm tube pitch is also used in all the investigations presented in sections 4.3, 4.4, 4.5 and 4.6.

The yielded results that demonstrate the influence of the tube width are depicted in Figure 4.4 and 4.5. For both operating modes and conditions, it is observed that as the tube width varies from 20 to 23 mm, both heat transfer rate and air-side pressure drop increase. However, the increase of the air-side pressure drop is found to be higher than of the heat transfer rate. This is due to the fact that the

increase of the tube width reduces the air flow area between the tubes. This thickens the boundary layer thickness, which shortens the tube critical height. Consequently, the air-side heat transfer and friction coefficient increase. For both dry and wet operating modes, air-side pressure drop ratio ($\Delta P_{23}/\Delta P_{20}$) for tube width of 23 mm and 20 mm is found to be greater than two , while the heat transfer rate ratio (Q_{23}/Q_{20}) is less than two.

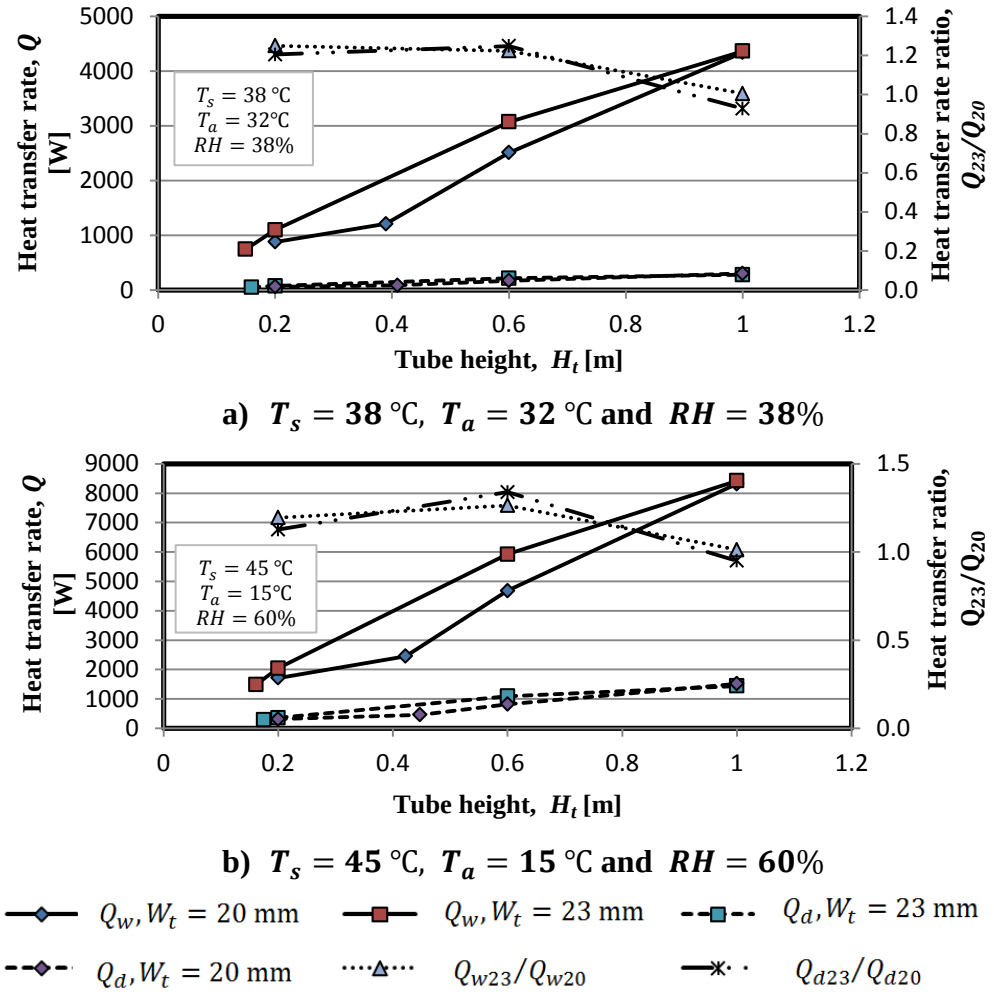

Figure 4.4: Effect of tube width on the heat transfer rate - one dimensional model

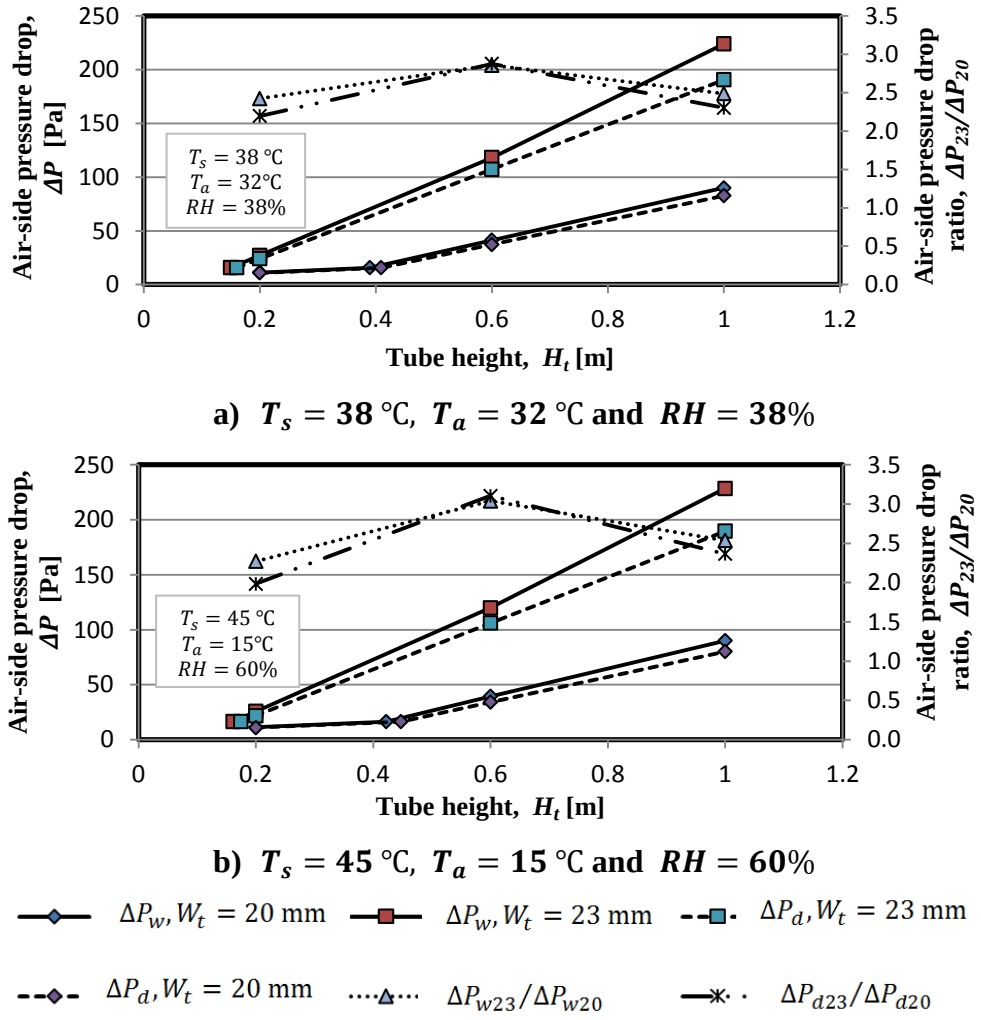

Figure 4.5: Effect of tube width on the air-side pressure drop - one dimensional model

4.3. Effect of deluge water mass flow rate on the heat transfer rate and air-side pressure drop

The effect of deluge water mass flow rate on the heat transfer rate and air-side pressure drop is examined at three deluge mass flow rates: $m_{dw1} = 5\,\Delta m_{dw}$, $m_{dw2} = 7.5\,\Delta m_{dw}$ and $m_{dw3} = 10\,\Delta m_{dw}$, whereby Δm_{dw} is the rate of evaporation. In order to demonstrate the effect of deluge water mass flow rate clearly, the heat transfer rate ($Q_{mdw1} = Q_{ref}$) and air-side pressure drop ($\Delta P_{mdw1} = \Delta P_{ref}$) achieved when the deluge water mass flow rate is equal to m_{dw1}, are taken to be reference data.

As can be seen in Figure 4.6 and 4.7, the variations in the obtained results are small. This indicates that, the performance of the flat tube bundle is insensitive to the changes in deluge water mass flow rate. However, from a closer observation it is found that as the deluge water mass flow rate increases from m_{dw1} to m_{dw3}

there is a slight decrease in the rate of heat transfer and insubstantial increase in the air-side pressure drop. The increase of the deluge water mass flow rate thickens the deluge water film; as a result the air flow area between tubes reduces. The thick deluge water film may build resistance to the heat transfer, which may result in the drop of the heat transfer rate. At the tube height of 0.6 m, the opposite changes in heat transfer rate are obtained. This is due to the effect of tube critical height which decreases as the deluge water mass flow rate increases.

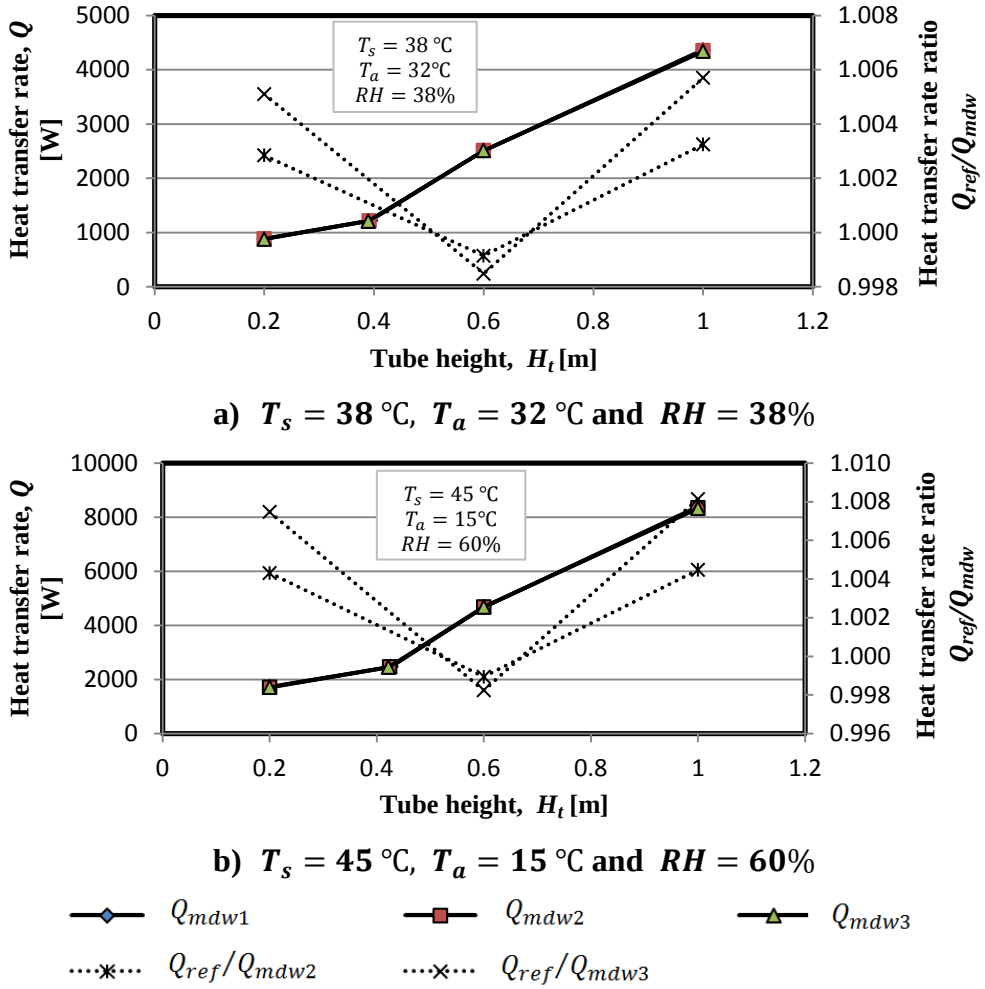

Figure 4.6: Effect of deluge water mass flow rate on the heat transfer rate - one dimensional model

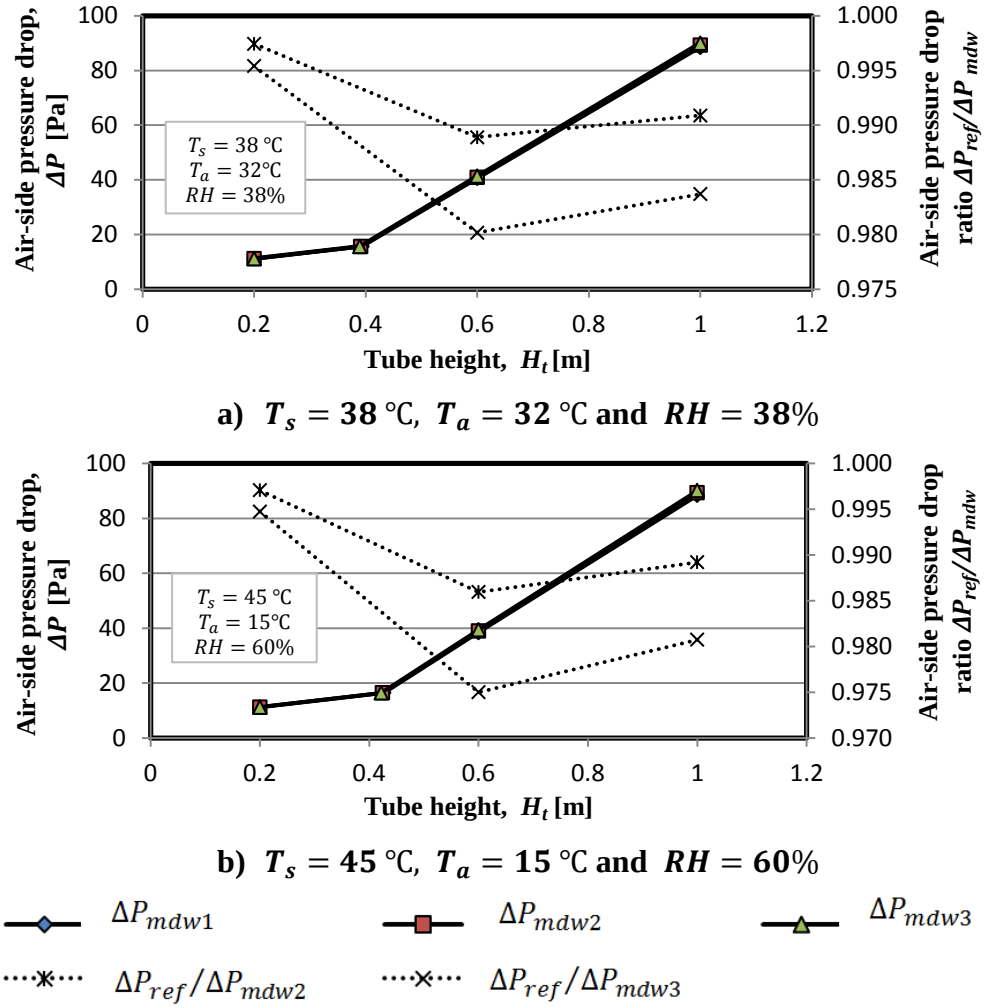

Figure 4.7: Effect of deluge mass flow rate on the air-side pressure drop - one dimensional model

4.4. Effect of frontal air velocity on the heat transfer rate and air-side pressure drop

In order to study the effect of frontal air velocity on the heat transfer rate and air-side pressure drop, three frontal air velocities of $v_{a1} = 2\ m/s$, $v_{a2} = 3\ m/s$ and $v_{a3} = 3.5\ m/s$ are considered. For the critical analysis of the effect of frontal air velocity, the heat transfer rate ($Q_{va3} = Q_{ref}$) and air-side pressure drop ($\Delta P_{va3} = \Delta P_{ref}$) obtained at air velocity of $v_{a3} = 3.5\ m/s$ are taken to be reference data.

For all considered operating conditions and modes, the heat transfer rate and air-side pressure drop are found to increase as the air velocity varies from 2 to 3.5m/s as depicted in Figure 4.8 and 4.9. Furthermore, it is noted that the changes in the air-side pressure drop is higher than in the heat transfer rate. This shows that the high frontal air velocity increases the tube bundle's performance; which is associated with high air-side pressure drop. For short tube heights, there is an

overlap in the heat transfer rate and air-side pressure drop values, which are attained at different air velocities. This is due to the effect of the tube critical height, which increases with the frontal air velocity.

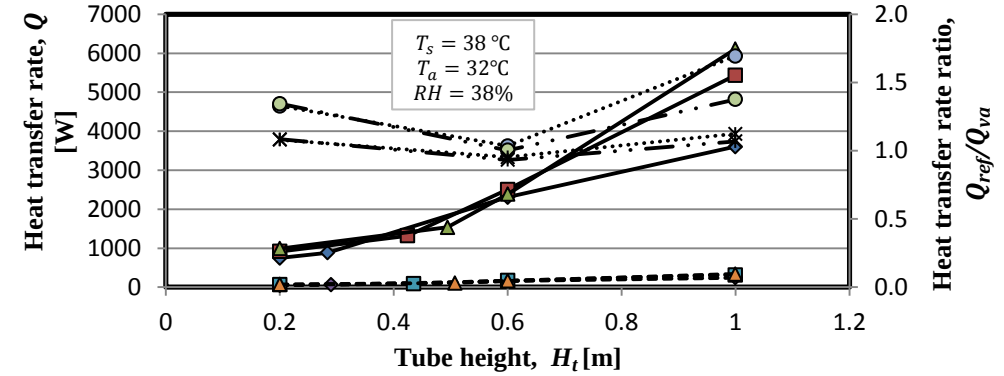

a) $T_s = 38$ ℃, $T_a = 32$ ℃ and $RH = 38\%$

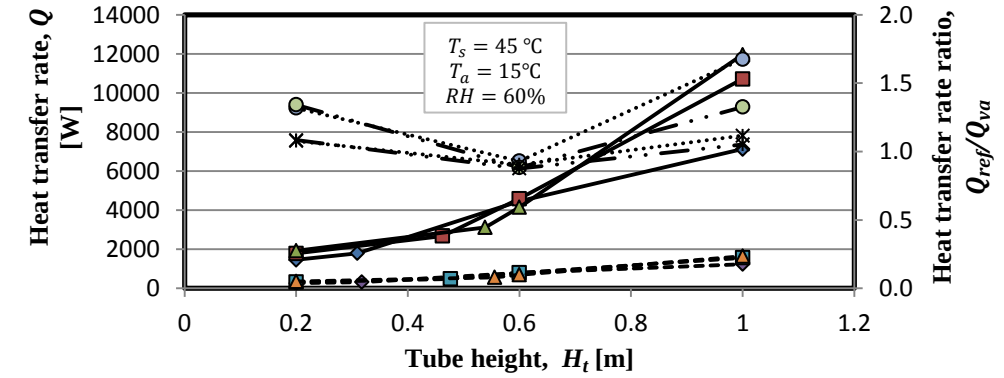

b) $T_s = 45$ ℃, $T_a = 15$ ℃ and $RH = 60\%$

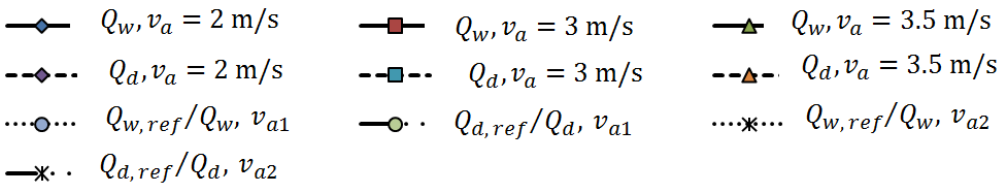

Figure 4.8: Effect of frontal air velocity on the heat transfer rate - one dimensional model

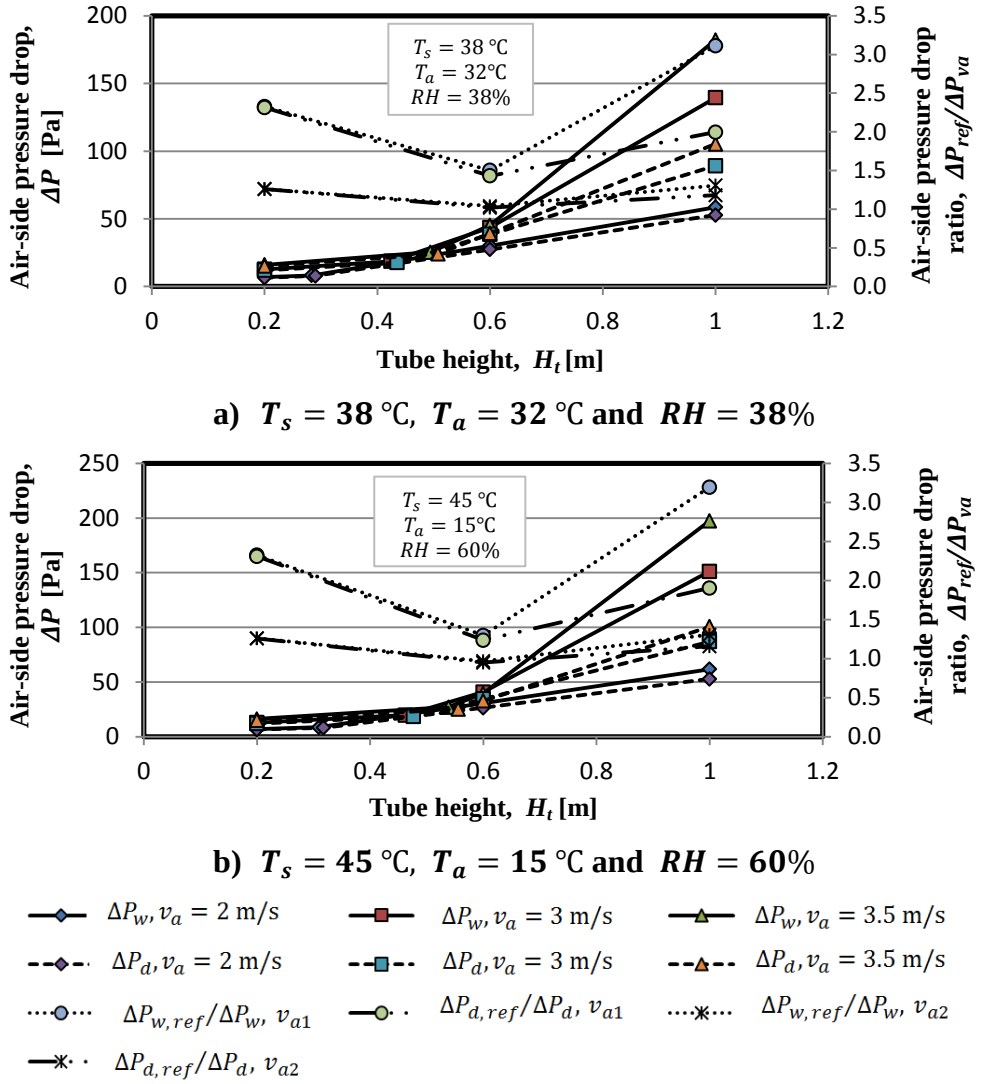

Figure 4.9: Effect of frontal air velocity on the air-side pressure drop - one dimensional model

4.5. Effect of steam operating conditions on the heat transfer rate and air-side pressure drop

The influence of steam operating conditions on the heat transfer rate and air-side pressure drop is investigated for two steam temperatures: $T_s = 45$ ℃ and $T_s = 60$ ℃ at an air temperature of $T_a = 15$ ℃. Figure 4.10 and 4.11 show that the steam temperature has more influence in the heat transfer rate than in the air-side pressure drop, and this is more noticeable in wet operating modes than in dry operating modes. When steam temperature changes from 45 to 60 ^{o}C, the heat transfer rate increases by 2 times and by 1.5 times for wet and dry operating mode respectively. The influence of the steam temperature on the air-side pressure drop is found to be inconsequential. However, the air-side pressure drop is slightly higher at high steam temperature than at low steam temperature.

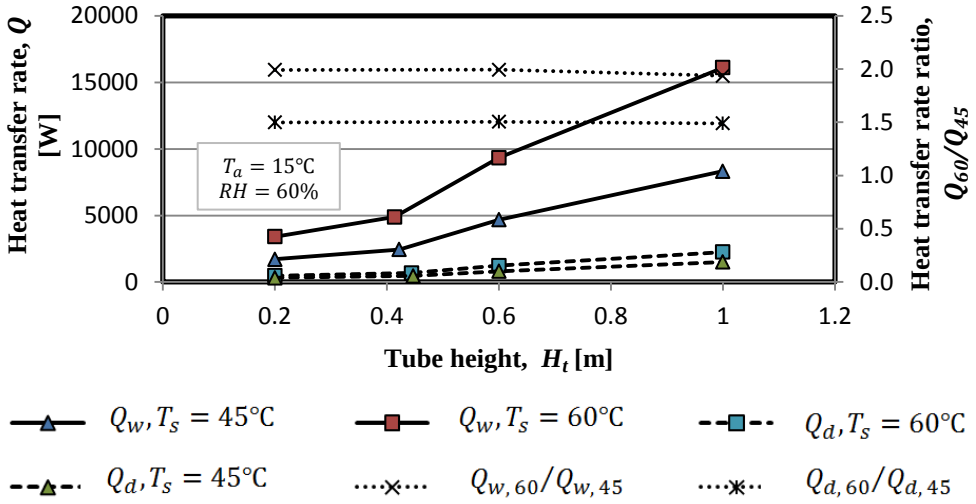

Figure 4.10: Effect of steam temperature on the heat transfer rate - one dimensional model

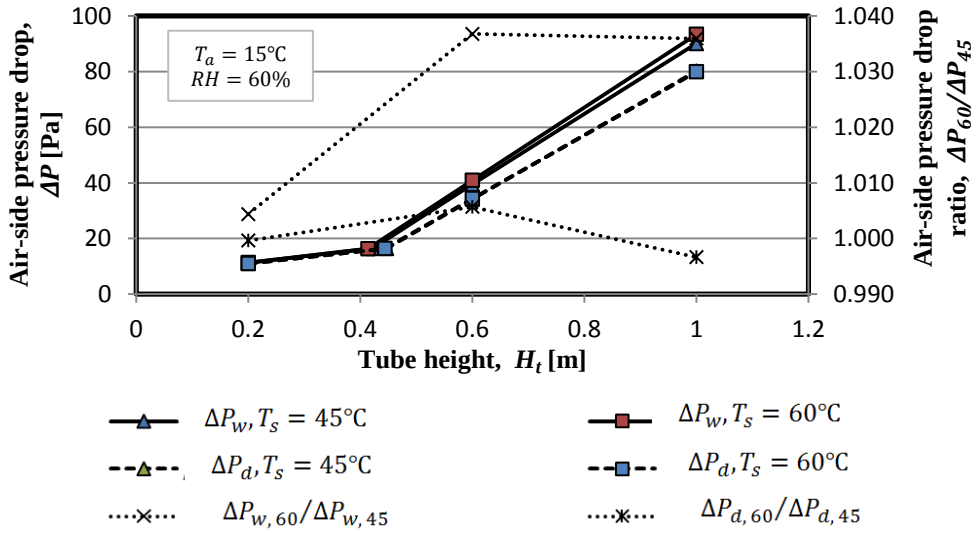

Figure 4.11: Effect of steam temperature on the air-side pressure drop - one dimensional model

4.6. Effect of air operating conditions on the heat transfer rate and air-side pressure drop

The impact of air operating conditions on the heat transfer rate and air-side pressure drop is investigated for two air operating conditions: $T_a = 15$ °C, $RH = 60$ %; and $T_a = 32$ °C, $RH = 38\%$; and at two different steam temperatures $T_s = 38$ °C and $T_s = 60$ °C. From the ratios of the heat transfer rate (Q_{15}/Q_{32}) and air-side pressure drop ($\Delta P_{15}/\Delta P_{32}$), which are obtained at different air operating conditions as depicted in Figure 4.12 and 4.13, the operating conditions of air are found to have a vast influence on the heat transfer rate than on the air-side pressure drop. This is highly noticeable at low steam temperatures in dry

operating modes than in wet operating modes. As the air temperature changes from 15 to 32 °C, for dry operating mode, the heat transfer rate drops by 4 times and by 1.5 times for the operation at steam temperature of $T_s = 38$ ℃ and $T_s = 60$ ℃ respectively. While for wet operating modes, the heat transfer rate drops by 1.2 times or less for both steam temperatures. From this analysis it is clear that the performance of the deluged tube bundle is independent from the ambient air conditions. Regardless of the steam temperature, the effect of air operating conditions on the air-side pressure drop is found to be less.

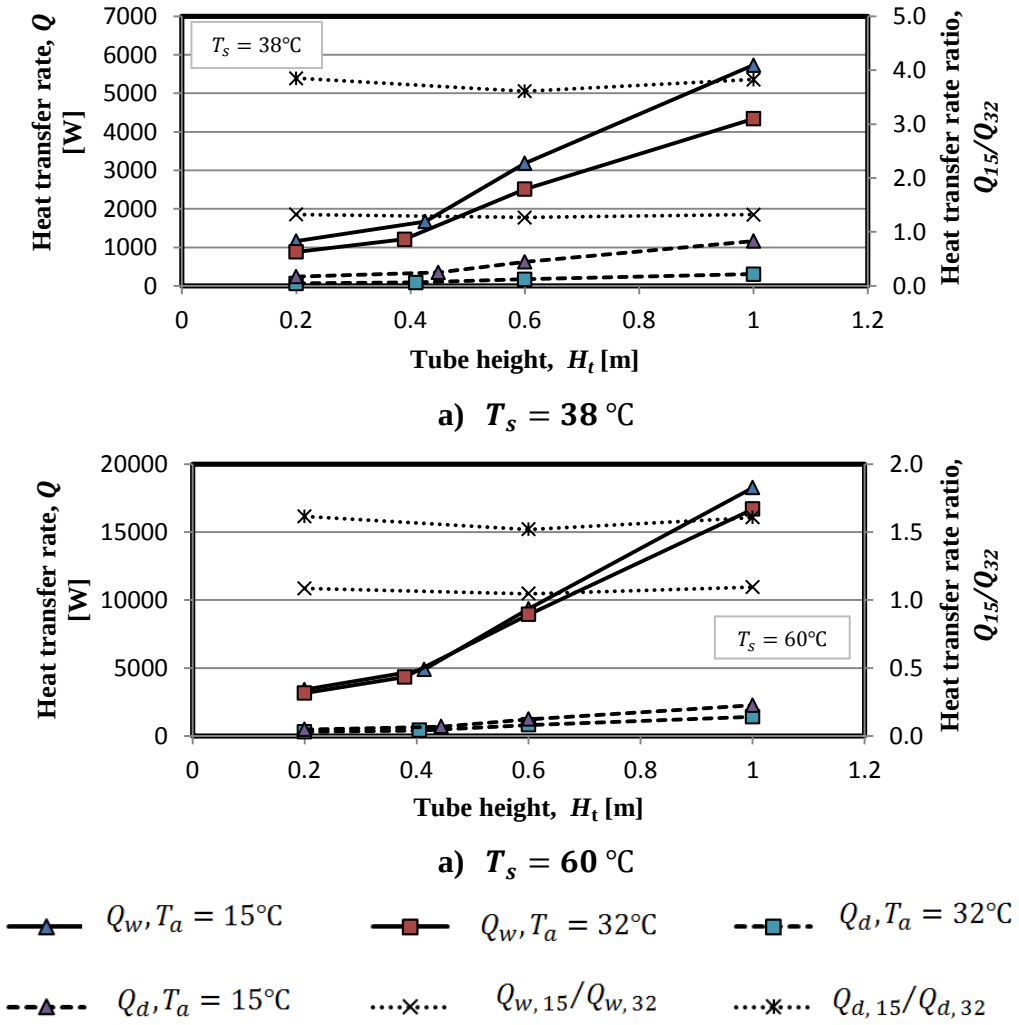

Figure 4.12: Effect of air operating conditions on the heat transfer rate - one dimensional model

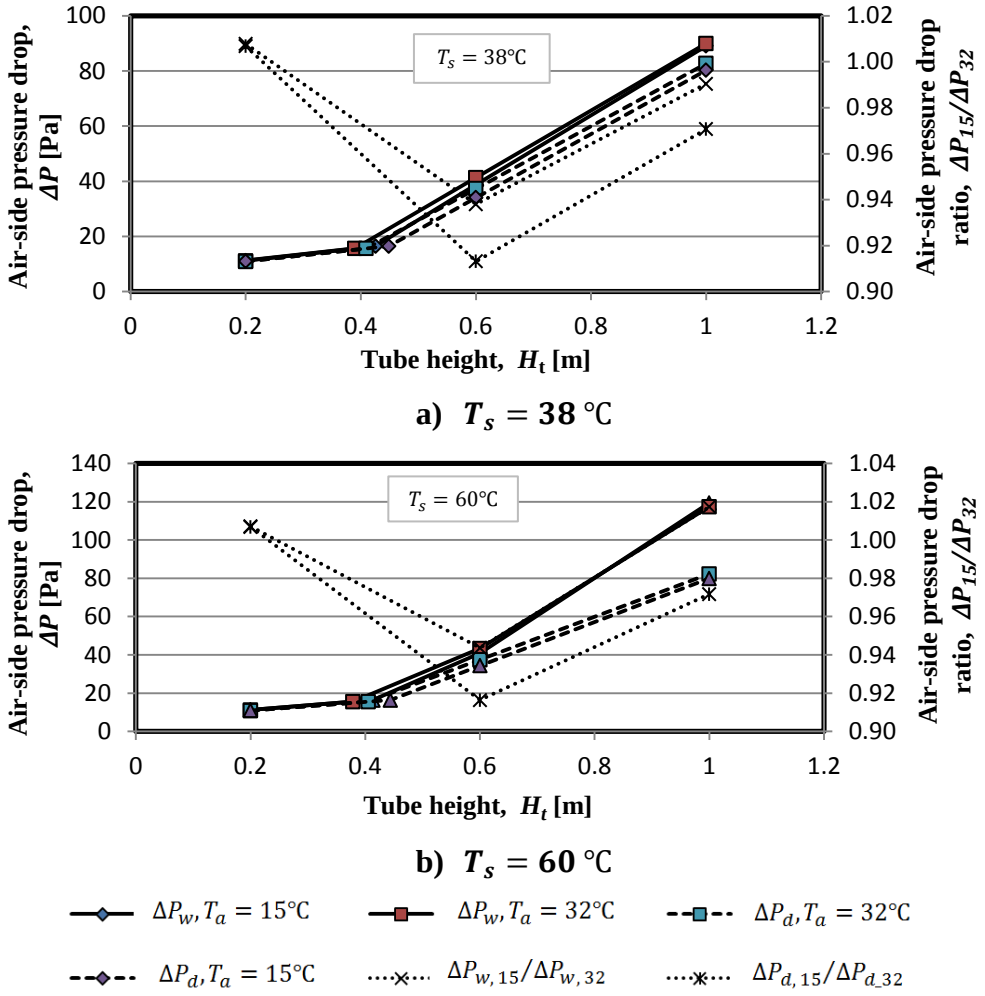

Figure 4.13: Effect of air operating conditions on the air-side pressure drop - one dimensional model

5. Tube bundle configurations

5.1. Introduction

The purpose of this chapter is to identify the configuration of the flat tube bundle for the second stage of induced HDWD, and also to compare its performance to the round tube bundle presented by Anderson (2014). The comparison is performed by investigating the effect of the tube pitch, tube height, and the steam flow area on the heat transfer rate ratio (Q_r/Q_f) and air-side pressure drop ratio ($\Delta P_r/\Delta P_f$) of the round and flat bundles. This study is conducted for the constant frontal area and fan power, which is equal to the value of the round tube bundle. Furthermore, the deluge water mass flow rate is taken to be seven and half times the evaporation rate ($m_{dw} = 7.5\,\Delta m_{dw}$), as also considered for the round tube bundle. The heat and mass transfer analogy method of analysis is employed in evaluation of the performance of the considered tube bundle configuration. The critical performance measures are identified to be heat transfer rate, air-side pressure drop, and fan power. The best tube bundle configuration is found to be the one that provides a higher rate of heat transfer at a reasonable air-side pressure drop.

In Figure 5.1, the round tube bundle considered by Anderson (2014), which is designed in an attempt to enhance the performance of round tube bundles presented by Heyns (2008) and Owen (2013), is depicted. The bundle is a multi-row with 39 tubes per row and 25 rows. The round tube bundle consists of tubes of 15.8 and 19 mm inner and outer diameter respectively, which are in a triangular arrangement with the tube pitch of 38 mm. The above mentioned bundle is found to be 2.87 m wide, 1 m high and 2.5 m long. The performance of this bundle is analysed by employing Merkel's approach and has its performance data shown in table 5.1.

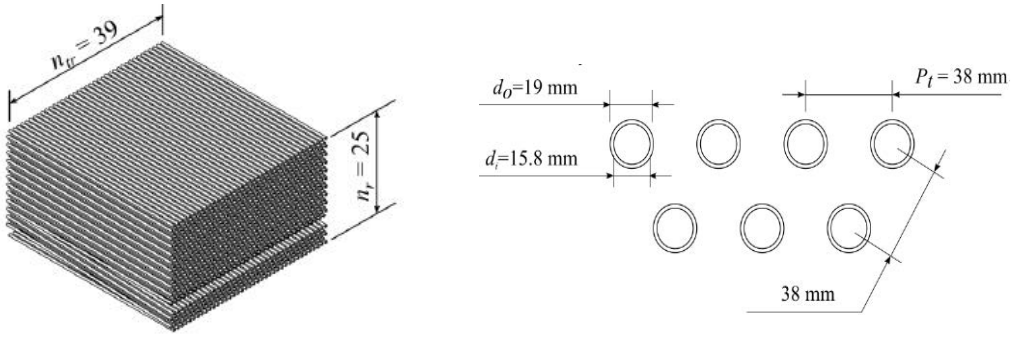

Figure 5.1: Tube bundle presented by Anderson (2014)

Table 5.1: The performance data of a round tube bundle presented by Anderson (2014)

Description	Symbol	Units	Operating mode	
			wet	dry
Heat transfer rate	Q	MW	5.126	0.627
Air-side pressure drop	ΔP	P_a	22.703	22.50
Fan power	P_F	W	417.98	417.892

5.2. Influence of tube pitch on the performance ratio of the bundles

To examine the impact of tube pitch on the performance ratio of the bundles, four tube pitches of 23; 25; 30 and 25 mm are considered. For each tube pitch, the performance ratio is analysed for three different steam flow areas of $A_{sf1} = 0.368\ \text{m}^2$, $A_{sf2} = 2A_{sf1}$, and $A_{sf3} = 3A_{sf1}$; whereby the first steam flow area is equal to the round tube bundle's steam flow area. The tube width corresponding to each steam flow area is computed. This investigation is conducted for both wet and dry operating modes, and the tube height is kept constant at 1 m. In Figure 5.2 and 5.3 the heat transfer rate ratios (Q_r/Q_f) and air-side pressure drop ratios ($\Delta P_r/\Delta P_f$) of the round and flat tube bundle are illustrated. The number of the tubes per row computed for each considered pitch is shown in table 5.2.

From Figure 5.2, it can be seen clearly that, for a constant tube pitch, there is a slight variation in the obtained results for different tube widths. However, a large difference in the yielded results at various tube pitches is observed. This shows that the tube pitch has a measurable effect on the bundle's performance than the tube width. Furthermore, it is found that for small tube pitches, the tubes with small width perform better than those with large widths. Additionally, it is also noted that at the large tube pitches, there is a slight increase in heat transfer rate for the wider tubes. This is due to the fact that for large tube pitches, the air-side pressure drop between the tubes is low. Therefore, since the fan power is constant, the air velocity between tubes is increased in order to achieve the targeted fan power. The air-side pressure drop ratio is found to increase as the tube pitch increases, and drop as the tube width increases.

Table 5.2: Number of tubes per row for the flat tube bundle configurations

Description	Symbol	Units				
Tube pitch	P_t	mm	23	25	30	35
Number of tubes per row	n_{tr}		125	115	96	82

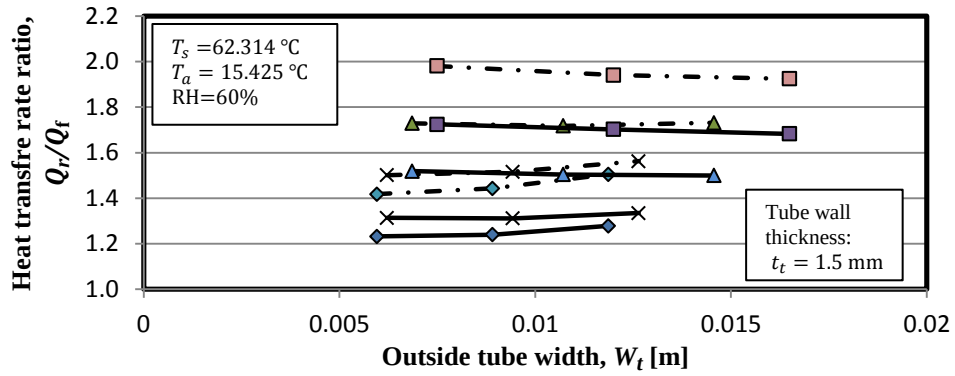

Figure 5.2: Effect of the tube pitch on the heat transfer rate ratio of round and flat tube bundle

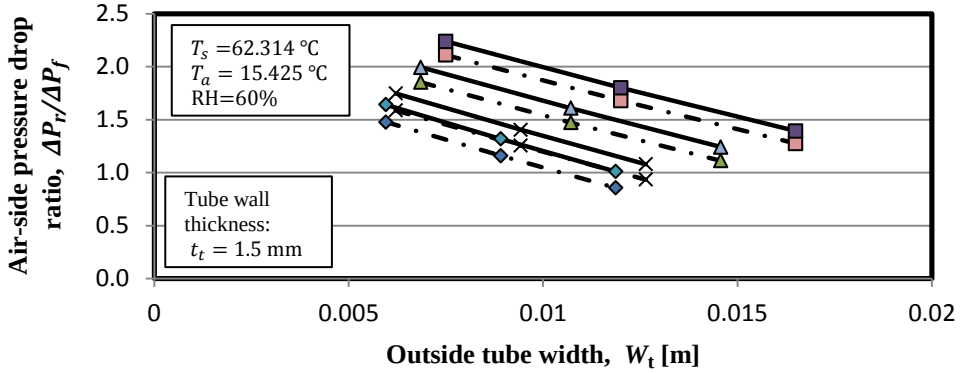

Figure 5.3: Effect of the tube pitch on the air-side pressure drop ratio of round and flat tube bundle

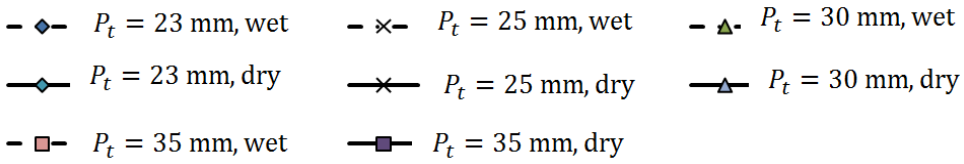

5.3. Influence of tube height on the performance ratio of the bundles

The effect of the tube height on the performance ratio of the bundles is examined for three tube heights of 0.5; 1; and 1.2 m. The tube pitch of 30 mm is considered in this investigation, despite a low performance obtained at this pitch compared to the performance yielded at the tube pitch of 23 and 25 mm. The study of the tube height effects at small tube pitches is found to become impossible and unrealistic for short tubes as the steam flow area changes from A_{sf2} to A_{sf3}.

Figure 5.4 and 5.5 displays the obtained ratios of the heat transfer rate (Q_r/Q_f) and air-side pressure drop ($\Delta P_r/\Delta P_f$) of a round and flat tube bundle. The results show clearly that the short tube height has a huge negative impact in the bundle

performance especially for the large tube width. This is due to the fact that for the constant steam flow area, the tube becomes wider when its height decreases.

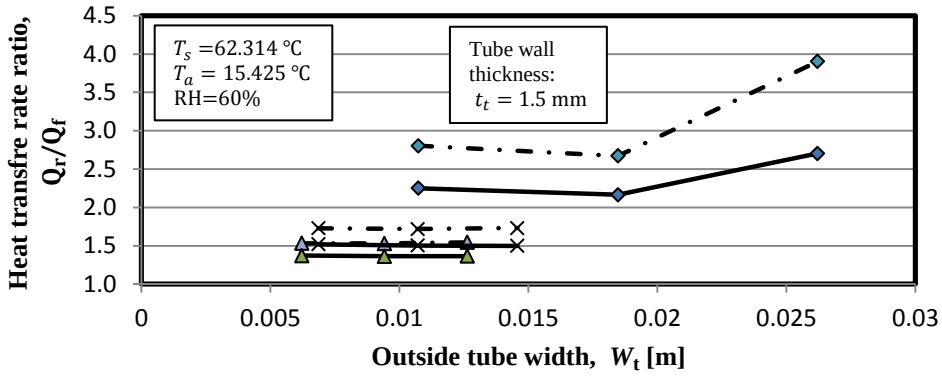

Figure 5.4: Effect of the tube height on the heat transfer rate ratio of round and flat tube bundle

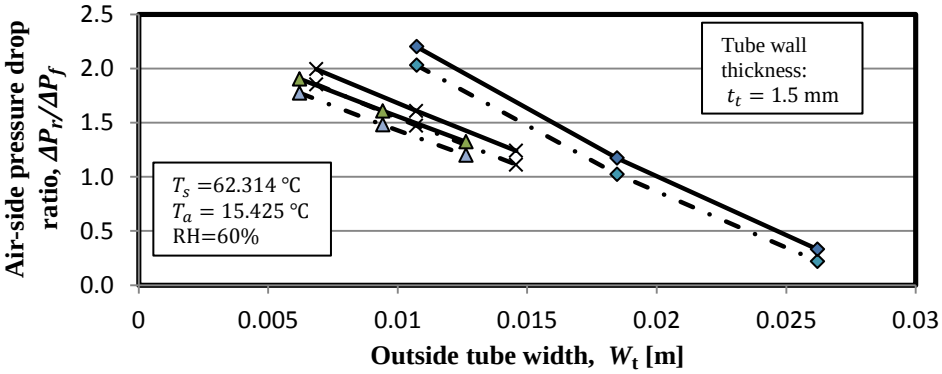

Figure 5.5: Effect of the tube height on the air-side pressure drop ratio of round and flat tube bundle

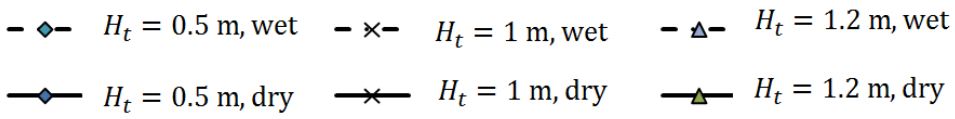

5.4. Tube bundle selection

The best flat tube bundle is selected based on the dimensions and steam flow area of the round tube bundle. From the data presented in section 5.2 and 5.3, the small tube pitches deliver high performance than large pitches. However, as mentioned early their performance analysis becomes unrealistic and impossible at some points. Therefore, the chosen bundle consists of tubes of 1 m long, inside and outside width of 3.86 and 6.86 mm respectively, and arranged with a tube pitch of 30 mm. The detailed data for both flat and round tube bundles are presented in table 5.3. The tube layout and dimensions of the flat tube bundle's configuration are demonstrated in Figure 5.6. As it is already illustrated in Figures 5.2 to 5.5, round tube bundle performs better than the flat tube bundle. In comparison with the selected flat tube bundle configuration, the performance of

the round tube bundle is found to be around 2 times, and 1.5 times, when both bundles operate as an evaporative and dry air-cooled condenser respectively.

Table 5.3: Comparison of the performances of flat and round tube bundles for wet operating mode

Description	Symbol	Units	Anderson (2004) bundle	Configurations
Tube shape			round	flat
Tube dimensions				
Tube height	H_t	m	-	1
Tube width	W_t	mm	∅19	6.86
Tube thickness	t_t	mm	3.2	1.5
Tube pitch	P_t	mm	38	30
Tube bundle properties				
Tube bundle height	H_b	m	1	1
Tube bundle width	W_b	m	2.87	2.87
Tube bundle length	L_b	m	2.5	2.5
Number of tubes per row	n_{tr}		75	96
Number of rows	n_r		25	1
Tube bundle frontal area	A_{frb}	m^2	7.172	7.172
Tube bundle minimum air flow area	A_{cb}	m^2	3.586	5.188
Performance data				
Heat transfer rate	Q	MW	5.215	3.017
Air-side pressure drop	ΔP	P_a	22.703	12.245
Fan power	P_F	W	417.92	417.727
Heat transfer rate ratio	Q_r/Q_f		1.729	
Air-side pressure drop ratio	$\Delta P_r/\Delta P_f$		1.854	

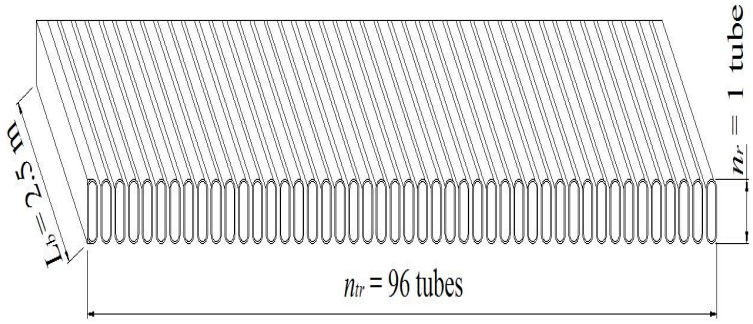

a) Tube layout

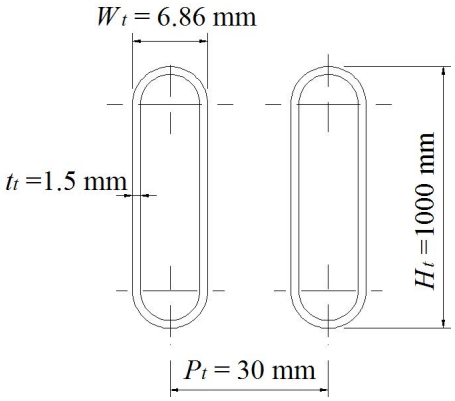

b) Tube dimensions

Figure 5.6: Tube bundle layout and dimensions

6. Conclusions and recommendations

In this study the modelling methods employed in the analysis of the thermal performance of the deluged flat tube bundle of a second stage of an induced draft HDWD of an ACSC are developed. Finally, these modelling methods are used to study the effects of the designing parameters on the bundle's performance.

6.1. Development of models

One and two dimensional models are presented by a set of governing differential equations. The one-dimensional governing equations are solved analytically by means of Merkel, Poppe, and heat and mass analogy methods of analysis. The two-dimensional governing equations are discretised using linear upwind difference method. The discretised algebraic equations are then solved numerically by employing heat and mass analogy methods of analysis.

The solutions of the two models are compared, and the one-dimensional solutions are found to be slightly higher than the two-dimensional solutions with a difference of 1.98%, 8.23%, and 10.79% in heat transfer rate for method of heat and mass analogy, Merkel, and Poppe respectively. The discrepancies in the results are mainly due to the assumed constant temperature difference between steam and deluge water or air in one-dimensional model. The difference in air-side pressure drop obtained by all the methods found to be insubstantial. Therefore, the two-dimensional model is validated for thermal performance analysis of a delugeable flat tube bundle of an ACSC.

6.2. Effect of designing parameters on the bundle performance

From the investigation of the influence of the designing parameters on the thermal performance of the flat tube bundle, it is found that the long tube height, large tube width, small tube pitch and high frontal air velocity increase the tube bundle's performance. However, this performance is associated with high air-side pressure drop. Therefore, a careful selection of these parameters is required during the designing of the tube bundle. The effect of deluge water mass flow rate on the bundle performance is found to be slight; this shows that the tube bundle's performance is insensitive to the variations of deluge water mass flow rate. The impact of steam temperature on the heat transfer rate is high for wet operating modes than dry modes, and its effect on the air-side pressure drop is insignificant. Therefore, operating the deluged tube bundle at high steam temperature is preferable. The influence of air operating conditions at high steam temperature, and for wet operating modes is found to be low, which shows that the performance of a deluged flat tube bundle depends less on air ambient conditions.

The best configuration of a delugeable flat tube bundle is identified through a comparison to round tube bundle presented by Anderson (2014). The performance of the flat tube bundle is found to be lower than that of the round tube bundle for both operating modes.

6.3. Significant of the project

Literature on this subject has limited data especially on the modelling of the performance of a delugeable flat tube bundle of ACSC, since most of the previous studies concentrated on the analysis of the round tube bundles performance. This study developed both analytical and numerical models which can be employed in the evaluation of a delugeable flat tube bundle performance. Therefore, this study fills a certain gap in the field of the engineering despite the fact that the performance of the identified flat tube bundle is lower than that of the round tube bundle. However, further studies can be conducted to enhance the performance of the flat tube bundle. The performance of the identified flat tube bundle is investigated at constant fan power and therefore an increase of the fan power might improve the performance, since the heat transfer rate is directly proportional to the air mass flow rate through the bundle.

References

Anderson, N. R., 2014. Evaluation of the performance characteristics of a hybrid (dry/wet) induced draft dephlegmator. *Master Thesis, University of Stellenbosch, RSA.*

Boulay, R. B., Miroslav , J. C. & Massoudi, M., 2005. Dry and Hybrid condenser cooling design to maximize operating income. *ASME Report, PWR2005-50225, Chicago, Illinois.*

Bosjnakovic, F., 1965. Technical thermodynamics. *Holt, Reinhart and Winston, New York,* pp. 326-331.

Branfield, G., 2003. Precooling of fin-tube heat exchanger inlet air using fine water spray. *B.Eng thesis, University of Stellenbosch, Rep. of South Africa.*

Bykov, A. V., Gogolin, V. A. & Tovaras, N. V., 1984. Investigation of heat, mass transfer and fluid flow characteristics in evaporative condensers. *International Journal of Refrigeration,* Volume 7, pp. 342-347.

Chan , S. H., Dae-Young , L. & Sung , T., 2003. Cooling enhancement in an air-cooled finned heat exchanger by thin water film evaporation. *International Journal of Heat and Mass Transfer,* Volume 46, p. 1241–1249.

Charles , K. & David , C., 2002. Assessment of Evaporative Cooling Enhancement Methods for Air-Cooled Geothermal Power Plants. *National Renewable Energy Laboratory (NREL/CP-550-32394).*

Conradie, T. A. & Kröger, D. G., 1991. Enhanced performance of a dry-cooled power plant through air precooling. *International power generation conference, San Diego, CA.*

Dreyer, A. A., 1988. Analysis of Evaporative Coolers and Condensers. *MSc Thesis, University of Stellenbosch, Rep. of South Africa.*

Duvenhage, K., 1993. Warmteruiling met adiabatiese voorverkoeling. *MSc Thesis, University of Stellenbosch, Rep. of South Africa.*

Erens, P. J. & Dreyer , A. A., 1989. A General Approach for the Rating of Evaporative Closed Circuit Coolers. *N&O JOERNAAL.*

Finlay, I. C. & Grant, W. D., 1972. Air coolers, cooling towers and evaporative coolers,. *National Engineering, Laboratory, East Kilbride, Glasgow, Report No. 534,* p. 165–328.

Finlay , I. C. & Grant , W. D., 1974. The accuracy of some simple methods of rating evaporative coolers. *Report No. 584, National Engineering Laboratory, East Kilbride, Glasgow.*

Gadhamshetty, V., Nirmalakhandan, N., Myint, M. & Ricketts, C., 2006. Improving aircooled condenser performance in combined cycle power plants. *Journal of Energy Engineering,* Volume 132 (2), p. 81 – 88.

Hasan, A. & Siren , K., 2003. Performance investigation of plain and finned tube evaporatively cooled heat exchangers. *Applied Thermal Engineering,* Volume 23, p. 325–340.

Hasan , A. & Siren , K., 2004. Performance investigation of plain circular and oval tube evaporatively cooled heat exchangers. *Applied Thermal Engineering,* Volume 24, p. 777–790.

Heyns , J. A., 2008. Performance characteristics of an air-cooled steam condenser incorporating a hybrid (dry/wet) dephlegmator. *Master Thesis, University of Stellenbosch, RSA.*

Heyns, J. A. & Kröger, D. G., 2010. Experimental investigation into the thermal-flow performance characteristics of an evaporative cooler. *Applied Thermal Engineering,* Volume 30, p. 492–498.

Heyns , J. A. & Kröger, D. G., 2012. Performance Characteristics of an Air-Cooled Steam Condenser with a Hybrid Dephlegmator. *R & D Journal of the South African Institution of Mechanical Engineering,* Volume 28, pp. 31-36.

Hwang , Y., Popli , S. & Radermacher , R., 2012. Enhancement of Round Tube-Louver Fin Heat Exchanger Performance Using Deluge Water Cooling. *International Refrigeration and Air Conditioning Conference,* p. 1264.

Incropera, F. P. & De Witt, D. P., 1990. *Fundamental of Heat and mass transfer, Third edition.* New York: John Wiley & Sons, Inc,.

Jafari , N. M. R. & Behfar , R., 2010. A novel design for evaporative fluid coolers. *Applied Thermal Engineering,* Volume 30, pp. 2746-2752.

Jahangeer, K. A., Andrew, A. O., Tay , M. & Raisul , I., 2011. Numerical investigation of transfer coefficients of an evaporatively-cooled condenser. *Applied Thermal Engineering,* Volume 31, pp. 1655-1663.

Kröger, D. G., 2004. *Air-cooled Heat exchangers and Cooling Towers: Thermal-Flow Performance Evaluation and Design.* Oklahoma, USA: PennWell Corporation, Tulsa,.

Leidenfrost, W. & Korenic, B., 1979. Analysis of Evaporative Cooling and enhancement of Condenser Efficiency and of Coefficient of Performance,. *Warme-Und-Stoffubertragung,* Volume 12, pp. 5-23.

Leidenforst, W. & Korenic , B., 1982. Evaporative Cooling and Heat Transfer Augmentation Related to Reduced Condenser Temperatures. *Heat Transfer Engineering,* Volume 3, pp. 38-59.

Maulbetsch , J. S., 2002. Comparison of alternative cooling technologies for California Power Plants: Economic, Environmental and Other Tradeoffs. *EPRI, Palo Alto, CA, and California Energy Commission, Sacramento, CA, 500-02-079F.*

Maulbetsch, J. & DiFilippo, M., 2003. Spray enhancement of air cooled condensers. *EPRI, Palo Alto, CA, California Energy Commission, Sacramento, CA and Crockett Cogeneration, CA. 1005360.*

Merkel, F., 1926. Verdunstungskuling. *VDI-Zeitschrift,* Volume 70, pp. 123-128.

Mizushina, T., Ito, R. & Miyashita, H., 1967. Experimental study of an evaporative cooler. *International Chemical Engineering,* pp. 727-732.

Nakayama, W., Kuwahara, H. & Hirasawa, S., 1988. Heat transfer from tube banks to air/water mist flow. *International Journal of Heat and Mass Transfer,* Volume 31(2), pp. 449-460.

Niitsu, Y., K. , N. & T. , A., 1969. Studies on characteristics and design procedure of evaporative coolers. *Journal of SHASE, Japan,* Volume 43.

Owen, 2013. Air-cooled condenser steam flow distribution and related dephlegmator design considerations. *Doctor Thesis, Stellenbosch University, RSA.*

Parker , R. O. & Treybal , R. E., 1961. The heat, mass transfer characteristics of evaporative coolers. *AIChE Chem Eng Progr Symp Ser 57,* Volume 32, p. 138–149.

Perez-Blanco, H. & Linkous, R. L., 1983. Use of an overall heat-transfer coefficient to calculate performance of an evaporative cooler. *OAK RIDGE NATIONAL Laboratory/ TM-8250.*

Poppe, M. & Rögener, H., 1984. Evaporative Cooling Systems. *VDI-Warmeatlas, Section Mh.*

Qureshi, B. A. & Zubair , S. M., 2005. The impact of fouling on performance evaluation of evaporative coolers and condensers. *International Journal of Energy Research,* Volume 29, p. 1313–1330.

Suhas, V. P., 1980. *Numerical heat transfer and fluid flow, Series in computational methods in mechanics and thermal sciences.* s.l.:Washington, D.C. : Hemisphere.

Verseteeg, H. K. & Malalasekera, M., 2007. *An introduction to computational fluid dynamics. The fnite volume Method, second edition.* London: Ashford Colour Press.

Wachtell , G. P., 1974. Atomized water injection to improve dry cooling tower performance. *Franklin Institute Research Laboratories, Pennsylvania.*

Yang , W. J. & Clark , D. W., 1975. Spray cooling of the air-cooled compact heat exchangers. *International Journal of Heat and Mass Transfer,* Volume 18, pp. 311-317.

Yunus, A. C. & Afshin , J. G., 2011. *Heat and Mass transfer, Fundamentals and Applications.* fourth ed. s.l.:New york: McGraw - Hill.

Zhang , F., Bock, J., Jacobi, A. M. & Wu, H., 2014. Simultaneous heat and mass transfer to air from a compact heat exchanger with water spray precooling and surface deluge cooling. *Applied Thermal Engineering ,* Volume 63, pp. 258-540.

Zheng , W. Y. et al., 2012. Experimental and computational analysis of thermal performance of the oval tube closed wet cooling tower. *Applied Thermal Engineering,* Volume 35, pp. 233-239.

Appendix

A. Properties of the fluids

A.1. The thermo-physical properties of dry air from 220 K to 380 K at standard atmospheric pressure(1 atm)

Density:

$$\rho_a(p_a, T_a) = p_a/(287.08\, T_a), \quad \mathrm{kg/m^3} \tag{A. 1}$$

Specific heat:

$$c_{pa}(T_a) = 1.045356 \times 10^3 - 3.161783 \times 10^{-1}\, T_a + 7.083814 \times 10^{-4}\, {T_a}^2 - 2.705209 \times 10^{-7} {T_a}^3, \quad \mathrm{J/kgK} \tag{A. 2}$$

Dynamic viscosity:

$$\mu_a(T_a) = 2.287973 \times 10^{-6} + 6.259793 \times 10^{-8}\, T_a - 3.131956 \times 10^{-11}\, {T_a}^2 + 8.15038 \times 10^{-15}\, {T_a}^3, \mathrm{kg/sm} \tag{A. 3}$$

Thermal conductivity:

$$k_a(T_a) = -4.937787 \times 10^{-4} + 1.018087 \times 10^{-4}\, T_a - 4.627937 \times 10^{-8}\, {T_a}^2 + 1.250603 \times 10^{-11}\, {T_a}^3, \mathrm{W/mK} \tag{A. 4}$$

A.2. The thermo-physical properties of saturated water vapour from 273.15 K to 380 K

Vapour pressure:

$$P_v(T_a) = 10^{z(T_a)}, \mathrm{N/m^2} \tag{A. 5}$$

Where

$$z_1(T_a) = 10.79586(1 - 273.16/T_a) \tag{A. 6}$$

$$z_2(T_a) = 5.02808\, log_{10}(273.16/T_a) \tag{A. 7}$$

$$z_3(T_a) = 1.50474 \times 10^{-4}\left[1 - 10^{-8.29692\{(273.16/T_a)-1\}}\right] \tag{A. 8}$$

$$z_4(T_a) = 4.2873 \times 10^{-4}\left[10^{4.76955(1-(273.16/T_a))} - 1\right] \tag{A. 9}$$

$$z_5 = 2.786118312 \tag{A. 10}$$

$$z(T_a) = z_1(T_a) + z_2(T_a) + z_3(T_a) + z_4(T_a) + z_5 \tag{A. 11}$$

Specific heat:

$$c_{pv}(T_a) = 1.3605 \times 10^3 + 2.31334\,T_a - 2.46784 \times 10^{-10}\,{T_a}^5 + 5.91332 \times 10^{-13}\,{T_a}^6, \mathrm{J/kgK} \quad \textbf{(A. 12)}$$

Dynamic viscosity:

$$\mu_v(T_a) = 2.562435 \times 10^{-6} + 1.816683 \times 10^{-8}\,T_a + 2.579066 \times 10^{-11}\,{T_a}^2 - 1.067299 \times 10^{-14}\,{T_a}^3, \mathrm{kg/ms} \quad \textbf{(A. 13)}$$

Thermal conductivity:

$$k_v(T_a) = 1.3046 \times 10^{-2} - 3.756191 \times 10^{-5}\,T_a + 2.217964 \times 10^{-7}\,{T_a}^2 - 1.111562 \times 10^{-10}\,{T_a}^3, \mathrm{W/mK} \quad \textbf{(A. 14)}$$

A.3. The thermo-physical properties of saturated water liquid from 273.15 K to 380 K

Density:

$$\rho_w(T_w) = (1.49343 \times 10^{-3} - 3.7164 \times 10^{-6}\,T_w + 7.09782 \times 10^{-9}\,T_w^2 - 1.90321 \times 10^{-20}\,{T_w}^6)^{-1}, \mathrm{kg/m^3} \quad \textbf{(A. 15)}$$

Specific heat:

$$c_{pw}(T_w) = 8.15599 \times 10^3 - 2.80627 \times 10\,T_w + 5.11283 \times 10^{-2}\,{T_w}^2 - 2.17582 \times 10^{-13}\,{T_w}^6, \mathrm{J/kgK} \quad \textbf{(A. 16)}$$

Dynamic viscosity:

$$\mu_w(T_w) = 2.414 \times 10^{-5} \times 10^{247.8/(T_w - 140)}, \mathrm{kg/ms} \quad \textbf{(A. 17)}$$

Thermal conductivity:

$$k_w(T_w) = -6.1455 \times 10^{-1} + 6.9962 \times 10^{-3}\,T_w - 1.01075 \times 10^{-5}\,{T_w}^2 + 4.74737 \times 10^{-12}\,{T_w}^4, \mathrm{W/mK} \quad \textbf{(A. 18)}$$

Latent heat of vaporization:

$$i_{fgw}(T_w) = 3.4831814 \times 10^6 - 5.8627703 \times 10^3\,T_w + 12.139568\,{T_w}^2 - 1.40290431 \times 10^{-2}\,{T_w}^3, \mathrm{J/kg} \quad \textbf{(A. 19)}$$

A.4. Thermo-physical properties of mixtures of air and water vapour

Density:

$$\rho_{av}(T_a, w) = (1 + w)[1 - w/(w + 0.62198)]\ \times \quad \textbf{(A. 20)}$$

$$p_a/(287.08\,T_a)\ ,\quad \text{kg air} - \text{vapour/m}^3$$

Specific heat:

$$c_{pav}(T_a, w) = (c_{pa}(T_a) + wc_{pv}(T_a))/(1+w), \text{J/K kg air} - \text{vapour} \quad \textbf{(A. 21)}$$

The specific heat of the air-vapour mixture per unit mass of dry air:

$$c_{pma}(T_a, w) = (c_{pa}(T_a) + wc_{pv}(T_a)), \text{J/K kg air} - \text{vapour} \quad \textbf{(A. 22)}$$

Dynamic viscosity:

$$\mu_{av}(T_a, w) = (X_a(w)\mu_a(T_a)M_a^{0.5} + X_v(w)\mu_v(T_a)M_v^{0.5})/(X_a(w)M_a^{0.5} + X_v(w)M_v^{0.5}), \text{kg/ms} \quad \textbf{(A. 23)}$$

where $M_a = 28.97$ kg/mole, and $M_v = 18.016$ kg/mole,

$$X_a(w) = 1/(1+1.608w) \quad \textbf{(A. 24)}$$

$$X_v(w) = w/(w+0.622) \quad \textbf{(A. 25)}$$

Thermal conductivity:

$$k_{av}(T_a) = (X_a(w)k_a(T_a)M_a^{0.33} + X_v(w)k_v(T_a)M_v^{0.33})/(X_a(w)M_a^{0.33} + X_v(w)M_v^{0.33}), \text{W/mK} \quad \textbf{(A. 26)}$$

Humidity ratio:

$$a_1(T_{db}, T_{wb}) = \frac{2501.6 - 2.3263(T_{wb} - 273.15)}{2501.6 + 1.8577(T_{db} - 273.15) - 4.184(T_{wb} - 273.15)} \quad \textbf{(A. 27)}$$

$$a_2(p_a, p_{vwb}) = \frac{0.6259 p_{vwb}}{p_a - 1.005 p_{vwb}} \quad \textbf{(A. 28)}$$

$$a_3(T_{db}, T_{wb}) = \frac{1.00416(T_{db} - T_{wb})}{2501.6 + 1.8577(T_{db} - 273.15) - 4.184(T_{wb} - 273.15)} \quad \textbf{(A. 29)}$$

$$w(T_{db}, T_{wb}, p_a, p_{vwb}) = a_1(T_{db}, T_{wb})a_2(p_a, p_{vwb}) - a_3(T_{db}, T_{wb})\ , \text{kg/kg dry air} \quad \textbf{(A. 30)}$$

The enthalpy of the air-vapour mixture per unit mass of dry air:

$$i_{ma}(T_a, w) = c_{pa}\left(\frac{T_a}{2} + 273.15\right) + w[i_{fgwo} + c_{pv}\left(\frac{T_a}{2} + 273.15\right)], \text{J/kg air} - \text{vapour} \quad \textbf{(A. 31)}$$

B. Theories and empirical correlations

B.1. Condensation heat transfer coefficient

The recommended correlation for determining the condensation heat transfer coefficient on a vertical flat plate, as presented in (Kröger, 2004) is

$$h_c = 0.943\left[\frac{\rho_c g(\rho_c-\rho_s){i_{fg}}^* k_c^3}{\mu_c(T_c-T_w)d_i}\right]^{0.25} \quad \textbf{(B. 1)}$$

where ${i_{fg}}^*$ is modified latent heat of vaporization, which determined as

$${i_{fg}}^* = i_{fg} + 0.68c_{pc}(T_c - T_w) \quad \textbf{(B. 2)}$$

B.2. Deluge water heat transfer coefficients

There are limited published literatures with recommended correlations for the deluged flat tube bundle. Several researchers such as, Parker and Treybal (1961), Niitsu et al. (1969) and Mizushina et al (1967) derived and recommended some correlations for determining the heat transfer coefficient between the tubes and deluge water, however, those correlations are only applicable to the round tube bundles. Therefore, the heat transfer coefficient between the tubes and deluge water is determined from the relation between the heat convection and conduction through the deluge water film as

$$h_w = \frac{k_{dw}}{\delta_{dw}} \quad \textbf{(B. 3)}$$

B.3. Air-side heat and mass transfer coefficients

a) Flow over the flat tube

For the flow over the flat tube the following theories, as presented in (Yunus & Afshin , 2011) are recommended to determine the heat transfer coefficient. The local Nusselt number at any location z, along the tube height

$$Nu_z = \frac{h_a z}{k_a} = 0.332{Re_z}^{0.5}Pr^{1/3} \quad \textbf{(B. 4)}$$

$$Nu_z = \frac{h_a z}{k_a} = 0.0296{\mathrm{Re}_z}^{0.5}\mathrm{Pr}^{1/3} \quad \textbf{(B. 5)}$$

where Eq. (B.4) is valid for $Re_z < 5\times10^5, Pr > 0.6$, and Eq. (B.5) is valid for $5\times10^5 \le \mathrm{Re}_z \le 10^7,\ 0.6 \le Pr \le 60$. The average Nusselt number for the flow over the entire tube's height

$$Nu = \frac{h_a H_t}{k_a} = 0.664{Re_{H_t}}^{0.5}Pr^{1/3} \quad \textbf{(B. 6)}$$

$$\mathrm{Nu} = \frac{h_a H_t}{k_a} = 0.037{\mathrm{Re}_{H_t}}^{0.5}\mathrm{Pr}^{1/3} \quad \textbf{(B. 7)}$$

where Eq. (B.6) is valid for $Re_{H_t} < 5 \times 10^5, Pr > 0.6$, and Eq. (B.7) is valid for $5 \times 10^5 \leq \mathrm{Re}_{H_t} \leq 10^7,\ 0.6 \leq Pr \leq 60$. The mass transfer convection coefficient is determined from the analogy between heat and mass transfer at the air-water interface. The local Sherwood number at any location z, along the tube height

$$Sh_z = \frac{h_D z}{\mathrm{D_{AB}}} = 0.332 {Re_z}^{0.5} Sc^{1/3} \quad \textbf{(B. 8)}$$

$$Sh_z = \frac{h_D z}{\mathrm{D_{AB}}} = 0.0296 {Re_z}^{0.5} Sc^{1/3} \quad \textbf{(B. 9)}$$

where Eq. (B.8) is valid for $Re_z < 5 \times 10^5, Sc > 0.5$, and Eq. (B.9) is valid for $5 \times 10^5 \leq Re_z \leq 10^7,\ 0.5 \leq Sc \leq 60$. The average Sherwood number for the flow over the entire tube's height

$$Sh = \frac{h_D H_t}{\mathrm{D_{AB}}} = 0.664 {Re_{H_t}}^{0.5} Sc^{1/3} \quad \textbf{(B. 10)}$$

$$Sh = \frac{h_D H_t}{\mathrm{D_{AB}}} = 0.037 {Re_{H_t}}^{0.5} Sc^{1/3} \quad \textbf{(B. 11)}$$

where Eq. (B.10) is valid for $Re_{H_t} < 5 \times 10^5, Sc > 0.5$, and Eq. (B.11) is valid for $5 \times 10^5 \leq Re_{H_t} \leq 10^7,\ 0.5 \leq Sc \leq 60$. Marrero and Mason (1972) recommended the following formula for defining the mass diffusion of water vapour

$$D_{H2O} = 1.87 \times 10^{-10} \frac{\left[\frac{T_{dws}+T_{am}}{2}+273.15\right]^{2.072}}{P_a} \quad \textbf{(B. 12)}$$

b) Flow in the duct

For the heat transfer coefficient of turbulent flow in the duct, Gnielinski (1976) recommended the following correlation

$$Nu = \frac{(f_D/8)(Re-1000)Pr}{1+12.7(f_D/8)^{0.5}\left(Pr^{2/3}-1\right)} \quad \textbf{(B. 13)}$$

which valid for $3000 < Re < 5 \times 10^6,\ 0.5 \leq Pr \leq 2000$. Petukhov (1970) recommended the following equation to determine the friction factor in turbulent flow in smooth tubes

$$f_D = (0.79\, lnRe - 1.64)^{-2} \quad \textbf{(B. 14)}$$

which valid for $3000 < Re < 5 \times 10^6$

B.4. Air-side pressure drop

For the flow over the flat tube, both local and average friction coefficients are determined from the formulas, as presented in (Yunus & Afshin , 2011). The local friction coefficients at any location z, along the tube's height

$$C_{f,z} = 0.664 Re_z^{-0.5} \quad \textbf{(B. 15)}$$

$$C_{f,z} = 0.059 Re_z^{-0.2} \quad \textbf{(B. 16)}$$

where Eq. (B.15) is valid for $Re_z < 5 \times 10^5$, and Eq. (B.16) is valid for $5 \times 10^5 \leq \mathrm{Re}_z \leq 10^7$. The average friction coefficient for the flow over the entire tube's height

$$C_f = 1.33 Re_{H_t}^{-0.5} \quad \textbf{(B. 17)}$$

$$C_f = 0.074 Re_{H_t}^{-0.2} \quad \textbf{(B. 18)}$$

where Eq. (B.17) is valid for $Re_{H_t} < 5 \times 10^5$, and Eq. (B.18) is valid for $5 \times 10^5 \leq \mathrm{Re}_{H_t} \leq 10^7$.

The pressure drop due to friction for external and internal flow is expressed as

$$\Delta P_f = C_f \left(\frac{A_a}{A_c}\right) \rho_a \frac{v_{am}^2}{2} \quad \textbf{(B. 19)}$$

$$\Delta P_f = f_D \left(\frac{H_t}{d_a}\right) \rho_a \frac{v_{am}^2}{2} \quad \textbf{(B. 20)}$$

C. Sample of calculation: Performance analysis of a delugeable flat tube air-cooled steam condenser bundle employing numerical method.

The thermal performance of a delugeable plain flat tube air-cooled steam condenser bundle is analysed numerically by employing heat and mass transfer analogy method of analysis.To attain the grid independent numerical solutions, the tube is divided into several intervals/rows (N_r). The variations in the numerical solutions are fixed at $N_r := 15$. In this sample of calculation only three rows, the first (1), middle (8) and last (15), are considered as illustrated in Figure C.1.

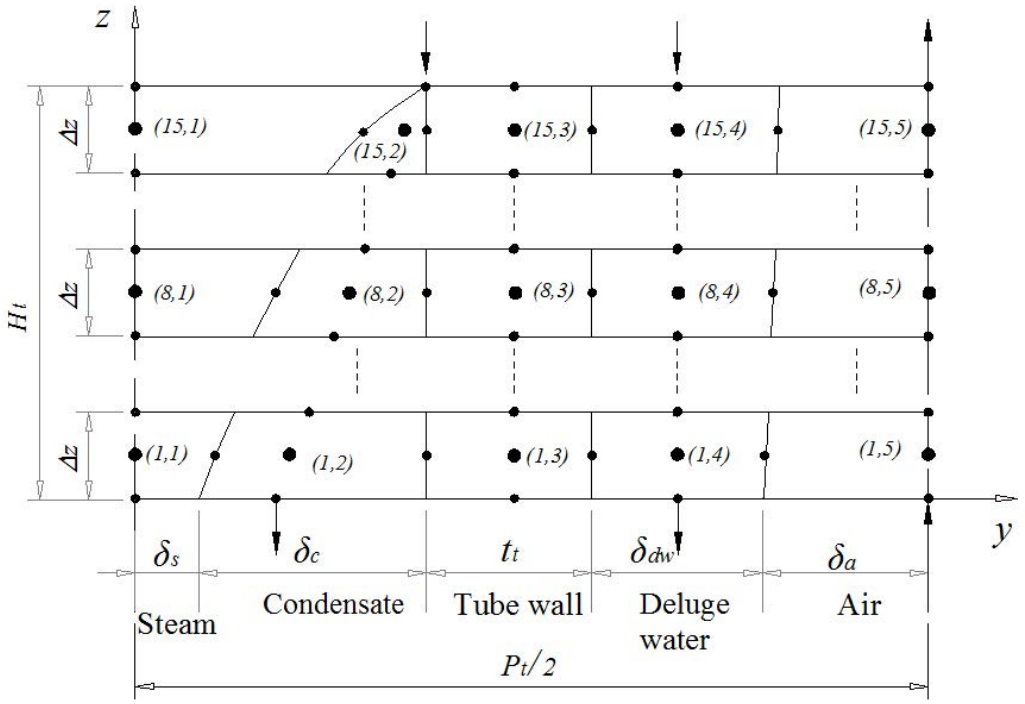

Figure C.1: The number of intervals/rows and grid points positions

C.1. Tube geometric parameters

Tube height	$H_t := 0.6$	m
Tube width	$W_t := 0.02$	m
Tube thickness	$t_t := 0.0015$	m
Tube length	$L_t := 1$	m
Tube pitch	$P_t := 0.028$	m
Tube wall thermal conductivity	$k_t := 45$	$\frac{W}{mK}$.

C.2. Operating conditions

Inlet air dry-bulb temperature	$T_{ai} := 15$	°C
$T_{ai\_K} := T_{ai} + 273.15$	$T_{ai\_K} = 288.15$	K
Relative humidity	$\phi := 60$	%
Inlet air wet-bulb temperature	$T_{wb} := 10.8$	°C
$T_{wb\_K} := T_{wb} + 273.15$	$T_{wb\_K} = 283.95$	K
Atmospheric pressure	$p_a := 101325$	$\frac{N}{m^2}$
Frontal air velocity	$v_{ai} := 2$	$\frac{m}{s}$
Steam temperature	$T_s := 45$	°C

C.3. Solution Parameters

The governing equations of a two dimensional numerical model are satisfied by the following values:

Outlet air temperature	$T_{ao} := 26.878$	°C
$T_{ao\_K} := T_{ao} + 273.15$	$T_{ao\_K} = 300.028$	K
Air mean temperature	$T_{am} := 22.05984887$	°C
$T_{am\_K} := T_{am} + 273.15$	$T_{am\_K} = 295.21$	K
Outlet air humidity ratio	$w_o := 0.0266148$	$\frac{kg}{kg}$ dry air
Inlet deluge water temperature	$T_{dwi} := 42.20803$	°C
$T_{dwi\_K} := T_{dwi} + 273.15$	$T_{dwi\_K} = 315.358$	K
Deluge water mean temperature	$T_{dwm} := 44.029145$	°C
$T_{dwm\_K} := T_{dwm} + 273.15$	$T_{dwm\_K} = 317.179$	K
Inlet deluge water mass flow rate	$m_{dwi} := 0.01388934$	$\frac{kg}{s}$
Steam mass flow rate	$m_s := 0.00176381$	$\frac{kg}{s}$
Tube critical height	$H_{cr} := 0.30317073$	m

C.4. Geometry relations

The height of grid cells on the steam-side, tube wall-side and deluge water-side

$$\Delta z := \frac{H_t}{N_r} \qquad \Delta z = 0.04 \text{ m}$$

The height of grid cells within critical region

$\Delta z_{cr} := \frac{H_{cr}}{N_r}$ $\Delta z_{cr} = 0.02021$ m

The tube height for the fully developed flow region

$H_{fd} := H_t - H_{cr}$ $H_{fd} = 0.29683$ m

The height of grid cells within fully developed flow region

$\Delta z_{fd} := \frac{H_{fd}}{N_r}$ $\Delta z_{fd} = 0.01979$ m

The effective heat transfer surface area on the steam-side, tube wall-side and deluge water-side

$A_{st} := 2\Delta z \cdot L_t$ $A_{st} = 0.08$ m^2

The effective air-side heat transfer surface area in the critical region

$A_{cr} := 2\Delta z_{cr} \cdot L_t$ $A_{cr} = 0.0404$ m^2

The effective air-side heat transfer surface area in the fully developed flow region

$A_{fd} := 2\Delta z_{fd} \cdot L_t$ $A_{fd} = 0.03958$ m^2

C.5. Analysis of the deluged flat tube bundle

The section of the tube bundle considered in this sample of calculation is shown in Figure 3.16. The analysis of the tube bundle is conducted from the air-side. The directions of the heat transfer to the air steam is presented in Figure C.2.

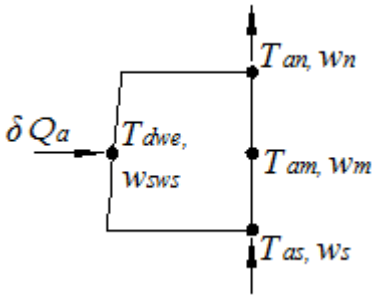

Figure C. 2: The grid cell from the air-side, showing the directions of the heat transfer to the air stream.

The vapour pressure is determined at the wet-bulb temperature $T_{wb\_K} = 283.95$ K as

$p_{vi} := \left(p_v\left(T_{wb} + 273.15\right)\right)$ $p_{vi} = 1294.383$ $\frac{N}{m^2}$

The inlet air humidity ratio is

$w_i := w\left(T_{ai}, T_{wb}, p_a, p_{vi}\right)$ $w_i = 0.00637$ $\frac{kg}{kg}$ dry air

The effective frontal area

$A_{fr} := L_t \cdot P_t$ $A_{fr} = 0.028$ m^2

The density of air-water vapour mixture entering the tube bundle

$\rho_{avi} := \rho_a\left[p_a, \left(T_{ai\_K}\right)\right]$ $\rho_{avi} = 1.225$ $\frac{kg}{m^3}$

The mass flow rate of the inlet air

$m_{avi} := \rho_{avi} \cdot v_{ai} \cdot A_{fr} \cdot \left(1 + w_i\right)$ $m_{avi} = 0.069$ $\frac{kg}{s}$

The dry air mass flow rate

$m_a := \frac{m_{avi}}{\left(1 + w_i\right)}$ $m_a = 0.0686$ $\frac{kg}{s}$

At the mean temperature of the deluge water, $T_{dwm\_K} = 317.179$ K the thermo-physical properties of saturated water liquid are

Density

$\rho_{dwm} := \rho_w\left(T_{dwm\_K}\right)$ $\rho_{dwm} = 990.74$ $\frac{kg}{m^3}$

Specific heat

$c_{pdwm} := c_{pw}\left(T_{dwm\_K}\right)$ $c_{pdwm} = 4177.188$ $\frac{J}{kgK}$

$c_{pvdwm} := c_{pv}\left(T_{dwm\_K}\right)$ $c_{pvdwm} = 1904.12$ $\frac{J}{kgK}$

Thermal conductivity

$k_{dwm} := k_w\left(T_{dwm\_K}\right)$ $k_{dwm} = 0.636$ $\frac{W}{mK}$

Dynamic viscosity

$\mu_{dwm} := \mu_w\left(T_{dwm\_K}\right)$ $\mu_{dwm} = 0.000604$ $\frac{kg}{ms}$

At the mean temperature of air, $T_{am\_K} = 295.21$ K the thermo-physical properties of air are

Density

$\rho_{am} := \overrightarrow{\rho_a\left(p_a, T_{am\_K}\right)}$ $\rho_{am} = 1.196$ $\frac{kg}{m^3}$

Specific heat

$c_{pam} := c_{pa}\left(T_{am\_K}\right)$ $c_{pam} = 1006.792$ $\frac{J}{kgK}$

Thermal conductivity

$k_{am} := k_a\left(T_{am\_K}\right)$ $k_{am} = 0.026$ $\frac{W}{mK}$

Dynamic viscosity

$\mu_{am} := \mu_a(T_{am\_K})$ $\mu_{am} = 0.0000182$ $\frac{kg}{ms}$

Prandlt Number

$Pr_{am} := \overrightarrow{Pr_a(T_{am\_K})}$ $Pr_{am} = 0.711$

The air temperature leaving the grid cells

$T_{an_{(15,5)}} := T_{ao}$ $T_{an_{(15,5)}} = 26.878$ °C

$T_{an_{(8,5)}} := 22.81119$ °C

$T_{an_{(1,5)}} := 16.7237$ °C

The air temperature entering the grid cells

$T_{as_{(15,5)}} := 26.36388$ °C

$T_{as_{(8,5)}} := 22.11927$ °C

$T_{as_{(1,5)}} := T_{ai}$ $T_{as_{(1,5)}} = 15$ °C

Therefore

$$T_{an} := \begin{bmatrix} T_{an_{(15,5)}} \\ T_{an_{(8,5)}} \\ T_{an_{(1,5)}} \end{bmatrix} \quad T_{an} = \begin{pmatrix} 26.878 \\ 22.811 \\ 16.724 \end{pmatrix} \text{ °C}$$

$$T_{as} := \begin{bmatrix} T_{as_{(15,5)}} \\ T_{as_{(8,5)}} \\ T_{as_{(1,5)}} \end{bmatrix} \quad T_{as} = \begin{pmatrix} 26.364 \\ 22.119 \\ 15 \end{pmatrix} \text{ °C}$$

The local air mean temperature

$$T_a := \frac{T_{an} + T_{as}}{2} \quad T_a = \begin{pmatrix} 26.621 \\ 22.465 \\ 15.862 \end{pmatrix} \text{ °C}$$

Then

$$T_{a\_K} := T_a + 273.15 \quad T_{a\_K} = \begin{pmatrix} 299.771 \\ 295.615 \\ 289.012 \end{pmatrix} \text{ K}$$

The humidity ratio of the air leaving the grid cells

$w_{n_{(15,5)}} := w_o$ $w_{n_{(15,5)}} = 0.027$ $\frac{kg}{kg}$ dry air

$w_{n_{(8,5)}} := 0.0194294$ $\frac{kg}{kg}$ dry air

$w_{n_{(1,5)}} := 0.00914669$ $\frac{kg}{kg}$ dry air

The humidity ratio of the air entering the grid cells

$w_{s_{(15,5)}} := 0.02569$ $\frac{kg}{kg}$ dry air

$w_{s_{(8,5)}} := 0.0182339$ $\frac{kg}{kg}$ dry air

$w_{s_{(1,5)}} := w_i$ $w_{s_{(1,5)}} = 0.006366$ $\frac{kg}{kg}$ dry air

Therefore

$$w_n := \begin{bmatrix} w_o \\ w_{n_{(8,5)}} \\ w_{n_{(1,5)}} \end{bmatrix} \qquad w_n = \begin{pmatrix} 0.0266148 \\ 0.0194294 \\ 0.00914669 \end{pmatrix} \quad \frac{kg}{kg} \text{ dry air}$$

$$w_s := \begin{bmatrix} w_{s_{(15,5)}} \\ w_{s_{(8,5)}} \\ w_{s_{(1,5)}} \end{bmatrix} \qquad w_s = \begin{pmatrix} 0.02569 \\ 0.0182339 \\ 0.00636603 \end{pmatrix} \quad \frac{kg}{kg} \text{ dry air}$$

The changes in air humidity ratio

$$\Delta w := w_n - w_s \qquad \Delta w = \begin{pmatrix} 0.0009248 \\ 0.0011955 \\ 0.00278066 \end{pmatrix} \quad \frac{kg}{kg} \text{ dry air}$$

The evaporation rate of the deluge water

$$\Delta m_{dw} := m_a \cdot \Delta w \qquad \Delta m_{dw} = \begin{pmatrix} 0.00006344 \\ 0.000082 \\ 0.00019074 \end{pmatrix} \quad \frac{kg}{s}$$

The mass flow rate of the deluge water at interface grid points

$m_{dwn_{(15,5)}} := m_{dwi}$ $m_{dwn_{(15,5)}} = 0.01389$ $\frac{kg}{s}$

$m_{dwn_{(8,5)}} := 0.01339647$ $\frac{kg}{s}$

$m_{dwn_{(1,5)}} := 0.01269114$ $\frac{kg}{s}$

Then

$$m_{dwn} := \begin{bmatrix} m_{dwn_{(15,5)}} \\ m_{dwn_{(8,5)}} \\ m_{dwn_{(1,5)}} \end{bmatrix} \qquad m_{dwn} = \begin{pmatrix} 0.0138893 \\ 0.0133965 \\ 0.0126911 \end{pmatrix} \quad \frac{kg}{s}$$

and therefore

$$m_{dws} := \begin{pmatrix} m_{dwn_1} - \Delta m_{dw_1} \\ m_{dwn_2} - \Delta m_{dw_2} \\ m_{dwn_3} - \Delta m_{dw_3} \end{pmatrix} \qquad m_{dws} = \begin{pmatrix} 0.0138259 \\ 0.01331447 \\ 0.0125004 \end{pmatrix} \quad \frac{kg}{s}$$

The mass flow rate at the nodal points is

$$m_{dw} := \frac{m_{dwn} + m_{dws}}{2} \qquad m_{dw} = \begin{pmatrix} 0.01385762 \\ 0.01335547 \\ 0.01259577 \end{pmatrix} \quad \frac{kg}{s}$$

The deluge water film thickness

$$\delta_{dw} := \left[\frac{3 \cdot \mu_{dwm} \cdot m_{dw}}{\rho_{dwm} \cdot 9.81 \cdot L_t \cdot \left(\rho_{dwm} - \rho_{am}\right)} \right]^{\frac{1}{3}}$$

$$\delta_{dw} = \begin{pmatrix} 0.00013773 \\ 0.00013604 \\ 0.00013341 \end{pmatrix} \quad m$$

The gap between the tubes

$$\delta_a := P_t - \left(W_t + 2\delta_{dw}\right) \qquad \delta_a = \begin{pmatrix} 0.00772454 \\ 0.00772791 \\ 0.00773317 \end{pmatrix} \quad m$$

The corresponding hydraulic diameter is simply twice the space between tubes.

$$d_a := 2 \cdot \delta_a \qquad d_a = \begin{pmatrix} 0.01544909 \\ 0.01545582 \\ 0.01546634 \end{pmatrix} \quad m$$

The minimum flow area of the air

$$A_c := L_t \cdot \delta_a \qquad A_c = \begin{pmatrix} 0.00772454 \\ 0.00772791 \\ 0.00773317 \end{pmatrix} \quad m^2$$

To minimise the number of the intervals/rows at which the tube should be divided in order to attain the grid independent solutions, the Reynolds number are determined at

$$z_{crRe} := \begin{pmatrix} 14 \cdot \Delta z_{cr} + \frac{3\Delta z_{cr}}{4} \\ 7 \cdot \Delta z_{cr} + \frac{3\Delta z_{cr}}{4} \\ \frac{3\Delta z_{cr}}{4} \end{pmatrix} \qquad z_{crRe} = \begin{pmatrix} 0.29811788 \\ 0.15663821 \\ 0.01515854 \end{pmatrix} \quad m$$

The local air-side Reynolds numbers of the saturated air flows over the deluge water film surface in the critical and fully developed flow region respectively are

$$Re_{acr} := \overrightarrow{\frac{m_{avi} \cdot z_{crRe}}{\mu_{am} \cdot A_c}} \qquad Re_{acr} = \begin{pmatrix} 145997.562 \\ 76677.149 \\ 7415.322 \end{pmatrix}$$

$$Re_{afd} := \overrightarrow{\left(\frac{m_{avi} \cdot d_a}{\mu_{am} \cdot A_c}\right)} \qquad Re_{afd} = \begin{pmatrix} 7565.897 \\ 7565.897 \\ 7565.897 \end{pmatrix}$$

The $Re_{acr} < 5 \cdot 10^5$, therefore the flow in the critical region is laminar, while $Re_{afd} > 2400$, and therefore the flow in the fully developed flow region is turbulent.

The locations along the tube critical height and from the leading edge (the bottom of the tube), at which the local values of Nusselt number, Sherwood number, heat and mass transfer coefficient are determined is

$$z_{cr} := \begin{pmatrix} 14 \cdot \Delta z_{cr} + \frac{\Delta z_{cr}}{2} \\ 7 \cdot \Delta z_{cr} + \frac{\Delta z_{cr}}{2} \\ \frac{\Delta z_{cr}}{2} \end{pmatrix} \qquad z_{cr} = \begin{pmatrix} 0.293065 \\ 0.1515854 \\ 0.0101057 \end{pmatrix} \quad m$$

The friction factor

$$f_D := \left(1.82 \log\left(Re_{afd}\right) - 1.64\right)^{-2} \qquad f_D = \begin{pmatrix} 0.0340469 \\ 0.0340469 \\ 0.0340469 \end{pmatrix}$$

The local Nusselt numbers for the flow over the tube in the critical and fully developed flow region respectively are

$$Nu_{acr} := \overrightarrow{\left[0.332 \cdot Re_{acr}^{0.5} \cdot \left(Pr_{am}\right)^{\frac{1}{3}}\right]}$$

$$Nu_{acr} = \begin{pmatrix} 113.207 \\ 82.042 \\ 25.513 \end{pmatrix}$$

$$Nu_{afd} := \overrightarrow{\frac{\left(\frac{f_D}{8}\right) \cdot \left(Re_{afd} - 1000\right) \cdot Pr_{am}}{1 + 12.7 \cdot \left(\frac{f_D}{8}\right)^{0.5} \cdot \left[\left(Pr_{am}\right)^{\frac{2}{3}} - 1\right]}}$$

$$Nu_{afd} = \begin{pmatrix} 23.89 \\ 23.89 \\ 23.89 \end{pmatrix}$$

The local air-side heat transfer coefficients in the critical and fully developed flow region respectively are

$$h_{acr} := \frac{\overrightarrow{k_{am} \cdot Nu_{acr}}}{z_{cr}} \qquad h_{acr} = \begin{pmatrix} 9.985 \\ 13.991 \\ 65.261 \end{pmatrix} \qquad \frac{W}{m^2 K}$$

$$h_{afd} := \frac{\overrightarrow{k_{am} \cdot Nu_{afd}}}{d_a} \qquad h_{afd} = \begin{pmatrix} 39.973 \\ 39.955 \\ 39.928 \end{pmatrix} \qquad \frac{W}{m^2 K}$$

The deluge water film surface temperature is found to be

$$T_{dwe} := \begin{pmatrix} 44.29406 \\ 43.90962 \\ 42.03331 \end{pmatrix} \qquad °C$$

and

$$T_{dwe\_K} := T_{dwe} + 273.15$$

At the air-water interface, the dry air properties of the air-water vapour mixture, determined at the average temperature can be used.

The mean deluge water film surface temperature

$$T_{dwem} := 43.73794307 \qquad °C$$

The average temperature between deluge water surface and air

$$T_{dwa} := \frac{T_{dwem} + T_{am}}{2} \qquad T_{dwa} = 32.899 \qquad °C$$

$$T_{dwa\_K} := T_{dwa} + 273.15 \qquad T_{dwa\_K} = 306.049 \qquad K$$

then

Density

$$\rho_{dwa} := \overrightarrow{\rho_a\left(p_a, T_{dwa\_K}\right)} \qquad \rho_{am} = 1.196 \qquad \frac{kg}{m^3}$$

Dynamic viscosity

$$\mu_{dwa} := \mu_a\left(T_{dwa\_K}\right) \qquad \mu_{dwa} = 0.0000187 \qquad \frac{kg}{ms}$$

Kinematic viscosity

$$\nu_{dwa} := \frac{\mu_{dwa}}{\rho_{dwa}} \qquad \nu_{dwa} = 0.0000163 \qquad \frac{m^2}{s}$$

The mass diffusivity of the water vapour in the air

$$D_{H2O} := 1.87 \cdot 10^{-10} \cdot \frac{\left(T_{dwa\_K}\right)^{2.072}}{p_a \cdot 10^{-5}}$$

$$D_{H2O} = 0.0000261 \qquad \frac{m^2}{s}$$

The Schmidt number

$$Sc := \frac{\nu_{dwa}}{D_{H2O}} \qquad Sc = 0.623$$

The local Sherwood numbers for the flow in the critical and fully developed flow region respectively are

$$Sh_{cr} := \overrightarrow{\left[0.332 \cdot \left(Re_{acr}\right)^{0.5} \cdot (Sc)^{\frac{1}{3}}\right]}$$

$$Sh_{cr} = \begin{pmatrix} 108.329 \\ 78.507 \\ 24.414 \end{pmatrix}$$

$$Sh_{fd} := \frac{\overrightarrow{\left(\frac{f_D}{8}\right) \cdot \left(Re_{afd} - 1000\right) \cdot Sc}}{1 + 12.7 \cdot \left(\frac{f_D}{8}\right)^{0.5} \cdot \left[(Sc)^{\frac{2}{3}} - 1\right]}$$

$$Sh_{fd} = \begin{pmatrix} 22.434 \\ 22.434 \\ 22.434 \end{pmatrix}$$

The local mass transfer convection coefficients in the critical and fully developed f low region respectively are

$$h_{Dcr} := \frac{\overrightarrow{Sh_{cr} \cdot D_{H2O}}}{z_{cr}} \qquad h_{Dcr} = \begin{pmatrix} 0.00965 \\ 0.01352 \\ 0.06306 \end{pmatrix} \frac{m}{s}$$

$$h_{Dfd} := \frac{\overrightarrow{Sh_{fd} \cdot D_{H2O}}}{d_a} \qquad h_{Dfd} = \begin{pmatrix} 0.0379 \\ 0.03789 \\ 0.03786 \end{pmatrix} \frac{m}{s}$$

The mean humidity ratio of the air and corresponding vapour pressure is

$$w_m := \frac{w_n + w_s}{2} \qquad w_m = \begin{pmatrix} 0.026152 \\ 0.018832 \\ 0.007756 \end{pmatrix} \frac{kg}{kg} \text{ dry air}$$

$$p_{va} := \frac{\overrightarrow{p_a \cdot w_m}}{\left(w_m + 0.622\right)} \qquad p_{va} = \begin{pmatrix} 4088.38 \\ 2977.56 \\ 1247.96 \end{pmatrix} \frac{N}{m^2}$$

The density of the water vapour away from the air-water interface

$$\rho_{ava} := \overrightarrow{\rho_{av}\left[p_{va}, \left(T_{a\_K}\right)\right]} \qquad \rho_{ava} = \begin{pmatrix} 0.029552 \\ 0.021825 \\ 0.009357 \end{pmatrix} \frac{kg}{m^3}$$

The vapour pressure at the air-water interface

$$p_{v\_int} := \overrightarrow{p_v(T_{dwe\_K})} \qquad p_{v\_int} = \begin{pmatrix} 9242.25 \\ 9060.19 \\ 8215.23 \end{pmatrix} \qquad \frac{N}{m^2}$$

The density of the water vapour at the air-water interface

$$\rho_{avs} := \overrightarrow{\rho_{av}[p_{v\_int}, (T_{dwe\_K})]} \qquad \rho_{avs} = \begin{pmatrix} 0.063087 \\ 0.061919 \\ 0.056479 \end{pmatrix} \qquad \frac{kg}{m^3}$$

The humidity ratio of air at the air-water interface

$$w_{sws} := \frac{0.62509 \cdot p_{v\_int}}{p_a - 1.005 \cdot p_{v\_int}} \qquad w_{sws} = \begin{pmatrix} 0.062771 \\ 0.061413 \\ 0.055177 \end{pmatrix} \qquad \frac{kg}{kg} \text{ dry air}$$

The local mass transfer coefficients in the critical and fully developed flow region respectively are

$$h_{dcr} := \overrightarrow{\left[\frac{h_{Dcr} \cdot (\rho_{avs} - \rho_{ava})}{(w_{sws} - w_m)}\right]} \qquad h_{dcr} = \begin{pmatrix} 0.008836 \\ 0.012729 \\ 0.062663 \end{pmatrix} \qquad \frac{kg}{sm^2}$$

$$h_{dfd} := \overrightarrow{\left[\frac{h_{Dfd} \cdot (\rho_{avs} - \rho_{ava})}{(w_{sws} - w_m)}\right]} \qquad h_{dfd} = \begin{pmatrix} 0.034712 \\ 0.035675 \\ 0.037624 \end{pmatrix} \qquad \frac{kg}{sm^2}$$

The evaporation rate of deluge water in the critical and fully developed flow region respectively is

$$\Delta m_{dwcr} := \overrightarrow{[h_{dcr} \cdot A_{cr} \cdot (w_{sws} - w_m)]}$$

$$\Delta m_{dwcr} = \begin{pmatrix} 0.000013 \\ 0.000022 \\ 0.00012 \end{pmatrix} \qquad \frac{kg}{s}$$

$$\Delta m_{dwfd} := \overrightarrow{[h_{dfd} \cdot A_{fd} \cdot (w_{sws} - w_m)]}$$

$$\Delta m_{dwfd} = \begin{pmatrix} 0.00005 \\ 0.00006 \\ 0.000071 \end{pmatrix} \qquad \frac{kg}{s}$$

Therefore, the total evaporation rate of deluge water

$$\Delta m_{dw2} := \overrightarrow{(\Delta m_{dwcr} + \Delta m_{dwfd})} \qquad \Delta m_{dw2} = \begin{pmatrix} 0.000063 \\ 0.000082 \\ 0.000191 \end{pmatrix} \qquad \frac{kg}{s}$$

The enthalpy of the water vapour at the deluge water mean temperature

$$i_v := c_{pvdwm} \cdot T_{dwm} + i_{fg}(273.15)$$

$$i_v = 2.585 \times 10^6 \qquad \frac{J}{kg} \text{dry air}$$

The latent heat transferred to the air in the critical and fully developed flow region respectively is

$$\delta Q_{amcr} := \Delta m_{dwcr} \cdot i_v \qquad \delta Q_{amcr} = \begin{pmatrix} 33.816 \\ 56.646 \\ 310.556 \end{pmatrix} \quad W$$

$$\delta Q_{amfd} := \Delta m_{dwfd} \cdot i_v \qquad \delta Q_{amfd} = \begin{pmatrix} 130.065 \\ 155.437 \\ 182.561 \end{pmatrix} \quad W$$

Total latent heat transferred to the air

$$\delta Q_{am1} := \overrightarrow{\left(\Delta m_{dw} \cdot i_v\right)} \qquad \delta Q_{am1} = \begin{pmatrix} 164.008 \\ 212.015 \\ 493.133 \end{pmatrix} \quad W$$

or

$$\delta Q_{am2} := \delta Q_{amcr} + \delta Q_{amfd}$$

$$\delta Q_{am2} = \begin{pmatrix} 163.881 \\ 212.083 \\ 493.117 \end{pmatrix} \quad W$$

The sensible heat transferred to the air in the critical and fully developed flow region respectively is

$$\delta Q_{accr} := \overrightarrow{\left[h_{acr} \cdot A_{cr} \cdot \left(T_{dwe} - T_a\right)\right]}$$

$$\delta Q_{accr} = \begin{pmatrix} 7.134 \\ 12.128 \\ 69.042 \end{pmatrix} \quad W$$

$$\delta Q_{acfd} := \overrightarrow{\left[h_{afd} \cdot A_{fd} \cdot \left(T_{dwe} - T_a\right)\right]}$$

$$\delta Q_{acfd} = \begin{pmatrix} 27.959 \\ 33.91 \\ 41.357 \end{pmatrix} \quad W$$

Total sensible heat transferred to the air

$$\delta Q_{ac} := \delta Q_{accr} + \delta Q_{acfd} \qquad \delta Q_{ac} = \begin{pmatrix} 35.093 \\ 46.038 \\ 110.399 \end{pmatrix} \quad W$$

The enthalpy of air at the interface grid points

$$i_{man} := \overrightarrow{i_{ma}\left(T_{an}, w_n\right)} \qquad i_{man} = \begin{pmatrix} 94974.35 \\ 72394.1 \\ 39998.94 \end{pmatrix} \quad \frac{J}{kg} \text{ dry air}$$

$$i_{mas} := \overrightarrow{i_{ma}\left(T_{as}, w_s\right)} \qquad i_{mas} = \begin{pmatrix} 92071.75 \\ 68632.05 \\ 31200.27 \end{pmatrix} \quad \frac{J}{kg} \text{ dry air}$$

The heat transfer rate to the air stream

$$\delta Q_{a1} := m_a \cdot (i_{man} - i_{mas}) \qquad \delta Q_{a1} = \begin{pmatrix} 199.1 \\ 258.052 \\ 603.532 \end{pmatrix} \quad W$$

or

$$\delta Q_{a2} := \delta Q_{ac} + \delta Q_{am1} \qquad \delta Q_{a2} = \begin{pmatrix} 199.1 \\ 258.053 \\ 603.532 \end{pmatrix} \quad W$$

The directions of heat transfer through the deluge water film are presented in Figure C.3.

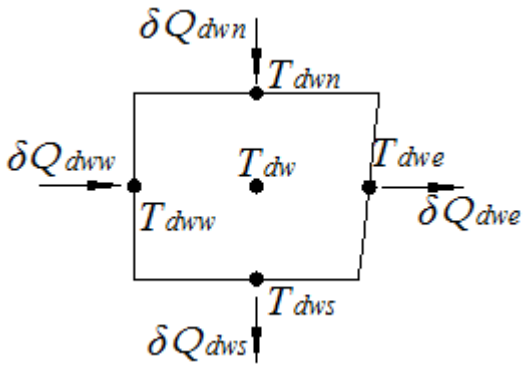

Figure C.3: The grid cell from the deluge water-side, demonstrating the directions of the heat transfer through the deluge water film

The heat transfer from deluge water film surface to the air stream

$$\delta Q_{dwe} := \delta Q_{a2} \qquad \delta Q_{dwe} = \begin{pmatrix} 199.1 \\ 258.053 \\ 603.532 \end{pmatrix} \quad W$$

The temperature of the deluge water on the outside surface of the tube wall

$$T_{dww} := \overrightarrow{\left[T_{dwe} + \frac{\delta Q_{dwe} \cdot \delta_{dw}}{k_{dwm} \cdot (A_{st})} \right]} \qquad T_{dww} = \begin{pmatrix} 44.833 \\ 44.6 \\ 43.616 \end{pmatrix} \quad °C$$

The deluge water weighted mean temperature

$$T_{dw} := T_{dww} - \frac{5 \cdot (T_{dww} - T_{dwe})}{8} \qquad T_{dw} = \begin{pmatrix} 44.496 \\ 44.168 \\ 42.627 \end{pmatrix} \quad °C$$

The temperature of the inlet deluge water

$$T_{dwn_{(15,4)}} := T_{dwi} \qquad T_{dwn_{(15,4)}} = 42.208 \quad °C$$

The temperature at the interface grid points of the grid cells

$T_{dws_{(15,4)}} := 44.4687975$ °C

$T_{dwn_{(8,4)}} := 44.19426$ °C

$T_{dws_{(8,4)}} := 44.13913$ °C

$T_{dwn_{(1,4)}} := 43.04549$ °C

$T_{dws_{(1,4)}} := 42.208026$ °C

Then

$$T_{dwn} := \begin{bmatrix} T_{dwi} \\ T_{dwn_{(8,4)}} \\ T_{dwn_{(1,4)}} \end{bmatrix} \qquad T_{dwn} = \begin{pmatrix} 42.20803 \\ 44.19426 \\ 43.04549 \end{pmatrix} \text{ °C}$$

$$T_{dws} := \begin{bmatrix} T_{dws_{(15,4)}} \\ T_{dws_{(8,4)}} \\ T_{dws_{(1,4)}} \end{bmatrix} \qquad T_{dws} = \begin{pmatrix} 44.4688 \\ 44.1391 \\ 42.208 \end{pmatrix} \text{ °C}$$

The temperature difference of the deluge water

$$\Delta T_{dw} := T_{dwn} - T_{dws} \qquad \Delta T_{dw} = \begin{pmatrix} -2.261 \\ 0.055 \\ 0.837 \end{pmatrix} \text{ °C}$$

The deluge water film thickness between tube wall and nodal point of each grid cell

$$\delta_{dw1} := \frac{\overrightarrow{(T_{dww} - T_{dw}) \cdot \delta_{dw}}}{(T_{dww} - T_{dwe})} \qquad \delta_{dw1} = \begin{pmatrix} 0.00008608 \\ 0.00008503 \\ 0.00008338 \end{pmatrix} \text{ m}$$

Therefore, the heat transfer to the deluge water film is

$$\delta Q_{dww1} := \frac{\overrightarrow{[k_{dwm} \cdot (A_{st}) \cdot (T_{dww} - T_{dw})]}}{\delta_{dw1}}$$

$$\delta Q_{dww1} = \begin{pmatrix} 199.1 \\ 258.053 \\ 603.532 \end{pmatrix} \text{ W}$$

The deluge water film thickness between the nodal points of the grid cells and the surface of the deluge water film

$$\delta_{dw2} := \frac{\overrightarrow{(T_{dw} - T_{dwe}) \cdot \delta_{dw}}}{(T_{dww} - T_{dwe})} \qquad \delta_{dw2} = \begin{pmatrix} 0.00005165 \\ 0.00005102 \\ 0.00005003 \end{pmatrix} \text{ m}$$

The heat transfer through the deluge water film

$$\delta Q_{dwe2} := \frac{\overrightarrow{k_{dwm} \cdot A_{st} \cdot (T_{dw} - T_{dwe})}}{\delta_{dw2}}$$

$$\delta Q_{dwe2} = \begin{pmatrix} 199.1 \\ 258.053 \\ 603.532 \end{pmatrix} \quad W$$

or

$$\delta Q_{dwe3} := \frac{k_{dwm} \cdot (A_{st}) \cdot (T_{dww} - T_{dwe})}{\delta_{dw}}$$

$$\delta Q_{dwe3} = \begin{pmatrix} 199.1 \\ 258.053 \\ 603.532 \end{pmatrix} \quad W$$

The directions of heat conducted through the tube wall are shown in Figure C.4.

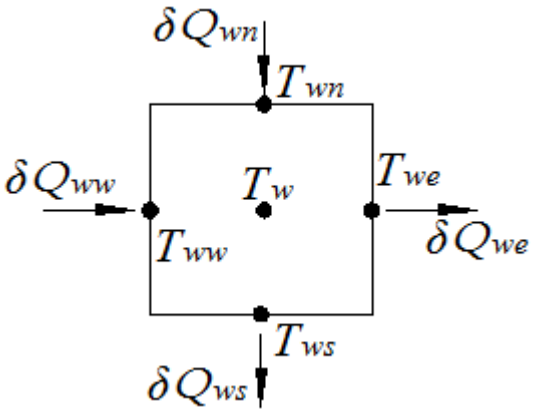

Figure C.4: The grid cell from the tube wall-side, showing the directions of heat conducted through the tube wall

The heat transferred from the outside tube wall to deluge water film

$$\delta Q_{we} := \delta Q_{dww1} \qquad \delta Q_{we} = \begin{pmatrix} 199.1 \\ 258.053 \\ 603.532 \end{pmatrix} \quad W$$

The outside tube wall temperature

$$T_{we} := T_{dww} \qquad T_{we} = \begin{pmatrix} 44.833 \\ 44.6 \\ 43.616 \end{pmatrix} \quad °C$$

The tube wall mean temperature

$$T_w := \overrightarrow{\left(T_{we} + \frac{\delta Q_{we} \cdot t_t}{2 k_t \cdot A_{st}}\right)} \qquad T_w = \begin{pmatrix} 44.874 \\ 44.653 \\ 43.742 \end{pmatrix} \quad °C$$

The inside tube wall temperature

$$T_{ww} := \overrightarrow{\left(T_{we} + \frac{\delta Q_{we} \cdot t_t}{k_t \cdot A_{st}}\right)} \qquad T_{ww} = \begin{pmatrix} 44.916 \\ 44.707 \\ 43.867 \end{pmatrix} \quad °C$$

The boundary value of the tube wall temperature is

$$T_{wn_{(15,3)}} := 44.91 \quad °C$$

The temperature at interface grid points

$$T_{ws_{(15,3)}} := 44.838967 \quad °C$$

$$T_{wn_{(8,3)}} := 44.662 \quad °C$$

$$T_{ws_{(8,3)}} := 44.644731 \quad °C$$

$$T_{wn_{(1,3)}} := 44.1476629 \quad °C$$

$$T_{ws_{(1,3)}} := 43.335506 \quad °C$$

Then

$$T_{wn} := \begin{bmatrix} T_{wn_{(15,3)}} \\ T_{wn_{(8,3)}} \\ T_{wn_{(1,3)}} \end{bmatrix} \qquad T_{wn} = \begin{pmatrix} 44.91 \\ 44.662 \\ 44.1477 \end{pmatrix} \quad °C$$

$$T_{ws} := \begin{bmatrix} T_{ws_{(15,3)}} \\ T_{ws_{(8,3)}} \\ T_{ws_{(1,3)}} \end{bmatrix} \qquad T_{ws} = \begin{pmatrix} 44.839 \\ 44.645 \\ 43.336 \end{pmatrix} \quad °C$$

The effective tube wall-side heat transfer surface area in z-direction

$$A_{wz} := 2 t_t \cdot L_t \qquad A_{wz} = 0.003 \quad m^2$$

The heat conducted through the tube wall in the z-direction

$$\delta Q_{wn} := \frac{2 k_t \cdot A_{wz} \cdot (T_{wn} - T_w)}{\Delta z} \qquad \delta Q_{wn} = \begin{pmatrix} 0.24 \\ 0.058 \\ 2.741 \end{pmatrix} \quad W$$

$$\delta Q_{ws} := \frac{2 k_t \cdot A_{wz} \cdot (T_w - T_{ws})}{\Delta z} \qquad \delta Q_{ws} = \begin{pmatrix} 0.24 \\ 0.058 \\ 2.741 \end{pmatrix} \quad W$$

The heat conducted through the tube wall in the y-direction

$$\delta Q_{ww} := \delta Q_{we} + \delta Q_{wn} - \delta Q_{ws} \qquad \delta Q_{ww} = \begin{pmatrix} 199.1 \\ 258.053 \\ 603.532 \end{pmatrix} \quad W$$

The directions of the heat transfer through the grid cells on the condensate-side are shown in Figure C.5.

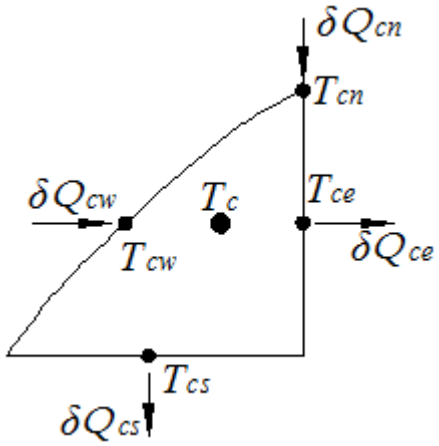

Figure C.5: The grid cell from the condensate-side, depicting the heat transfe directions

The condensation film surface temperature is assumed to be constant and equal to condensing temperature, therefore

$$T_{cw} := T_s \qquad T_{cw} = 45 \quad °C.$$

The inside tube wall temperature for each grid cell

$$T_{ce} := T_{ww} \qquad T_{ce} = \begin{pmatrix} 44.91597 \\ 44.70713 \\ 43.86732 \end{pmatrix} \quad °C$$

The weighted mean temperature of the condensate at nodal points

$$T_c := T_s - \frac{3\left(T_s - T_{ce}\right)}{4} \qquad T_c = \begin{pmatrix} 44.93698 \\ 44.78035 \\ 44.15049 \end{pmatrix} \quad °C$$

The boundary values of condensate temperature is

$$T_{cn_1} := T_s \qquad T_{cn_1} = 45 \quad °C$$

The temperature at the interface grid points for each grid cell

$$T_{cs_{(15,2)}} := 44.9211412 \quad °C$$

$$T_{cn_{(8,2)}} := 44.7914096 \quad °C$$

$T_{cs_{(8,2)}} := 44.76805548$ °C

$T_{cn_{(1,2)}} := 44.321876$ °C

$T_{cs_{(1,2)}} := 43.979104$ °C

Then

$$T_{cn} := \begin{bmatrix} T_s \\ T_{cn_{(8,2)}} \\ T_{cn_{(1,2)}} \end{bmatrix} \qquad T_{cn} = \begin{pmatrix} 45 \\ 44.791 \\ 44.322 \end{pmatrix} \text{ °C}$$

$$T_{cs} := \begin{bmatrix} T_{cs_{(15,2)}} \\ T_{cs_{(8,2)}} \\ T_{cs_{(1,2)}} \end{bmatrix} \qquad T_{cs} = \begin{pmatrix} 44.921 \\ 44.768 \\ 43.979 \end{pmatrix} \text{ °C}$$

The temperature difference of the condensate

$$\Delta T_c := \left(T_{cn} - T_{cs}\right) \qquad \Delta T_c = \begin{pmatrix} 0.079 \\ 0.023 \\ 0.343 \end{pmatrix} \text{ °C}$$

The positions of the nodal points from the top of the tube

$$z_{np} := \begin{pmatrix} \frac{\Delta z}{2} \\ 7\cdot\Delta z + \frac{\Delta z}{2} \\ 14\cdot\Delta z + \frac{\Delta z}{2} \end{pmatrix} \qquad z_{np} = \begin{pmatrix} 0.02 \\ 0.3 \\ 0.58 \end{pmatrix} \text{ m}$$

Then the condensation film thickness at each nodal point

$$\delta_c := \overrightarrow{\left[\frac{8\cdot\mu_c\cdot k_c\cdot\left(T_{cw} - T_{ce}\right)\cdot z_{np}}{\rho_c\cdot 9.8\cdot\left(\rho_c - \rho_{vs}\right)\cdot\left(i_{fgc} + c_{pvs}\cdot T_s\right)}\right]^{\frac{1}{4}}}$$

$$\delta_c = \begin{pmatrix} 0.000022 \\ 0.000058 \\ 0.000096 \end{pmatrix} \text{ m}$$

The condensation film thickness between the film surface and nodal points

$$\delta_{c1} := \overrightarrow{\left[\frac{\left(T_{cw} - T_c\right)}{\left(T_{cw} - T_{ce}\right)}\cdot\delta_c\right]} \qquad \delta_{c1} = \begin{pmatrix} 0.000016 \\ 0.000043 \\ 0.000072 \end{pmatrix} \text{ m}$$

The changes in the condensate's mass flow rate

$$\Delta m_c := \left[\frac{\overrightarrow{\left[k_c \cdot A_{st} \cdot \left(T_{cw} - T_c\right)\right]}}{\delta_{c1} \cdot \left(i_{fgc} + c_{pvs} \cdot T_s\right)}\right] \qquad \Delta m_c = \begin{pmatrix} 0.00008 \\ 0.000104 \\ 0.000243 \end{pmatrix} \quad \frac{kg}{s}$$

or

$$\Delta m_{c2} := \left[\frac{\overrightarrow{\left[k_c \cdot A_{st} \cdot \left(T_{cw} - T_{ce}\right)\right]}}{\delta_c \cdot \left(i_{fgc} + c_{pvs} \cdot T_s\right)}\right] \qquad \Delta m_{c2} = \begin{pmatrix} 0.00008 \\ 0.000104 \\ 0.000243 \end{pmatrix} \quad \frac{kg}{s}$$

The enthalpy released from the condensed steam

$$\delta Q_{cw} := \Delta m_c \cdot \left(i_{fgc} + c_{pvs} \cdot T_s\right) \qquad \delta Q_{cw} = \begin{pmatrix} 199.044 \\ 257.986 \\ 603.381 \end{pmatrix} \quad W$$

The boundary values of condensate mass flow rate is

$$m_{cn_{(15,2)}} := 0 \quad \frac{kg}{s}$$

The condensate mass flow rate at interface grid points

$$m_{cn_{(8,2)}} := 0.000624504 \quad \frac{kg}{s}$$

$$m_{cn_{(1,2)}} := 0.001520464 \quad \frac{kg}{s}$$

Then

$$m_{cn} := \begin{bmatrix} m_{cn_{(15,2)}} \\ m_{cn_{(8,2)}} \\ m_{cn_{(1,2)}} \end{bmatrix} \qquad m_{cn} = \begin{pmatrix} 0 \\ 0.0006245 \\ 0.0015205 \end{pmatrix} \quad \frac{kg}{s}$$

and therefore

$$m_{cs} := \begin{pmatrix} m_{cn_1} + \Delta m_{c_1} \\ m_{cn_2} + \Delta m_{c_2} \\ m_{cn_3} + \Delta m_{c_3} \end{pmatrix} \qquad m_{cs} = \begin{pmatrix} 0.0000803 \\ 0.0007285 \\ 0.0017637 \end{pmatrix} \quad \frac{kg}{s}$$

The enthalpy transferred by the condensate at interface grid points

$$\delta Q_{cn} := \overrightarrow{\left[m_{cn} \cdot c_{pc} \cdot \left(T_{cn} - T_c\right)\right]}$$

$$\delta Q_{cn} = \begin{pmatrix} 0 \\ 0.02888 \\ 1.08925 \end{pmatrix} \quad W$$

$$\delta Q_{cs} := \overrightarrow{\left[m_{cs} \cdot c_{pc} \cdot \left(T_c - T_{cs}\right)\right]}$$

$$\delta Q_{cs} = \begin{pmatrix} 0.00531 \\ 0.03743 \\ 1.26354 \end{pmatrix} \quad W$$

The heat transferred through the condensation film is then

$$\delta Q_{ce1} := \delta Q_{cw} + \delta Q_{cn} - \delta Q_{cs} \qquad \delta Q_{ce1} = \begin{pmatrix} 199.038 \\ 257.977 \\ 603.207 \end{pmatrix} \quad W$$

or

$$\delta Q_{ce2} := \frac{k_c \cdot \left(A_{st}\right) \cdot \left(T_{cw} - T_{ce}\right)}{\delta_c} \qquad \delta Q_{ce2} = \begin{pmatrix} 199.044 \\ 257.986 \\ 603.381 \end{pmatrix} \quad W$$

The friction coefficient

$$C_f := \begin{pmatrix} \frac{0.664}{Re_{acr}^{\frac{1}{2}}} \end{pmatrix}$$

$$C_f = \begin{pmatrix} 0.0017378 \\ 0.0023979 \\ 0.0077109 \end{pmatrix}$$

The mean air velocity

$$v_{am} := \overrightarrow{\left(\frac{m_{avi}}{\rho_{am} \cdot A_c}\right)} \qquad v_{am} = \begin{pmatrix} 7.475 \\ 7.471 \\ 7.466 \end{pmatrix} \quad \frac{m}{s}$$

The frictional force

$$F_f := \overrightarrow{\left(C_f \cdot A_{cr} \cdot \rho_{am} \cdot \frac{v_{am}^2}{2}\right)}$$

$$F_f = \begin{pmatrix} 0.0023 \\ 0.0032 \\ 0.0104 \end{pmatrix} \quad N$$

The air-side pressure drop due to friction in the critical and fully developed flow region respectively are

$$\Delta P_{cr} := \frac{\overrightarrow{F_f \cdot v_{am}}}{v_{am} \cdot A_c} \qquad \Delta P_{cr} = \begin{pmatrix} 0.30372 \\ 0.41854 \\ 1.34314 \end{pmatrix} \quad Pa$$

$$\Delta P_{fd} := \overrightarrow{\left[f_D \cdot \left(\frac{H_{fd}}{d_a} \right) \cdot \rho_{am} \cdot \frac{v_{am}^{\,2}}{2} \right]}$$

$$\Delta P_{fd} = \begin{pmatrix} 21.84746 \\ 21.8189 \\ 21.77441 \end{pmatrix} \quad \text{Pa}$$

Total air-side pressure drop

$$\Delta P := \Delta P_{cr} + \Delta P_{fd} \qquad \Delta P = \begin{pmatrix} 22.151 \\ 22.237 \\ 23.118 \end{pmatrix} \quad \text{Pa}$$

The fan power

$$P_F := \overrightarrow{\left(\Delta P \cdot v_{am} \cdot A_c \right)} \qquad P_F = \begin{pmatrix} 1.27895 \\ 1.28393 \\ 1.33474 \end{pmatrix} \quad \text{W}$$